Multi-disciplinary 3-D reservoir characterization and flow simulation of Aptian/Albian silicate sandstone reservoirs in Bredasdorp Basin, offshore South Africa.

By

Alfred OMOLOLU ONANEYE

Thesis presented in fulfilment of the requirements for the degree of **Master of Science** ***in the Faculty of Science at Stellenbosch University***

Supervisor: **Prof. Daniel Mikeš**

Co-supervisor: **Prof. Abraham Rozendaal**

December 2014

DECLARATION

I, the undersigned, hereby declare that the work contained in this thesis is my own original work and has not previously in its entirety or in part been submitted at any other university for a degree or examination. Where use was made of the work of others it has been acknowledge in the text.

…….. 2nd April 2014

Signature Date

ABSTRACT

Geological models remain the required input in flow simulators for use by reservoir engineers to simulate performance and optimize oil recovery. The lack of complete subsurface information however, continues to pose a challenge to accurate geological characterisation. A 3-D geologic reservoir model of identified reservoir sand-bodies (WBRED-A, WBRED-B, WBRED-C and WBRED-D) was created to evaluate reservoir fluid-flow performance by way of a systematic workflow that integrates reservoir characterisation, reservoir modelling, upscaling and fluid-flow simulation using a range of data sets. These include: 2-D seismic profiles, well logs, cores, sedimentary logs, and well tests from three exploratory wells. The modelling /approach employed deterministic geological processes in a stochastic framework, hence combining benefits of both deterministic and stochastic modelling methods arranged in nested steps defined primarily by: (1) the creation of a 3-D reservoir model with an anatomy based on concepts of depofacies and their distribution and partitioning, (2) upscaling (i.e. selection of an optimal upscaling method) of the 3-D reservoir model for realistic and representative reservoir anatomy and (3) fluid-flow simulation (i.e. steady state simulation based on assigned two-phase flow parameters of depofacies).

The juxtaposing and organisation of observed lithofacies features (sedimentary structures and facies associations) in a down-dip depositional profile allowed for the reconstruction of depositional lithofacies architecture and geometric elements. Six depofacies were recognised (proximal mouth bar, distal mouth bar, delta front, distributary channel, overbank/inter-channel and floodplain/inter-channel deposit), which are broadly grouped into four main lithofacies associations (massive sandstone, interbedded sandstone, claystone, and soft-sediment deformation). Reservoir sandbodies are indicative of a depositional system characterised by a succession of superimposed deltaic cycles which control vertical and horizontal reservoir

connectivity. A description of reservoir petrophysics revealed that the WBRED-D presents the lowest average poro-perm results of the four units investigated. Moderate to excellent poro-perm relationship is confirmed within the two main reservoir types-distributary channel-fill and inter-channel reservoirs for WBRED-B, WBRED-C and WBRED-D. Effective porosity values in WBRED [A-D], ranges from 0.14 to 0.35 indicating moderate to very good reservoir quality, while permeability values ranges from 6mD to 602mD and is attributed to well sorted sands. The key control of effective porosity and permeability is the continuity and connectivity of the channel sands and inter-channel deposits. Besides, average water saturation values in the units range from 12% to 69% representative of a reservoir system considered satisfactory for hydrocarbon production. Ten stratigraphic flow units are mapped within WBRED [A-D] and define predictable hydraulic conductivity, storage and porosity of reservoir sandbodies. Flow unit 6 and 10 are identified as possible flow barriers.

Upscaling results of WBRED-C show that to preserve reservoir connectivity, the upscaling of the inter-channel deposits proved important. Permeability and porosity upscaling using arithmetic mean and flow-based methods proved effective in generating an excellent agreement between upscaled and fine grid model for WBRED-C. Upscaling describes the replacement of a number of heterogeneous fine grid-blocks with one equivalent coarse homogeneous grid block. The impact of two-phase flow parameters, as modelled for three depofacies characterizing WBRED-C against cumulative production, reveal that relative permeability/wettability is the dominant two-phase flow property. Vertical and lateral facies heterogeneity governs successful mobile oil and gas productivity. To these ends, results of this study are of particular significance to Bredasdorp Basin where geological complexity exists and will assist in planning enhanced oil recovery strategies.

UITTREKSEL

Geologiese modelle word benodig vir reservoir vloei simulators wat gebruik geword deur reservoir ingenieurs om reservoir verrigting na te boots en te optimaliseer. Weens 'n gebrek aan akkurate ondergrondse inligting, is die karakterisering van geologiese kenmerke steeds 'n uitdaging. 'n 3-D geologiese reservoir model van geïdentifiseerde reservoir sandliggame (WBRED-A, WBRED-B, WBRED-C en WBRED-D) is geskep om reservoir vloeiprestasie te evalueer deur middel van 'n sistematiese werkvloei wat reservoir karakterisering, reservoir modellering, skalering en vloeistof vloei simulasie met 'n verskeidenheid van datastelle. Dit sluit in 2D seismiese profiele, boorgat logs, kern logs, sedimentêre logs, en toetse vanuit drie verkennende boorgate. Die modellering gebruik deterministiese geologiese prosesse in 'n stogastiese raamwerk, dit wil sê die kombinasie van die voordele van beide deterministiese en stogastiese modellering metodes, georden in substappe gedefinieer hoofsaaklik volgens: (1) die skepping van 'n 3-D reservoir model met 'n anatomie wat gebaseer is op die konsepte van depofacies en hul verspreiding en skeiding, (2) die skalering van die 3-D reservoir model vir ŉ realistiese en verteenwoordigende reservoir anatomie en (3) die vloei simulasie.

Die afwisseling van die waargenome lithofacies funksies (sedimentêre strukture en fasies verenigings) in 'n afwaartse-helling afsettings profiel het toegelaat vir die rekonstruksie van die afsettings lithofacies argitektuur en geometriese elemente. Ses depofacies is geïdentifiseer (proksimale mond bar, distale mond bar, delta front, vertakking kanaal, inter-kanaal en vloedvlakte), wat gegroepeer is volgens vier lithofacies (massiewe sandsteen, interbedded sandsteen, claystone en sagte sediment deformasie). Reservoir sandliggame is 'n aanduiding van 'n afsettings omgewing gekenmerk deur 'n reeks van oorvleuelende deltaisch siklusse wat die vertikale en horisontale reservoir verbindings beheer.

Reservoir petrofisika beskrywings het aangetoondat WBRED-D bied die laagste gemiddelde poro-perm resultate van die vier eenhede ondersoek. Matige tot n uitstekende poro-perm verhouding is bevestig binne die twee belangrikste reservoir tipes-vertakking naamlik kanaalvul en interkanaal reservoirs vir WBRED-B, WBRED-C en WBRED-D . Effektiewe porositeit in WBRED [nC], wissel van 0,14tot0,35 wat dui op matige tot goeie reservoir gehalte, terwyl deurlaatbaarheid waardes wissel van6mD tot 602mD en wordtoegeskryf gesorteerde sande. Diebeheer van effektiewe porositeit en permeabiliteit is hoofsaaklik die kontinuïteit en verbinding van die kanaal sand en interkanaal afsetting. Gemiddelde water versadigingwaardes in die eenhede wissel van 12% tot 69 %, wat 'n reservoir stelsel aandui met bevredigende potensiaal vir koolwaterstof produksie. Tien stratigrafiese vloei eenhede is gekarteer binne WBRED [nC] en definieer voorspelbare hidrouliese geleiding, die stoor en porositeit van reservoir sandliggame. Vloei eenheid 6 en 10 is geïdentifiseer as moontlike vloei hindernisse.

Opskalering resultate van WBRED-C toon dat om reservoir verbinding te bewaar, die opskaling van die inter- kanaal afsettings belangrik is. Deurlaatbaarheid en porositeit opskalering gebruik rekenkundige gemiddelde en vloeigebaseerde metodes wat doeltreffend bewys is en lewer 'n uitstekende ooreenkoms tussen opskalering en detailrooster model vir WBRED-C. Opskaling beskryf die vervanging van 'n aantal van heterogene detail rooster - blokke met een ekwivalent growwe homogene rooster blok. Die impak van tweefase vloei parameters, soos gemodelleer vir drie depofacies wat WBRED-C met kumulatiewe produksie vergelyk , toon dat relatiewe deurlaatbaarheid/benatting is die dominante twee fase vloei eienskap.. Vertikale en laterale fasies heterogeniteit veroorsaak suksesvolle mobiele olie en gas produktiwiteit. Resultate van hierdie studie is van besondere belang vir Bredasdorpkom waar geologiese kompleksiteit bestaan en sal help met die beplanning vir verbeterde olie ontginning strategieë.

ACKNOWLEDGEMENT

It is my great pleasure to thank so many people, after the numerous challenges embarked upon adapting to the multidisciplinary nature of this research study. First of all, I would like to thank my Heavenly father for the grace, wisdom, understanding and good health bestowed upon me during the period of this study. I wish to express my sincere gratitude to my supervisor Prof. Daniel Mikeš and Prof. Abraham Rozendaal for their patience, long suffering, assistance, guidance, and giving me considerable flexibility in how to approach this study. I thank Prof. Daniel Mikeš particularly for giving me the opportunity to take on this project despite the initial lack of research funds. I believe without doubt that his knowledge, critic mind and kindness will benefit me throughout the rest of my life.

Special thanks to Inkaba ye Africa for funding this research study and allowing for various international academia engagements during the period of this research work. Many thanks, to Prof. Maarten de Wit and Elronah Schaap at the (Inkaba Office) for their leadership and guidance and indulgence during times of need. The efforts of the technical team at the Petroleum Agency of South Africa for giving the permission to access data and for easy facilitation to physically examine cores at their core bank are appreciated. Many thanks, to Jacques Roux at the Petroleum Agency South Africa for guidance into the start of the research project.

Special thanks to all my fellow research colleagues (Mareli, Rick, Donovan, Fabian, Andy, Bose, Ernie, Happiness, Palesa, Renitia and Malika) for their advice and direction. I gratefully acknowledge Wasiu Sonibare and Samir Guma Elamri for insightful views and technical suggestions to improve this report. I wish to express sincere gratitude to my finance (Bolutife Adefehinti) and brother (Frederick Adebayo Onaneye) for their support and encouragement.

DEDICATION

I dedicate this work to my mother and my sister, YETUNDE RACHEL ONANEYE and OMOTOLA OLUWAFUNMILAYO BABAJIDE, the pillars of inspiration in my life. Their continue care and love proved invaluable during difficult times.

TABLE OF CONTENTS

SECTION 1

SECTION 3

LIST OF FIGURES

Pages

CHAPTER 1

CHAPTER 2

CHAPTER 5

LIST OF TABLES

CHAPTER 4

CHAPTER 5

LIST OF NOMENCLATURE AND ABBREVIATION

WBRED = WBRED [A-D] reservoir sandstone units

V_{shale} = Volume of shale

S_w = Water saturation

S_{HC} = Hydrocarbon saturation

$S_{W\ IND}$ = Water saturation (Indonesia)

F_{eff} = Effective porosity

GRlog = Gamma ray log

SECTION 1

CHAPTER 1

INTRODUCTION

1.1 Structure of the Thesis

1.1.1 Elements

This thesis reports the results of a three-dimensional reservoir characterization and flow simulation study (i.e. window-study) of identified Lower Cretaceous Aptian and Albian reservoir sandstones, approximately 20km east from the Sable oilfield in the Western Bredasdorp Basin offshore South Africa (Figure 1.1). For the purpose of this study, the identified reservoir units are labelled "WBRED", and grouped into WBRED-A, WBRED-B, WBRED-C and WBRED-D.

This evaluation study comprises of three major sections which on subdivision compile seven chapters. These sections demonstrate an organized progression of incorporating the different multi-disciplines (i.e. geology, geophysics, petrophysics and reservoir engineering) involved in the reservoir characterization and modelling building process.

1.1.2 Section 1

Section one gives a brief overview of the focus of this thesis. It begins with Chapter One which presents the research frame work, aims and the flowchart of stepwise techniques utilized in this study. It includes a literature review which involves a comprehensive search in publications relating to reservoir geology, stratigraphy, and facies architecture of sedimentary basins, gridding and upscaling techniques for reservoir simulation and a brief discussion on geostatistics and flow simulation. This section ends with the methodology adopted for the study and a review of the geology of the Bredasdorp Basin in chapter two and three respectively.

1.1.3 Section 2

This section covers all aspects of the conceptual geological model creation and 3-D facies modelling process which includes qualitative core description, log analysis, depositional lithofacies analysis, lithology property data analysis and property modelling. Chapter four examines lithofacies analysis, log analysis, well log correlation, core description and interpretation of the three available wells in the study area. Chapter five further describes in detail the construction of the geological (reservoir) model involving both qualitative and quantitative petrophysical evaluation of selected wire-line log data of the three wells (i.e. E-L1, E-AH1, and E-BD2) available for this study.

1.1.4 Section 3

Chapter six and seven embodies section three. This section describes the upscaling of reservoir properties, fluid model, rock-physics characterization and definition of simulation cases. It presents various development strategies, simulation case scenarios, reservoir performance and future production forecast results. The thesis ends in Chapter Seven with an extensive conclusion and relevant recommendations. The framework diagram for the present study illustrating the components of the thesis is presented in (Figure 1.2).

1.2 Study Area

The sedimentary basin selected for this study is the larger Bredasdorp sub-basin, located in the southern offshore region of South Africa (Figure 1.1). This basin comprises mostly of marine Aptian to Maastrichtian sediments, covering an area of approximately 18,000 sq. km in fairly shallow water depths (less than 200m), ranging from 50m in the extreme northwest and a maximum depth of 116m in the southwest (Grobbler, 2005; Petroleum Agency SA Hand book, 2007).

The selected area for this study is situated in the western section of Block 9 in the Bredasdorp Basin and east of the Sable oilfield with geographic coordinates located between latitude 19^0E and 22^0 and longitude 34.4^0 and 35^0. The modelled section of the study area is 356 sq. km hosting three cored wells (E-L1, E-AH1 and E-BD2) approximately 11.14 km apart (Figure 1.3).

1.2.1. Exploration and production activity profile - Western Bredasdorp Basin

The larger Bredasdorp Basin has experienced intensive petroleum exploration and drilling and consequently made available large collection of geological data sets. This specifically has helped to provide a better understanding of the geology of the basin. Recent exploration activities show that, the Western Bredasdorp Basin suggests an area with significant hydrocarbon potential; favourable oil and gas prone source rocks and good reservoir rocks and traps with effective seal parameters (Davies, 1997a; 1997b, Brown et al., 1995; Roux, 2007).

In addition, several play concepts and basin floor fans associated with bright seismic anomalies indicating possible oil seeps or hydrocarbon accumulation have been recognised. Various producing oilfields have also been discovered around this area (e.g. Sable Oil Field). The exploration and production ventures have been driven mainly by South Africa's national exploration company (PetroSA) and a few independent oil companies. Further exploration activities however, are still needed to confirm untested structures with up-dip potential within the Western Bredasdorp Basin. This would clear doubts on hydrocarbon potential and in turn provide more geological understanding. The ranking of prospective regions in the Outeniqua Basin which includes the Western Bredasdorp Basin by the Petroleum Agency of South Africa is presented in (Figure 1.4 and Table1.1).

1.2.2 Previous Work

A number of reservoir characterization studies related to the Bredasdorp Basin have been carried out, but remain in the form of internal reports and property of PetroSA. The majority of these reports were not accessible for this study.

A review of the general literature reveals that to date only a few syntheses of geology and stratigraphy of the Western Bredasdorp Basin are published and focused mainly on the 13A and 14A sequences. Current study interests are concentrated on obtaining better understanding on the complexity surrounding the evolution of the Bredasdorp Basin and petroleum system elements. The works of (Barton and Frewin, 1998; Burden, 1996; Turner, 2000) gives a good account of the different regional geological models formulated for the 14A sequence consisting of Middle Albian sediments. This subsequently came after a detailed sequence stratigraphic study of the Bredasdorp Basin was carried out under the auspices of the University of Texas at Austin in 1988. The geological models developed for sequence 14A prior to 1995 were based mainly on geophysical log correlation and petrographic studies with no account of seismic mapping. According to Turner, 2000 and Burden and Davies, (1997a), the current 14A model combined all the elements of the previous models and the following aspect are considered proven: (1) the geographic distribution of the sandstones is concentrated within two east-west trending fairways, (2) the existence of a sequence boundary between 14At1 and 14mfs based on biostratigraphy evidence, (3) the 14A sand units consist of channelized deposits consisting of three distinct sub units which are a lower siltstone, a middle massive amalgamated sandstone unit and an upper interbedded sandstone and claystone unit interpreted as abandonment channel–fill deposits.

At the moment, an extensive exploration program is on-going in the Bredasdorp Basin, however with more focus on the central area, there are still much to be evaluated as it relates to uncertainties associated with the sandstone fairways, distribution of facies and fluid-flow regime in the western section of the basin (Turner, 2000; Petroleum Agency SA, Brochure 2008).

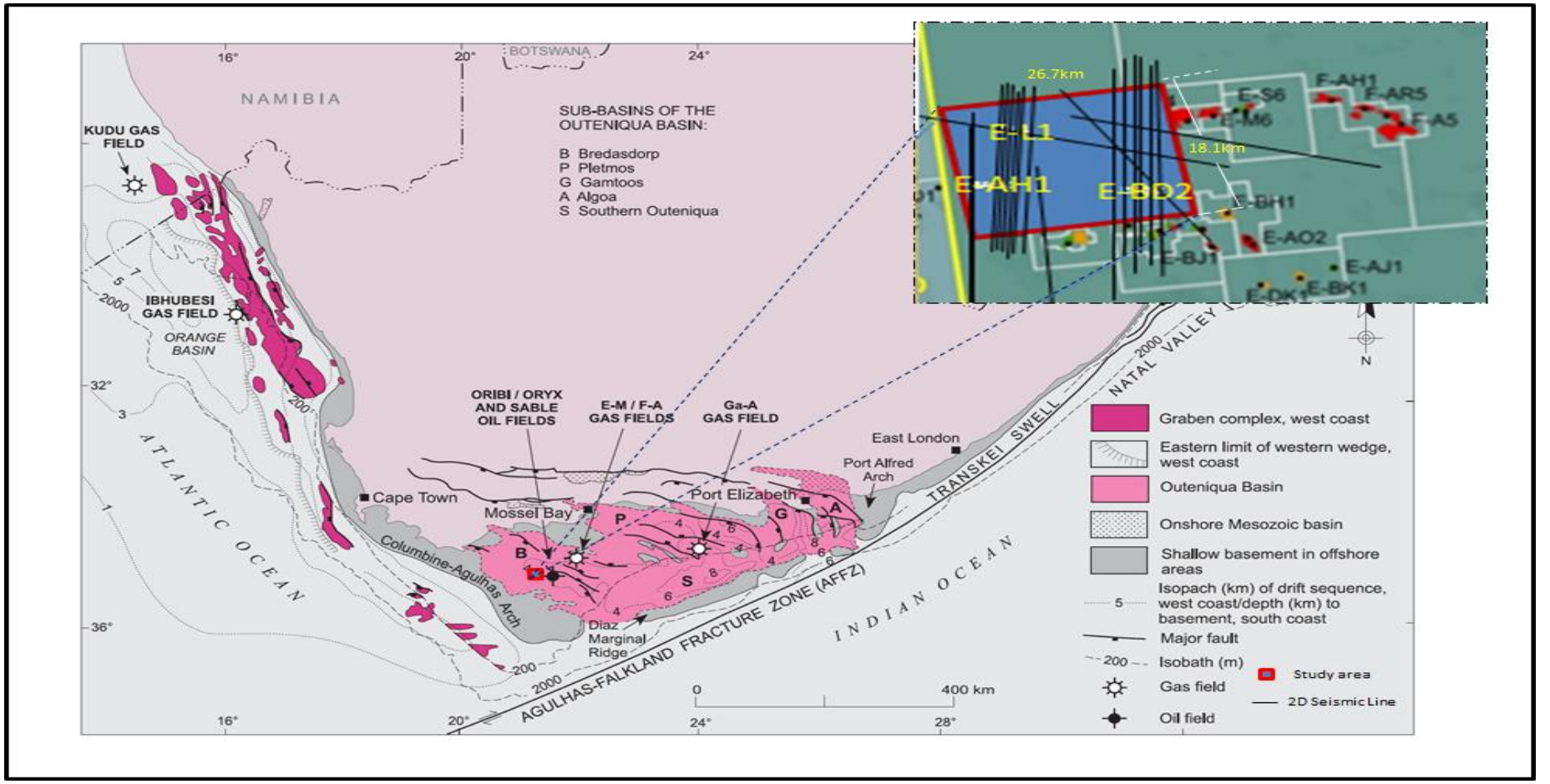

Figure 1.1: Map of study area located approximately 20km east of Sable oilfield in the Bredasdorp Basin offshore South Africa (area marked in blue ; modified from Broad et al., 2006).

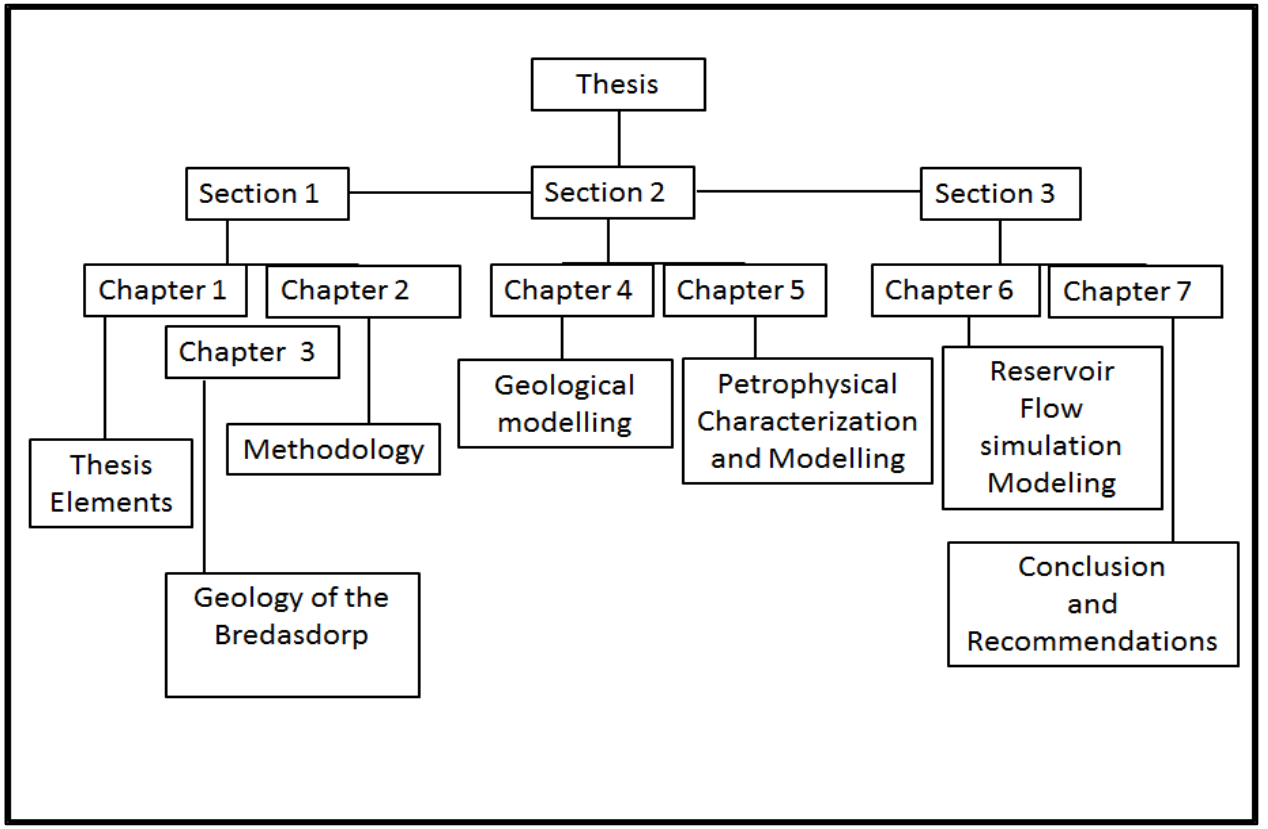

Figure 1.2: Structure diagram of the thesis illustrating its components.

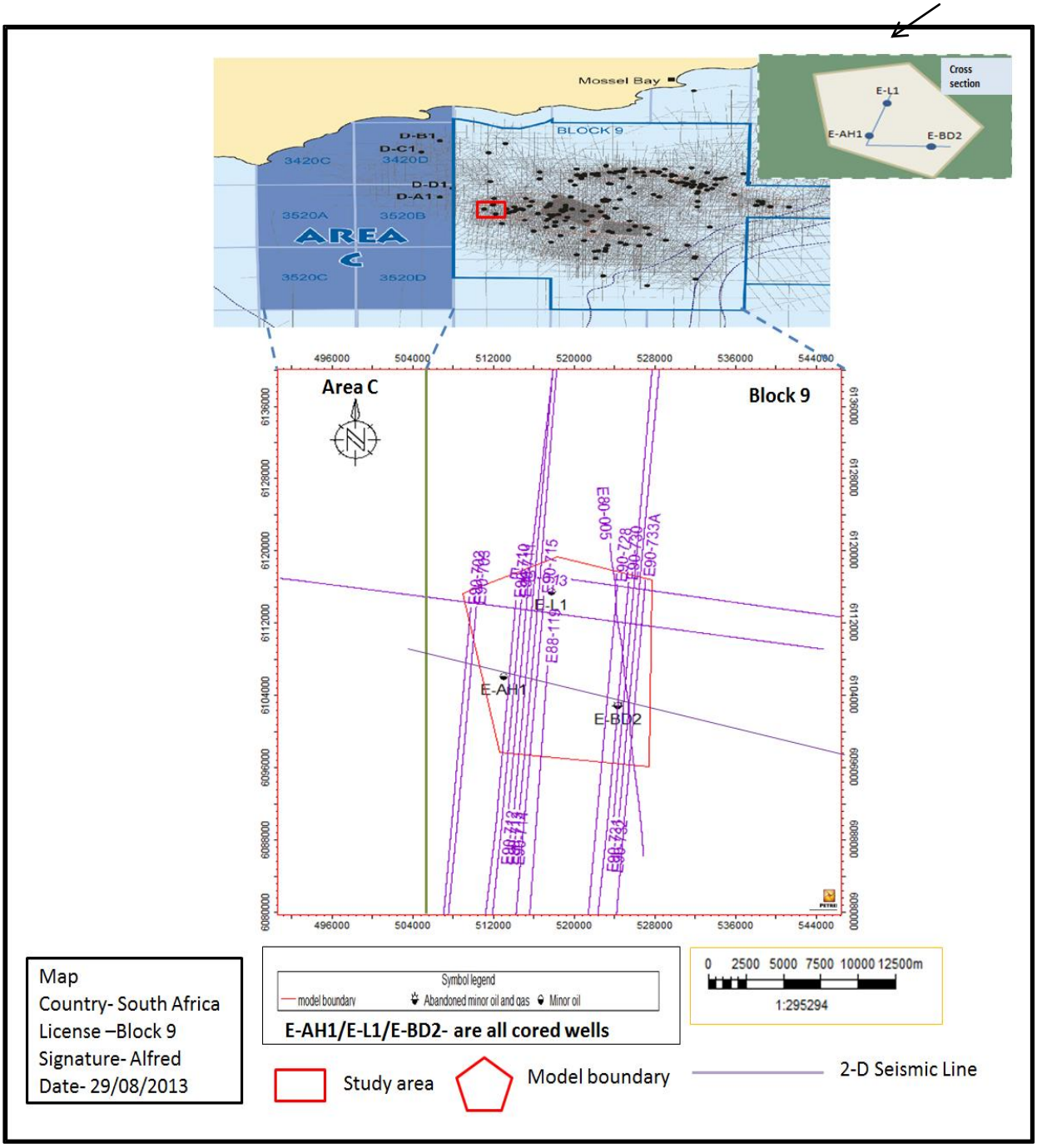

Figure 1.3: Well location map (UTM coordinate) as generated in PETREL, marked by a blue line in the upper right rectangular green box is the cross section profile of the selected wells.

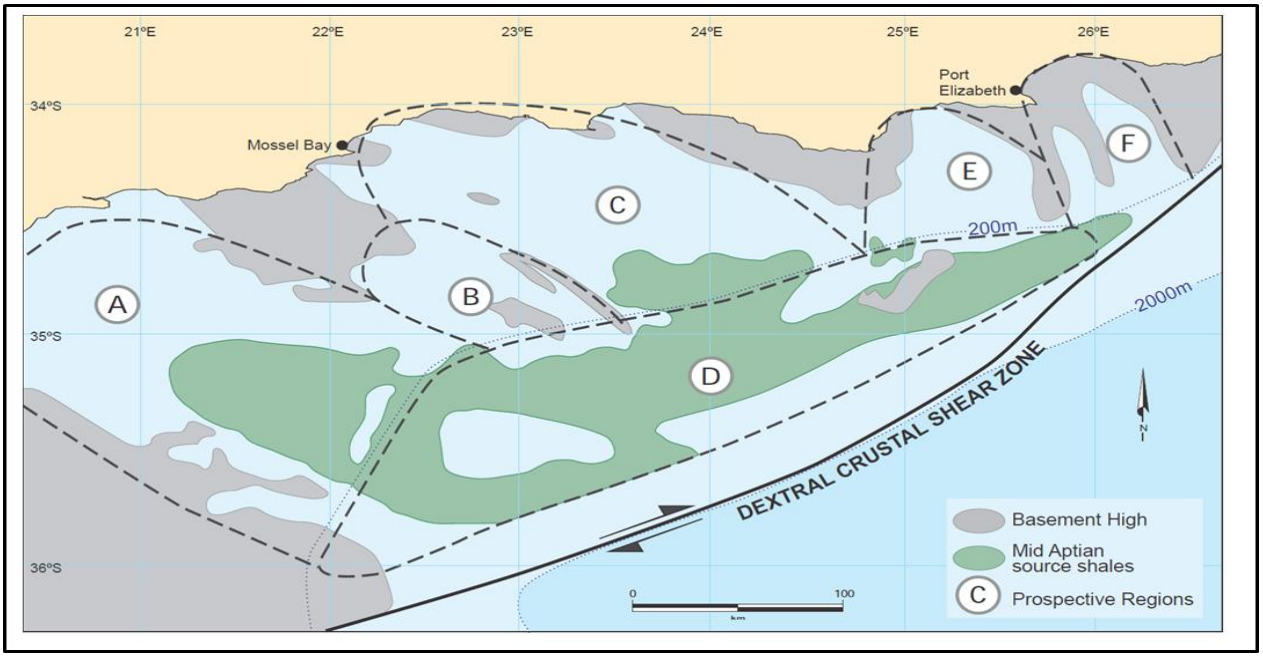

Figure 1.4: Ranking of prospective regions across the Outeniqua Basin (consisting of Bredasdorp-A, Infanta Embayment-B, Pletmos-C, Gamtoos-E and Algoa-F sub-basins) off shore South-Africa (from Petroleum Agency SA Brochure, 2010).

Table 1.1: Ranking of prospective regions of each sub-basin in the Outeniqua Basin offshore South Africa based on a number of petroleum system elements.

Prospective regions					
A Bredasdorp	B Infanta Embayment	C Pletmos	D Southern Outeniqua	E Gamtoos	F Algoa
Kitchen area					
Large	Small	Moderate	Large	Small	Small
Traps					
Abundant	Limited	Abundant	Abundant	Limited	Limited
Effective seals					
Widespread	Limited	Widespread	Widespread	Limited	Limited
Oil and gas finds					
Proven oil and gas potential	Little potential	Proven gas potential	Undrilled	Gas shows	Oil shows
Hydrocarbon potential					
Excellent	Poor	Good	Excellent	Good for gas	Excellent

1.3 Background

A 3-D reservoir model generally refers to a conceptual three dimensional representation of the observed and estimated characteristics of an identified subsurface reservoir (Peaceman and Donald, 2000). Over the years, reservoir models have provided a consistent approach to link all existing data in characterizing subsurface oil and gas reservoirs and an input for flow simulation computation (Kamali et al., 2013). Pressing forward, the need for reliable 3-D reservoir models have continued to be paramount due to the ever depleting hydrocarbon reserves and geological complexities encountered in major hydrocarbon reservoirs worldwide (Ringrose et al., 1993). This is also based on efforts to optimize recovery mechanisms. Recent studies have shown that in recent years it is now realistically achievable to construct 3-D reservoir models; a development referred to by notable scholars as the most resourceful tool for reservoir management purposes (Robinson, 2008; Branets et al., 2009). Another significance of 3-D reservoir models is that it reliably promotes reservoir production forecast and offers best possible drainage mechanism under various development scenarios (e.g. Dubrule and Damsleth, 2001; Massonnat et al., 2002).A outcome considered a big leap in the characterization of geologically complex subsurface reservoirs (Branets et al., 2009).

However, there are still pertinent challenges to having realistic 3-D reservoir models that serves as input for flow simulation. To analyse these challenges, (Tamhane et al., 1999; Dubrule and Damsleth, 2001) emphasised the need to address inadequate assimilation and true reflection of geological knowledge in the creation of realistic reservoir models. A manifestation ascribed often to practices of stochastically characterizing petroleum reservoirs (Mikeš et al., 2006). In recent years, it is observed that the role of reservoir geology is diminishing with respect to 3-D stochastic reservoir modelling (Tamhane et al., 1999).

Stochastic simulation remains however, a popular means of quantifying reservoir heterogeneity when considering oil industry reservoir modelling practice. The question would be why is this so? Geoscientist and geo-modellers attribute this practice to the impossibility of physically characterizing subsurface reservoirs and therefore result to obtaining approximate solutions with often little subsurface information. However, reservoir geology generates a significant understanding towards defining the reservoir in terms of continuity, lithology, facies distribution, structural geometry and style, yet, it acknowledges that most petroleum reservoirs reside within sedimentary settings that are often complex in architecture and heterogeneous at a wide range of scale (Massonnat, 1997). Therefore, accurately resolving reservoir rock architecture and heterogeneity at multiple scales for use in 3-D flow simulation modelling presents a huge task; the various scales are presented in Figure 1.5.

Nevertheless, a great number of geoscience studies (e.g. Haldorsen and Lake, 1984; Weber and van Geuns, 1986; Ringrose et al., 1993; Aarnes et al., 2006: Wen et al., 1998; Branets et al., 2009: Barker and Thibeau, 1997; Poppelreiter et al., 2005; Tye and Hickey, 2001: Gauthier et al., 2002; Darman et al., 2002, Campbell, 1967) have recognized these challenges and mostly the effect of multiple scales of heterogeneity in characterizing fluid flow behaviour in petroleum reservoirs. In response they have proposed different concepts and technologies (e.g. advanced gridding techniques, powerful hybrid upscaling algorithms, intelligent reservoir to simulation modelling workflows, development of multi-scale data reservoir software-with the possibility of incorporating the effect of small scale geological structures etc.) for improved multi-scale 3-D geological (reservoir) modelling. Another typical challenge is the availability of incomplete reservoir data information often arising due to cost and time factor decisions. Yet, conventional 3-D geological (reservoir) modelling practice depends on fast and flexible procedures in handling reservoir data which are unfortunately, often incomplete; making the establishment of ground truth not entirely possible even though in reality the reservoir is deterministic (Tamhane et al., 1999;

Durlofsky et al., 2005). Under this circumstance, oil industry reservoir modelling workflows have extended more focus to the larger scale resulting from the form of measurements available, reservoir data missing scales, computational capability, and technical knowhow (Wen et al., 2005). Despite these challenges, the geologist's contribution to the physical frame work of the reservoir is enormous and often essential. As result, their effort often involves providing as much geological information as possible in the model to validate realistic reservoir descriptions and also reduce subjectivity.

The benefits of data integration is seen vital to decreasing uncertainties of the model, but may not necessarily amount to a more "accurate" reservoir model (Tamhane et al., 1999). This can be hinged on the fact that the constructed model cannot be verified alongside the actual subsurface reservoir in question (Oreskes et al., 1994). Considering however, the challenges associated with integrating reservoir data from various sources into a consistent 3-D volume.

Also,he availability of high speed computers as enabled geoscientist and geo-modellers to embrace the use of geostatistics also referred to as stochastic modelling. For the purpose of integrating multi-scale data, simulating unknown reservoir properties and quantifying reservoir heterogeneity (Tamhane et al., 1999). The geostatistical methods employs statistical means to quantify and exploit spatial correlation by harnessing and integrating available data from various sources and scales of measurement (i.e. seismic and geologic features, core measurements, well logs, borehole image logs and production data) (Hohn, 1988).

Nonetheless, reservoir studies (e.g. Raba'a and Heine, 2006; Philips and Wen, 2007; Ringrose et al., 1993), demonstrated the effect of characterizing and modelling sedimentary deposit (i.e. petroleum reservoirs) as totally homogenous bodies which generally connotes to gross simplification of reservoir potential when considering sedimentary and structural heterogeneities. They suggested the practical and effective way to resolve realistic reservoir fluid flow performance

often entails adopting the best practice of modelling the depositional facies that primarily controls the spatial distribution of reservoir heterogeneity. Under this circumstance, creating a facies dependent 3-D reservoir model commonly considers two categories of facies modelling techniques (Schlumberger reservoir modelling manual, 2011). They are categorized as either deterministic or stochastic (e.g. object based simulation, sequential indicator simulation, truncated gaussian simulation and pixel based methods) (Journel, 1989; Tamhane et al., 1999). The deterministic technique creates models which mathematically expressed as having outcomes being precisely determined through known relationships that give little or no room for random variation (Schlumberger reservoir modelling manual, 2011). Input in this case would provide the same output. Typically, this technique is used when there is dense subsurface data (e.g., many wells, wells plus seismic), a case that rarely exist at the exploration phase (Schlumberger reservoir modelling manual, 2011).

Stochastic technique also, utilizes statistical processes that use input data variables to predict ranges of assumptions; this simply explains that any uncertainty in the input data would be quantified by averaging over multiple realizations. This is often applied in conditions where sparse subsurface data with poor vertical and lateral resolution are present to have a possible result that is used to produce multiple, equally and probable realizations (Schlumberger reservoir modelling manual, 2011). Stochastic modelling thereby offers the advantage and capability of analysing uncertainties and risks (Tamhane et al., 1999). Today, reservoir modellers use stochastic modelling which includes upscaling as routine tools to better model heterogeneity, accesses uncertainties and integrate data (Kamali et al., 2013). Upscaling is a tool which helps to bridge the scale gap that exists between the finely gridded geological model and the simulation grid. In effect to effectively compute equivalent reservoir rock properties of the fine grid fit for reservoir simulation purpose (Qi and Hesketh, 2004). As a whole this describes the upscaling process or workflow. Moreover, the implementation of the upscaling workflow is considered comparatively trivial alongside other

input workflows in reservoir modelling. It plays a major role in effectively preserving the geological knowledge scale and obtaining accurate upscaled representation of modelled properties. To this end, geological studies (e.g. Mikeš et al., 2006) demonstrates that to optimise the use of the upscaling tool an "integrated upscaling procedure" must be designed. The procedure establishes the need towards incorporating the effects of all geological structures that characterize hydraulic flow through each step of evaluating the rock record to reservoir flow simulation. The steps consist of reservoir data acquisition, geological description, facies analysis, facies modelling, upscaling of the geological model and finally reservoir flow simulation. The above stated reviewing heterogeneities that affect fluid flow should then be analysed with the aim of critically optimizing the upscaling process. Based on the discussions, a number of issues surrounding improved reservoir characterisation for flow simulation have been mentioned. This is intended to report the current state of fluid flow studies and stimulate thoughts towards the following questions: (1) To what extent can we preserve the geological detail utilizing routine geological and simulation modelling workflows against the balance of available computational resources? (2) Can upscaling be avoided, considering the expected growth towards the need of fine scale geological descriptions against the rapid development of cost saving high speed computers and reasonable simulation run times?

1.4 Sedimentary facies - clastic reservoirs

Accurate knowledge and description of sedimentary facies (i.e. reservoir lithofacies), distribution and geometry along different styles of platform depositional environment (i.e. clastic or carbonate) is crucial to obtaining true productive capacity of a target reservoir. This is because petrophysical properties of the rock making up the reservoir vary by lithofacies types. Moreover, lithofacies describes a three dimensional mass of sedimentary rock distinguishable from adjacent units on the basis of its lithology, texture, geometry, sedimentary structure and palaeontology (IPIMS, 2011).

Four major benchmarks are often used to define various lithofacies types in a clastic environment: (1) the utmost number of recognizable lithofacies using petrophysical wire-line logs curves and other variables; (2) the minimum number of lithofacies needed to accurately represent lithologic and petrophysical heterogeneity; (3) the utmost distinction of core petrophysical properties among types; and 4) the relative contribution of a lithofacies type to storage and flow (Schaller, 2009). This is essential to the construction of a geostatistical reservoir model as the assigning of cells with lithofacies is vital to characterizing petrophysical properties that vary among lithofacies.

1.5. Gridding, upgridding and upscaling geological models for flow simulation

Grid and gridding within the realm of geostatistics are seemingly similar words but in geological (reservoir) modelling the word grid is considered before any numerical reservoir description. The grid, gridding and the gridding algorithm are defined by a geophysicist respectively, as spatial arrangements of points (i.e., x- y coordinates), the act of determining values for grid elements on a map, and the computational procedure incorporated in the methods that determine the values assigned to grid elements. While, upgridding describes the process of determining the 3-D computational grid of the simulation model (King, 2007). Grid generation for practical reservoir to simulation modelling presents daunting challenges due to complex structure of subsurface reservoir geometry (Branets et al., 2008). Nonetheless, advanced gridding techniques and grid options (e.g. local gridding, stair step gridding, unstructured grids etc.) have been developed to confront these challenges. Unstructured grids (e.g. voronoi grids) are designed to be more flexible such that it mimics realistic representation of reservoir geometry and architecture. A critical review of reservoir grid types and upscaling methods are provided by (Mattax and Dalton, 1990; Christie 1996; Barker and Thibeau 1997; Farmer, 2002). 3-D geological (reservoir) models generated using geostatistical methods typically consist of millions of grid cells. Models of this scale cannot be simulated with reasonable use of computing resources. Consequently, flow simulation models are

made by coarsening the grid and re-sampling properties of the fine scale model (Li, 1995). This as a whole describes upscaling and an illustration displayed in Figure 1.6.

The choice of the upscaling technique for any reservoir simulation study is vital in ensuring that all derived and defined reservoir rock properties (e.g. facies, porosity, permeability and fluid saturations) at the fine grid scale (i.e. geological reservoir model) are reproduced on scale up into the coarse grid (i.e. simulation grid) (Qi and Hesketh, 2004). Often, adopted upscaling techniques are not carefully researched for optimal use. Mansoori et al., 1993, 1994, highlighted the importance of exploiting upscaling techniques that are optimal against the balance of preserving geologic features that characterize fluid flow in the fine grid reservoir model and flow simulation time on the coarse grid. This is a good quality control measure for reducing upscaling errors and inefficiency as part of the reservoir simulation modelling process (Schlumberger reservoir modelling manual, 2011). Contributions from researchers active in the field of upscaling (e.g. Darman et al., 2002; Barker and Dupouy, 1999; He et al., 2002; Durlofsky L. J., 1998; Zijl and Trykozko, 2002; Qi and Hesketh, 2004; Mikeš et al., 2006) described various ways by which geological (reservoir) models should be conceived and possible choices of upscaling them for flow simulation computation. A summary of this makes available a list of requirements to be considered in order for an upscaled reservoir model to accurately represent the fine scale grid reservoir properties. The requirements include the following: (1) the geometry, geology and physical uniqueness of the original model must be described accurately, (2) the mathematically computed solutions of the original model must match the upscaled model so that flow equations are accurate, (3) the governing reservoir fluid mechanics must be reproduced, (4) the saturation and pressure profiles of both the fine geological model and simulation model must be as similar as possible.

1.5.1 Upscaling techniques for reservoir simulation

Over the last two decades, there is vast literature and many techniques for upscaling reservoir geological models for use in fluid flow simulation (Wen and Gomez-Hernandez, 1996; Christie, 1996; Renard and Marsily, 1997) (Table1.2).

A number of these techniques are currently being reviewed due to new ideas that relate to the functionality of existing conventional and traditional upscaling methods (Barker and Thibeau, 1997; Farmer, 2002). In addition, new geostatistical reservoir description algorithms have also helped to instigate new and better upscaling techniques that can find practical use. (Ewing, 1997; Hoosbeek and Bryant, 1992; Renard and De Marsily, 1997, Pickup and Stephen, 2005; Christie and Blunt, 2001; Moulton et al., 1998; King, 1989), are a few of numerous authors pioneering these new ideas in the research field of upscaling. The classifications of the available techniques are quite numerous and proposed by different authors. However, literature has shown that no single classification is unequivocal. A summarized classification of the upscaling methods and upscaling stages associated with reservoir modelling to simulation are shown in (Figure 1.7).

Qi and Hesketh, 2004, described that the sole essence of upscaling as averaging. Averaging methods have continued to find their use in upscaling; the averaging methods constitute aspects of the framework used in building most conventional upscaling techniques. Even though, they are best used to describe circumstances of perfectly layered or perfectly random heterogeneity distribution that actually don't conform to real reservoir descriptions (Li et al., 2001).The widely used averaging methods are the power law average i.e. harmonic, and geometric. There are two main types of averaging upscaling methods based on the upscaling property (i.e. continuous averaging method and discrete averaging method). An overview of the averaging methods and other major types of upscaling techniques for reservoir simulation is presented in Table 1.2 and

Table 1.3. Table 1.3 provides a brief description some of the major numerical upscaling methods and their limitations.

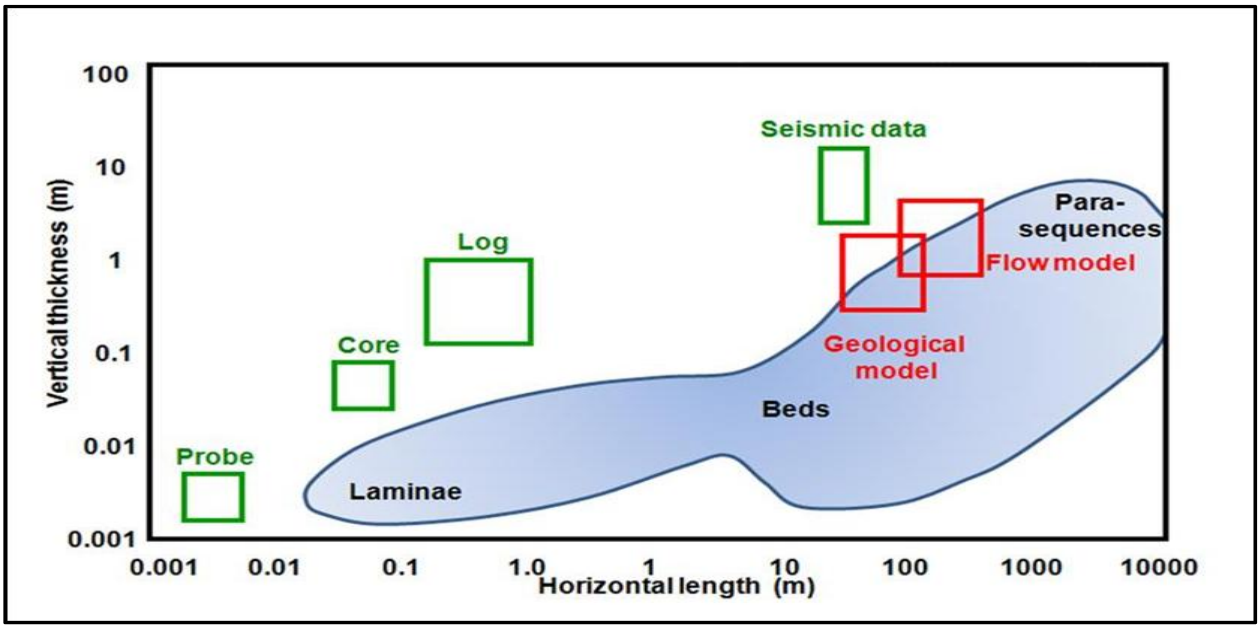

Figure 1.5: Typical reservoir data scale resolution used in reservoir characterization (after Pickup and Hern 2002).

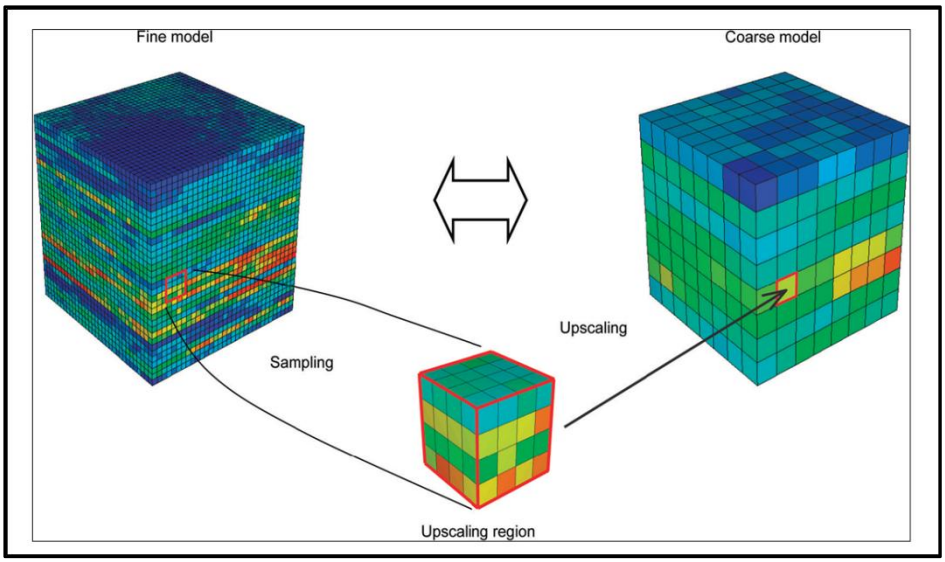

Figure 1.6: Concept of upscaling as it relates to reservoir modelling (modified after Christie, 2001).

[A]

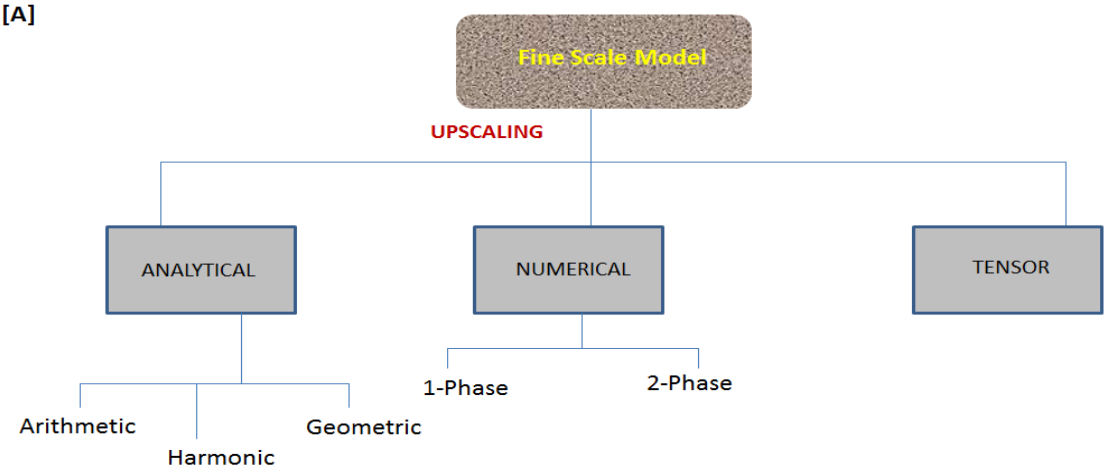

[B]

	Single phase Upscaling	Two Phase Upscaling	Reference
Upscaling Methods	Pressure Solver Method	Pseudofunctions	Christie, 1996
	Renormalization	Pore volume weighted method	Barker and Thibeau (1997) King (1989)
	Stream line Method		
	Power-law average		Warren and Price, (1960)

Figure 1.7: (A): Classification of upscaling techniques (A) modified after Mansoori, (1994) and Li, (1995) and (B), the various types of single phase and two-phase upscaling methods.

Table 1.2 Summarized description of the common averaging upscaling methods with their limitations

Average Upscaling Methods	Governing Equations	Functions	Notes	Limitations	References
Arithmetic (mean)	$K_{arithm} = \frac{\sum_{i=1}^{n} K_i}{n}$	Typically used for additive properties such as porosity, saturation and net-to-gross. Offers the best method for porosity.	The averaging procedures offers the simplest upscaling techniques for computing discrete (i.e. facies) and continuous rock petrophysical grid properties. They do not require any numerical solutions, making them convenient and very efficient computationally.	They tend to smear extreme ends of permeability.	Wen and Gomez-Hernandez, (1996)
Median		This averaging method considers sorting out grid input values and select center value. For example, if there are 7 input values these are sorted by magnitude and the entry number 4 is selected.			Warren and Price, (1961)
Harmonic	$K_{harm} = n\left(\sum_{i=1}^{n} \frac{1}{K_i}\right)^{-1}$	The harmonic mean works well with log normal distributions. It provides exact effective permeability vertically if the reservoir is layered with constant permeability in each layer. Used for permeability because it is sensitive to lower values. The method is not defined for negative values.			Deutsch and Journel, (1998)
Geometric	$P = \sqrt{\frac{\sum_i w_i p_i^2}{\sum_i w_i}}$	Gives the exact effective permeability vertically if the reservoir is layered with constant permeability in each layer. The harmonic mean works well with log normal distributions. It is used for permeability because it is sensitive to lower values. The method is not defined for negative values.			Begg et al., (1989)
Root mean squared (RMS)	$P = \sqrt{\frac{\sum_i w_i p_i^2}{\sum_i w_i}}$	It sets bias towards higher values.			
Midpoint		This samples or picks input values halfway. Random choice and likely to give a property with the same distribution of values as the original.			
Minimum		Samples the minimum values.			
Maximum		Selects the highest value from the original cells that contribute to an upscaled cell.			
Power	$P = \sqrt[x]{\frac{\sum_i w_i p_i^x}{\sum_i w_i}}$	This method generalizes several of the above methods by accepting an exponent parameter. The method has relative biases toward higher or lower values, i.e. generally, minimum < harmonic < geometric < arithmetic < RMS < maximum.			

Table 1.3 Summarised description of numerical upscaling methods and their limitations

Upscaling methods	Governing Equations	Functions	Limitations	Reference
Pressure solver	$k_e^x = -\mu \nabla x Q/A$	It offers a standard way to estimate effective permeability of a grid block	Results depend on assumed boundary conditions. It is time consuming when used for large grids. Usable for cases of simple heterogeneity and anisotropy	Christie, (1996) King and McDonald, (1997)
Renormalization		Highly applicable for multiphase upscaling	It offers systematic errors that tend to be greater when there is a larger anisotropy present	Qi and Hesketh, (2004)
Tensor		Its effective use considers utilizing tensors on pressure solvers. Consequently, calculating accurate tensor effective permeabilities. Based on solving a second-order elliptic differential equation describing single phase, incompressible, steady-state fluid flow in a region without sources and sinks (i.e. wells). The process provides I, J, and K or X, Y, and Z permeabilities from input as permeability in I, J and K directions.	It cannot be directly entered into a commercial reservoir simulator. It is currently been developed for practical use.	Cristie, (1996) Qi and Hesketh, (2004)

1.6 Uncertainty analysis in three-dimensional reservoir characterization

In the petroleum industry, uncertainty is a common word. It implies less than 100% of being sure about something. However, in reality uncertainty is not an inherent character of petroleum reservoirs. The uncertainty arises due to inadequate geological knowledge and understanding of the reservoir, thereby, resulting to uncertainty been modelled or analysed. Uncertainty analysis therefore, describes the process of investigating the combined uncertainties for all uncertain parameters. This assumes that all the key uncertainty parameters are independent of each other (Schlumberger reservoir modelling manual, 2011).

Trusting production forecast capabilities of a 3-D realistic reservoir model for optimum decisions and critical investment require characterizing and quantifying all associated uncertainties (Singh et al., 2013). Examples of associated uncertainties includes reservoir raw data analysis, interpretation, reservoir structure mapping, stratigraphy, facies and petrophysical modelling, transmissibility calculations, upscaling procedure and flow simulation inherent in the 3-D static and dynamic model. Considering the wide uncertainty range associated with 3-D reservoir modelling, uncertainty management workflows are designed. Majority of these uncertainty management workflow tools are benchmarked on satisfying the following requirement: (1) Spot and filter out relevant elements of uncertainty, (2) Ability to evaluate a wide range of uncertainties; which includes ability to capture, quantify and store different multiple scenarios of geological models in a consistent integrated framework, so as to quantify their cumulative impact. This study proposes to perform uncertainty analysis in the three defined phase of reservoir characterization and modelling construction process and rank uncertainties based on their highest cumulative impact to lowest.

1.7 Aims and Objectives

1.7.1 Justification of study

In the Bredasdorp Basin, the significance of developing working geological models towards the development and prediction of present and future reservoirs has long been recognised, particularly following oil discoveries within post-rift sediments (i.e. 9A to 14A sequences). As a result, numerous models have been proposed, but little has been done in the western section of the basin to combine all available data and current geological knowledge in compiling a working 3-D geological (reservoir) model within selected reservoir sands (i.e. between 9A and 14A sequences) for improved fluid-flow characterisation (Davies, 1997a; Roux 2007; Petroleum Agency SA Brochure, 2008).

Based on the reservoir characterization scheme proposed for this study, the working model upon creation would provide the following benefits: (1) provide more insights on the geological complexity associated with the reservoirs sands within the 9A and 14A sequences, (2) provide a 3-D depositional lithofacies model of reservoir sands that is lacking, (3) identify at reservoir scale geological elements that constitute the yet undefined petroleum system, (4) deliver substantial information on true prediction of reservoir performance and associated uncertainties. It must be recalled that within an active exploration and /or appraisal program such as existing in the Bredasdorp Basin, availability of new data (seismic and geological), new ideas/concepts and technological advancements must be assimilated into redefining prevailing geological knowledge. This will result in the creation of models that can be maintained for effective exploration, appraisal and development programs.

1.7.2 Goals

Considering an extension of existing knowledge in the study area, the underlying goal is to integrate existing upscaling and geological reservoir modelling techniques together with fluid-flow simulation procedures to better characterize identified reservoir units for optimum oil recovery predictions. To this end, the study goals are fourfold.

The first is to present a better understanding of the internal 3-D architecture of the reservoir sands within the 9A and 14A sequences of the slope to shallow marine play in the Western Bredasdorp Basin. The second is to calculate numerically the connected fluid-flow behaviour of the identified sandstone reservoirs, the average porosity and effective permeability. This is considered in effect to be the dominant control on the transition between reservoir facies (hydrocarbon–bearing) and non-reservoir facies (non-hydrocarbon bearing) (King et al., 2001). The third is to compare upscaling techniques and determine which provides useful estimates of reservoir properties of identified reservoir units. In addition, suggest explanations or answers on challenges involved in upscaling a geological model (10^8 cells) to a fluid-flow model (10^5 cells). The last objective is to seek the effect of sedimentary architecture on two phase fluid flow performance. Consequently, a broad range of reservoir modelling techniques that includes qualitative facies analysis, petrophysical analysis, upscaling, and flow simulation computations are employed to effectively explore reservoir rock properties and fluid-flow characteristics. In addition, associated geological uncertainties are accessed based on available data, modelling input parameters, and selected reservoir modelling techniques and approach.

All available reservoir data (i.e. geological and geophysical) which includes 2D seismic, petrophysical wire-line logs and core data are honoured extensively to construct a 3-D geological reservoir model and appropriately upscaled for flow simulation. The whole

process of constructing a flow simulation model using real field data (i.e. in the Bredasdorp Basin) strategically aims at:

- Presenting a robust 3-D internal facies architecture which includes hydraulic elements of the identified sandstone reservoir units in the study area.
- Establishing a reservoir modelling workflow that effectively integrates an upscaling procedure that captures heterogeneity from the rock record to flow simulation using all available conventional data and resources.
- Understanding sedimentary controls on porosity, permeability and fluid saturation as well as understanding the vertical and horizontal heterogeneity within selected reservoir intervals.
- Testing sensitivities of static (i.e. facies geometry) and dynamic (relative permeability) properties as it relates to production.
- Establishing a relative permeability curve for field applications in the Bredasdorp Basin
- Making recommendations on the location of appraisal wells where necessary.
- Creating production profiles.

Based on the stated research aims the following research questions are underlying:

- What is the depositional control on reservoir facies characteristics?
- What is the poro-perm relationship?
- What are the main controlling factors of gas/oil production?
- What is the impact of multi-scale facies variations on two phase fluid-flow?

CHAPTER 2

METHODOLOGY

2.1 Introduction

This chapter presents the geological characterization and modelling techniques adopted to construct the 3-D geological (reservoir) model, approach and aspects weighed in preparing the model, and the modelling workflow. The chapter also includes figures introducing the different aspects/workflows associated with constructing the facies and petrophysical models, upscaling the reservoir geological model and finally the flow simulation model. As a whole, this describes the stepwise process used to meet most of the aforementioned objectives of this study. The methodology adopted takes into account the assimilation of true geological knowledge in the creation of the geological (reservoir) model by comparing, integrating, constraining all available disparate data, interpretations and performing prudent adjustments to each provided input. All reservoir data available for this study are presented in APPENDIX A.

2.2 Modelling Methodology

2.2.1 Approach

In view of a range of approaches and frameworks available for modelling petroleum reservoirs for fluid-flow behaviour and prediction, Weber and van Geuns (1990), proposed an engineering solution. This solution considers characterization that allows most petroleum reservoirs to be classified appropriately from the viewpoint of the required modelling approach. Mijnssen (1991) and Mikeš et al., (2006), suggested the approach of creating a "standard facies model", which includes all facies, their spatial distribution, shape, flow boundaries and bedding types as template for reservoir models so as to incorporate all

heterogeneity levels and ensure accurate prediction of reservoir fluid flow. The above stated proposals simply describes: (1) identification and definition of petroleum reservoirs into three basic geometrical build-up types (i.e. layer cake, jigsaw-puzzle, and labyrinth) employing prevailing facies distribution of possible known depositional environment (2) extensions of this simple system reservoir-type definitions into covering and reflecting geometrical build-up of facies as it relates to bedding type and characterizing hydrodynamic or flow units. The essence of these proposals is the disregard of routine homogenization of the reservoir model for better ground truth characterization.

The modelling approach adopted exploits an integrated modelling workflow that comprise of geological techniques that aid in successively characterizing multi-scale geological features for reliable reservoir fluid flow prediction within the consideration of available resources. The approach employs a hierarchical object and a sequential gaussian simulation based procedure, powered by a data driven conceptual geological model and delivers a 3-D flow simulation model in PETREL^{TM}. The PETREL^{TM} reservoir software application is selected as it offers an integrated modelling workflow environment permitting a number of flexible geological reservoir modelling and simulation procedures. It offers a list of capabilities for this study: i.e. 3-D visualization, 3-D mapping, 2D seismic interpretation, well log correlation, 3-D grid design for the geological model, depth conversion, seismic well tie, velocity modelling, upscaling of reservoir structure/rock properties, map plotting, and finally simulation (i.e. using the Eclipse black oil simulator platform).

2.3 Geological and reservoir flow simulation modelling

A reservoir characterization and modelling workflow is developed for two modelling stages (static and dynamic). The static modelling stage is defined primarily by the geological modelling of reservoir facies within mapped stratigraphic zones based on successive workflows that consist of arranged nested steps (i.e. identification of potential reservoir unit, establishment of reservoir stratigraphic framework, erection of a 2D conceptual sedimentological model, modelling of depofacies units and corresponding petrophysical properties and lastly upscaling of reservoir geological model), whereas, the dynamic modelling stage is defined by the numerical flow simulation of the selected 3-D upscaled model. Figures 2.1 and 2.2 present a typical shared earth modelling construction workflow in PETREL, showing its relation to reservoir geological modelling and simulation.

2.3.1 Description of each step of the Work Flow

The workflow as configured in PETREL together with the methodology scheme is presented in Figures 2.3 and 2.4 respectively. The figures show several nested steps pull together with each step having its own detailed workflow. Details of these are discussed in Table 2.1 in a manner that shows an organized progression of steps alongside selected reservoir characterization methods as appropriate.

All applicable reservoir data needed to carry out each stage involved in this study are organized and configured into a database. The preparation is tailored towards enhancing the process of reservoir data handling and analysis for this study. In parts, it involves storing, organization, geostatistical analysis, validation, and modelling of reservoir data. Full details of data preparation and quality checking are presented in APPENDIX B.

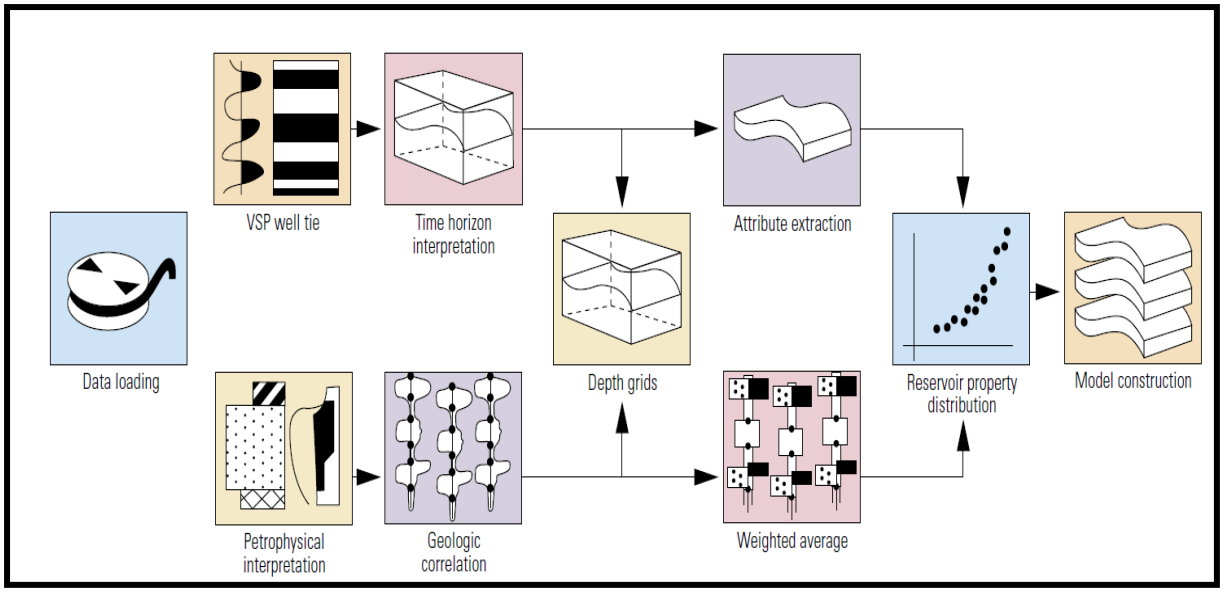

Figure 2.1: A typical and flexible geological reservoir modelling construction workflow in PETREL seismic-to-simulation software, modified as appropriate for use in the modelling stage for this study (Schlumberger Oil field review, 2008)

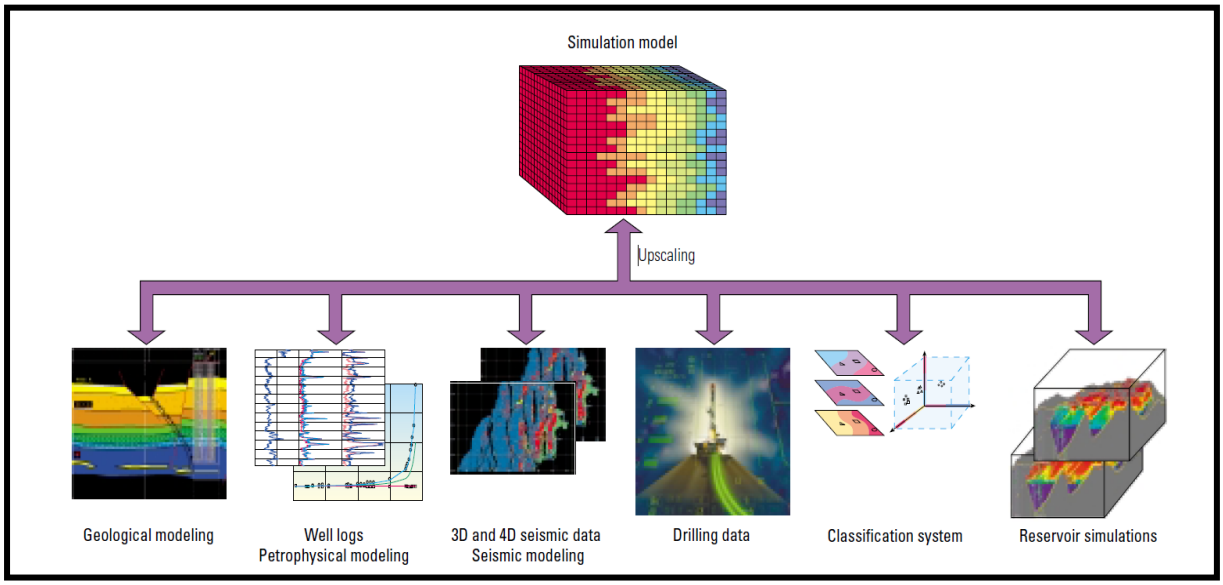

Figure 2.2: Shared earth model (i.e., digital numerical representation of the subsurface comprising key input elements housed in a database and shared amongst exploration and production asset team members for use in petroleum reservoir simulation (Schlumberger Oil field review, 2008).

Table 2.1: Description of each step characterizing the methodology scheme designed for this study.

Sedimentological analysis- cores and logs   In carrying out detailed sedimentological descriptions of the three cored wells, log and core analysis have been relied on to provide vital ground truth information, hence delineation of reservoir units. Sedimentological core descriptions of the selected wells are carried out and it involved physical examination of cores followed by digitisation of observations into sedimentary logs and finally, the interpretation of lithofacies and corresponding association (APPENDIX C). The definition of a characteristic suite of well log responses for each facies association is performed, and then subsequently used for the interpretation of a facies log throughout the studied interval of the selected wells. Various characteristics of selected well logs and their basic interpretation goals are shown in APPENDIX D.
Petrophysics and depositional lithofacies-well log correlation   The primary goal of this phase is the generation of interpreted petrophysical logs in the selected cored wells using qualitative and quantitative methods. The first step carried out in the log analysis process is the identification and selection of reservoir units of interest within established stratigraphic markers (9A to 14A) based on the definition of clean and shale baselines on GR logs complemented with SP and porosity logs of the selected wells (E-AH1, E-L1, and E-BD2). Using the facies association scheme created, cored intervals are split and grouped into facies successions between marked top and bottom depths. The second step, involved generating log facies, corresponding log derived petrophysical properties (porosity, permeability, and fluid saturations) in the studied log interval of selected cored wells. Based on this flow units are obtained within the studied inter-well volume of each well. Cut-offs of volume of shale (V_{sh}), porosity, water saturation and permeability are used to estimate net pay, in addition, various petrophysical cross plots (e.g. Hingle, SML and Pickett plots) are integrated and used for cut-off definition for determining other rock petrophysical properties (i.e. water saturation). Derived vertical facies successions are used to define, group and correlate depositional sequences throughout the modelled area. Finally, quality checking of the log-core analysis process is performed by core to log calibration. Core sample data depths are depth shifted as appropriate to true log depth, while core derived fluid properties are plotted and overlaid against plots of log derived rock fluid properties of each well (E-AH1, E-L1, and E-BD2) to confirm excellent match. Data derived from special and routine core analysis is shown in (APPENDIX E).
Stratigraphic framework analysis – Seismic interpretation   Stratigraphic correlation between the studied inter-well volume of the cored wells (E-L1, E-AH1 and E-BD2) is considered the objective of this phase. Seismic interpretation takes a central role in achieving this objective.   Seismic interpretation involves the extraction of subsurface geologic information from seismic data while seismic stratigraphy is a technique to interpret stratigraphic information from seismic data (AAPG Explorer Hand book, 2013). For this study, correlating the derived vertical reservoir facies successions within mapped stratigraphic log reservoir units is crucial to determining reservoir geometry. Based on the log correlated reservoir unit tops and bottom depths, stratigraphic horizon interpretations are carried out on the seventeen 2D seismic reflection profiles cutting across the model boundary area. Well markers are matched against seismic reflection events observed on seismic sections. These observations are transferred and made consistent in selecting reflections events, taking into account seismic amplitude and continuity of reflections, especially in areas that lack well control. Continuous velocity logs of the selected wells are used to obtain vertical travel times in milliseconds and vertical depth on calibration with seismic data, allowing for seismic to well log tie. To these ends, five stratigraphic horizons, R1, R2, R3, R4, and R5 within the inter-well volume of the selected wells are mapped, hence, four stratigraphic reservoir unit intervals. The depth/ thickness of these horizons are converted using a time-depth relation curve based on travel time data of horizons and well survey information (check shot and vertical seismic profile VSP). Besides, synthetic seismograms are also generated by convolving the reflectivity obtained from acoustic and density logs with extracted representative wavelet from seismic within and outside the defined reservoir intervals. This is carried out to compare correlation markers picked on well logs with major reflections on the selected seismic profiles. The quality–checking workflow designed to enhance the modelling stage is presented in Figure 2.3.
Construction of a conceptual sedimentological model   Conceptual sedimentological models have played a significant role in reservoir modelling practice even before the advent of modern computers. The model offers the most detailed image of the geologist understanding of representing a petroleum reservoir (Al-Khalifa et al., 2006). Following the correlation of interpreted vertical facies successions within the inter-well volume of the selected wells and a review of regional geology information, conceptual sedimentological models of the potential reservoirs units are established. For this study, the significance thereof centres on reducing the uncertainties associated with incomplete reservoir information (i.e. rock property data), spatial variability and the inherent heterogeneous nature of reservoir rock properties. The starting point of creating a conceptual geological model is aimed at providing the geologic framework of identified reservoir sandbodies. It considers an integrated and flexible workflow that anchors and exploits the strength of the geological knowledge (i.e. comprising and utilizing both geological rules and geological experience). The geological knowledge evolves from what is known to investigating the unknown. In this instance, it describes knowledge of regional geology, previous studies alongside qualitative interpretation of well log data and cores within the studied stratigraphic interval. The conceptual sedimentological model creation is guided by the integration of following steps: (1) Review of regional geology information and previous reservoir geological modelling studies of the Bredasdorp Basin, (2) Subsurface facies analysis–well log analysis, core description and interpretation and log correlation within the inter-well volume of the identified reservoir units.

Table 2.1: (continuation from page 30)

Definition of the 3-D stratigraphic framework

This phase brings together the integration of seismic horizon interpretation, well to well correlation and stratigraphic modelling. The essence of the 3-D grid construction is to build a lattice to be used as a base for the 3-D cell generation. The simple make grid process is selected in PETREL; thou often used as a suitable alternative to model non-faulted reservoirs and simulation grids. The first step in constructing the 3-D grid block involves defining the orthogonal 3-D grid cells dimension along X, Y and Z directions. An optimal (25m X 25m X 20 layers) grid cell size is chosen to capture vertical and lateral heterogeneity as well incorporate the well spacing pattern. At this level, all interpreted seismic horizons and corresponding generated surfaces (R1, R2, R3, R4, and R5) are inserted and organized in stratigraphic order into the make grid panel. This is performed to initiate the creation of the 3-D stratigraphic grid frame work. However, each stratigraphic grid based on the defined modelling zones/flow units is divided uniformly so as to incorporate minimum observed thickness of facies in each layer within identified sequences at the selected wells.

Generation of 3-D facies and petrophysical models- stochastic property modelling

Stochastic property modelling involves the use of stochastic simulation in interpolating between data measurements (usually wells) in generating multiple equiprobable realizations of a reservoir or field (Schlumberger Oilfield Glossary). Considering the lack of a complete representative reservoir data together with the natural variability associated with reservoir rock properties and the need to quantify uncertainties, stochastic modelling proves invaluable. A number of different stochastic reservoir modelling methods exist; however, cross-fertilization between the methods is common and generating promising outcomes (Farmer, 1988, Dubrule, 1989; Haldorsen and Damsleth, 1990). The 3-D stochastic modelling scheme adopted for this study make use of both the hierarchical object and truncated gaussian simulation (TGS) methods as an efficient means to simulate the interpreted depositional lithofacies (e.g. channel fills, overbank/inter-channel deposit, delta-front and mouth bar sandbodies) based on the established 2D conceptual sedimentological model of defined reservoir units. Afterwards, the sequential gaussian simulation method (SGS) is selected to model continuous petrophysical properties (i.e. porosity, permeability and fluid saturations), by constraining and conditioning existing 3-D facies models of the selected reservoir unit intervals. The (SGS) is a technique that is robust and applicable in generating realizations of continuous variables. The realizations are conditioned to honour well data input distributions, histogram computation, areal and vertical trends and patterns of spatial correlation (variogram) defined using the reservoir data analysis tools in PETREL.

The sequential indicator simulation (SIS) and (SGS) methods both use the same basic algorithm in generating multiple equiprobable realizations of a property, rather than simply estimating the mean. The essence simply, is that it adds some variability to undo the smoothing effect that can occur when simply estimating the mean using the kriging algorithm. This often gives a superior representation of the inherent variability of the simulated property. The (SIS) makes use of indicator kriging while, the (SGS) operates on the simple kriging algorithm. The simple kriging algorithm relies on a random variable (data) under the condition of a normal (Gaussian) distribution. The hierarchical object facies modelling carried out in (PETREL) starts with the population of discrete facies model with defined bodies having different geometries, facies codes and fractions. To this end, a large scale facies model is defined and an additional smaller scale facies model is generated to model local variations within the larger scale facies model. The hierarchical object modelling algorithm is conditioned to well information from separate discrete well logs of selected wells describing facies at each of these scales; source points, aerial distribution and vertical distribution. Equally, the sequential indicator simulation is used to stochastically distribute defined lithofacies property using a pre-defined histogram. Directional settings such as variogram and extensional trends are honoured, allowing a stochastic distribution of facies based on a given transition between facies and trend direction defined within the inter-well volume of the selected reservoir unit intervals. A major interdependent process in (PETREL) is followed in order to generate the 3-D facies and petrophysical models of the selected reservoir sandbodies. It is called well log upscaling or blocking of well logs. Well log upscaling is carried out as a requirement prior to the population of the 3-D grid. It involves assigning log property values both discrete and continuous (facies and log derived petrophysical values) to the grid cells penetrated by the selected wells.

Transfer of geological reservoir model to fluid flow simulator-Upscaling

This step involved the upscaling of selected 3-D geological reservoir model for fluid flow simulator computations. The upscaling process adopted for this study is discussed more extensively in Chapter 5.

Numerical flow simulation modelling (dynamic)

The main objective here is to determine the fluid-flow behaviour of the selected reservoir units/interval by performing numerical simulation upon calibration of upscaled fluid model to dynamic data. Numerical flow simulation involves the mathematical modelling of fluid flow so as to obtain accurate numerical solutions of the reservoir data input alongside providing the basis for reservoir performance predictions. The following pre and post processing simulation procedures are carried out successively in PETREL and ECLIPSE black oil simulator in order to execute reservoir fluid flow behaviour simulations; fluid model parameter assigning (i.e. derivation of rock physics and saturation functions), definitions of development strategies and simulation case scenarios. Upon final configuration of the simulation model, runs are submitted into ECLIPSE black oil simulator based on the defined development strategies and simulation case scenarios. Simulation output results are displayed and analysed.

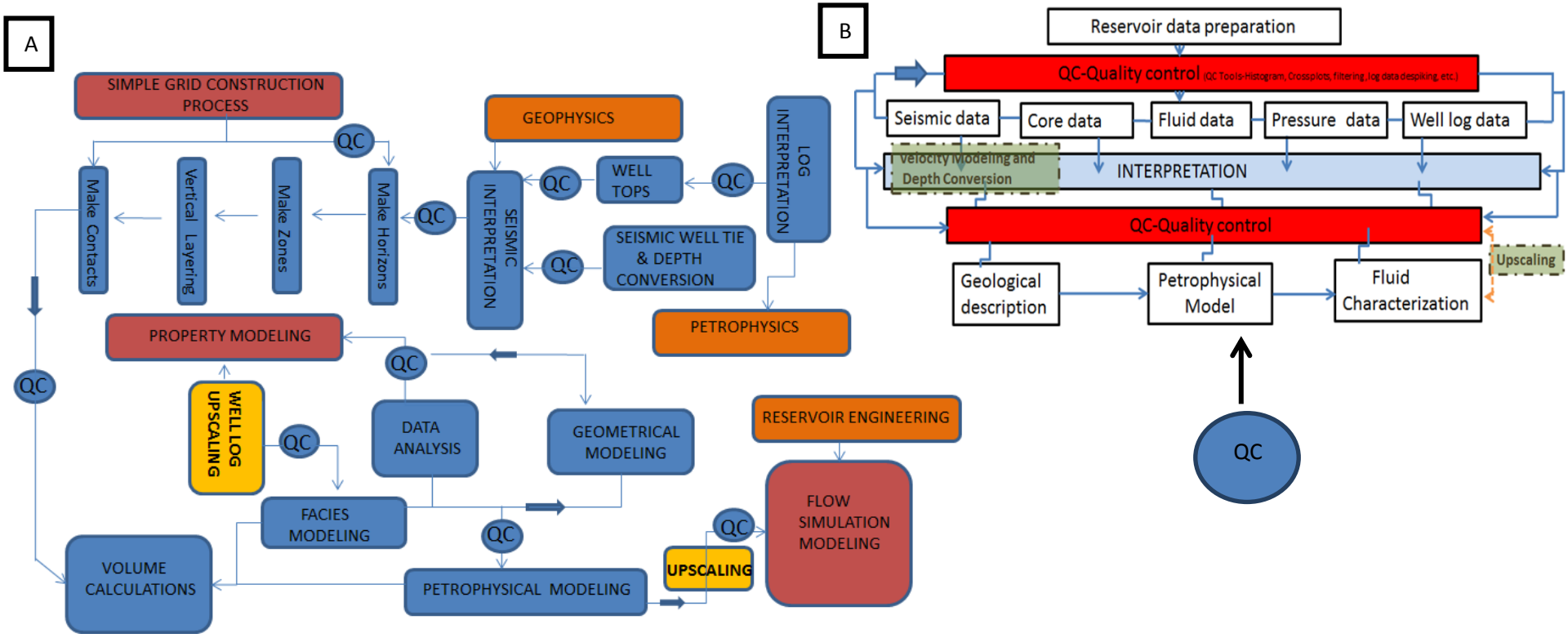

Figure 2.3: Multi-disciplinary modelling workflow created in PETREL for this study. The workflow is aimed at effectively preserving the observed rock record through each step in the modelling process for true fluid flow prediction. On the right hand (fig B) is the schematic workflow created for reservoir data preparation as it applies to quality checking of the modelling process.

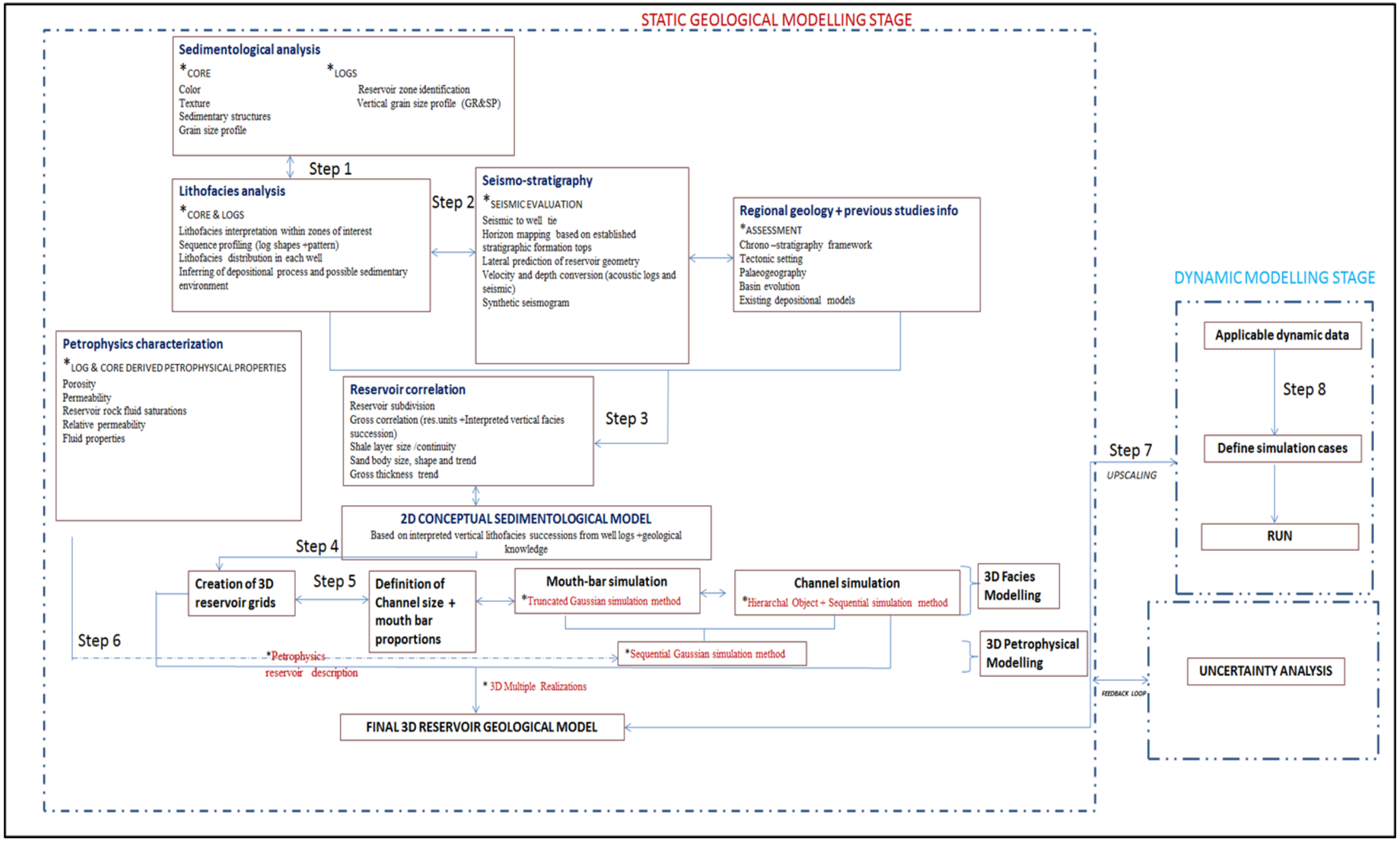

Figure 2.4 Methodology scheme for geological to flow simulation modelling for this study.

CHAPTER 3

GEOLOGY OF THE BREDASDORP SUB-BASIN

3.1 Introduction

The South African offshore environment parades a coastline of nearly 3000km and a continental margin which comprises a continental shelf of approximately 165,000km^2 down to the 200m isobath and closely 400,000km^2 out to the 2000m isobaths (Broad et al., 2006). The Southern African offshore environment has three distinct tectonostratigraphic zones based on the basins therein: western, southern and eastern offshore (Petroleum Agency SA Brochure, 2008). The southern offshore region referred as the Outeniqua Basin comprises of a series of en-echelon sub-basins (i.e. Bredasdorp, Pletmos, and Gamtoos and Algoa basins) (Du Toit, 1976; Dingle et al., 1983) (Fig 1.1). These basins arbitrarily extend to the 200-metre isobath demonstrating a history of strong strike-slip fault movement during the Late Jurassic-Early Cretaceous plate margin shearing and separation of Goodwin (Broad et al., 2006). The rifting that appears to have been initiated by these occurrences resulted in a series of complex oblique rift half graben structures overlain with drift sediments bounded by rocks of the Ordovician-Devonian Cape Supergroup, forming prominent arches structures between in each of these basins (McMillan et al., 1990; Broad et al., 2006).

3.2 Regional geological setting

3.2.1 The structural configuration and development of the Bredasdorp Basin

The aftermath of a major break–up and separation of the West Godwana supercontinent into the African and South American plates initiated and led to the existence of the South Africa continental margins which further orchestrated process that initiated the formation of the Outeniqua Basin (McMillan et al., 1990) (Figures 3.1A and 3.1B). In the west and southwest

of the Bredasdorp Basin are the Agulhas Arch and the Northeast the Infanta Arch respectively (Fig 1.1). The Bredasdorp Basin opens south-eastwards connecting with the Southern Outeniqua Basin, terminated on the southeast by the Agulhas-Falkland Fracture Zone (AFFZ) (Fig 1.1). Broad et al., 2006, highlighted that major processes which includes extensional forces, rifting, continental-separation and drifting constructed South Africa's continental margin, in addition to, the break–up and drifting that occurred in the Early Mesozoic and Early Cretaceous respectively. Further down southeast of the basin is the 1200km long ridge to ridge offset, Agulhas–Falkland Fracture Zone (AFFZ) a major structural feature that overlooks the Bredasdorp Basin (Fig 1.1). It spans through the southern and eastern plate margin of South Africa and originated due to the dextral (right-lateral) strike slip movement of the African and South American continental plates as they slid past each other, preceded by drifting of the Falkland plateau from the African plate (Ben-Avraham et al., 1997; Broad et al., 2006) (Fig 1.1). However, a number of these various dynamic processes led to the formation of the South Africa offshore rift sub-basins. Specifically, the commencement of strike slip movement of the (AFFZ) in Early Cretaceous at the start of drifting resulted in truncation of the pre-existing rift basins structural trends (i.e. Outeniqua-Bredasdorp, Pletmos, and Gamtoos and Algoa basins). The latter developed structures were termed failed rifts, due to the reasoning that they could have opened up and developed into mid–oceanic spreading centres. In the event of this, marine conditions prevailed and the deposition of Upper Jurassic and Lower Cretaceous synrift continental and marine strata alongside post rift Cretaceous and Cenozoic divergent margin rocks commenced across the basin. Among the four major depocenters that constitutes the Outeniqua Basin and the Bredasdorp show less developed typical faults with sediments deposited mostly in the non-marine and marginal environments which resulted to widespread advancement of red and green clay-stones overlain by clean, porous glauconitic littoral sandstones. The Outeniqua

Basin is composed primarily mid-Aptian to Maastrichtian deposits which spread over pre-existing rift basins showing transverse structural gain. The rift period that characterized the south coast terminated in the lower Valanginian, showing much association with the drift–onset unconformity (1At1). However, visible from seismic sections that cut across the basin are widespread normal faults and complex horst and graben structures (McMillan et al., 1990). In addition, (Dingle et al., 1983; Jungslager, 1999) identified three major stages of drift history recorded with the paleogeography of the Bredasdorp and related by:

1. An initial post rift basin, which exhibited several all embayment's that closely conformed to the residual synrift sub-basins (super cycle 1-5, 126-117.5 Ma).
2. An enlarged basin that flooded and integrated the initial post rift embayment with connections with to the Proto-Indian Ocean (super cycles 6-12, 117.5-112 Ma).
3. An expanding basin with increasing connection to the early Atlantic Ocean (super cycles 13, 14, 15-16 and 17-20, 112-68 Ma), defines a pre-rift geology and post-rift geology describing basin paleogeography in response to varying tectonic events. The duration of the rift episode saw the supply of clastic sediments into residual synrift sub basin that shaped out an enlarged post rift basin with several embayment's that connects to the Proto Indian Ocean. A series of these isolated embayments join both the Southern Outeniqua Basin and Early Indian Ocean via a narrow passage in a south-easterly direction Clifton (1981).

3.3 Local geological setting

3.3.1 Stratigraphy of the Western Bredasdorp Basin

In the Western section of the Bredasdorp Basin two episodes of sedimentation is associated with the stratigraphy of the basin, the synrift and the drift. Synrift and drift episodes clearly defined active rift tectonics and sedimentation associated with the early period of continental break-up and a post-rift phase involving thermal subsidence respectively (Dingle et al., 1983; Broad et al., 2006). However, geologic and geophysical evidences both show that the synrift and drift events are less distinct in the Western Bredasdorp Basin when compared to Orange Basin for instance (Petroleum Agency SA Brochure, 2008).

Synrift and Drift successions

Investigating the synrift episode controlled by active boundary faults in the Bredasdorp sub-basin, Jungslager (1999) identified two phases of synrift sedimentation i.e., synrift I and synrift II successions. A summary of the subdivisions associated with each of the synrift phases and drift episodes is presented in Tables 3.1 and 3.2 respectively. The splitting up of the synrift and drift successions into unconformity-bounded sedimentary sequences exploited the use of lithogenetic facies analysis and sequence stratigraphy principles, and in effect, adopted the sequence naming convention of Brown et al, (1995). A schematic cross section across the Bredasdorp Basin is presented (Figure 3.2).

Table 3.1: Summarised descriptions of synrift I and II successions (Petroleum Agency SA Brochure, 2008).

Synrift I Succession (Jurassic- Hauterivian)	Synrift II Succession Hauterivian
Lower fluvial interval: represents initial graben fill made up of clay stones, sandstones and conglomerates deposit in alluvial fans and fluvial environments.	Contain deep-water shales
Lower shallow marine interval: represents the first marine incursion into the basin, made up of glauconitic fossiliferous sandstones symbolizing progradational beach deposit. This interval is poorly developed within the synrift depocenters of the Western Bredasdorp Basin.	
The upper shallow marine interval: this unit is poorly developed and characterized mainly by massive glauconitic fossiliferous sandstones of late Valanginian age deposited as trangressive beach facies along the north and south flanks of the Bredasdorp Basin.	

Table 3.2: Summarised descriptions of the drift phase episodes (Petroleum Agency SA Brochure, 2008).

Drift Phase	
Hauterivian to Aptian	**TRANSITIONAL (EARLY DRIFT PHASE) (1At1-13At1)** Pro-gradational expansion of shelf in the northern-part over the Arniston Half-graben and a continued deepening of the Southern sub-basin.
Albian to Maastrichtian	**DRIFT PHASE (LATE DRIFT SEQUENCE) (13At1 to present)** This phase describes regional subsidence driven by thermal cooling, sediment loading and continued movement of the Arniston Fault.
Palaeocene to Present day	**UPPER DRIFT PHASE (LATE DRIFT SEQUENCE)** Oil prone source in synrift depocenters as well as Central Bredasdorp Basin entered main stage of oil generation. Continued minor subsidence disrupted by Early Tertiary alkaline intrusion activity over the central high. Late tilting of the Bredasdorp Basin combined with uplift of the northern flank resulted in late erosion of up to 600m in places.

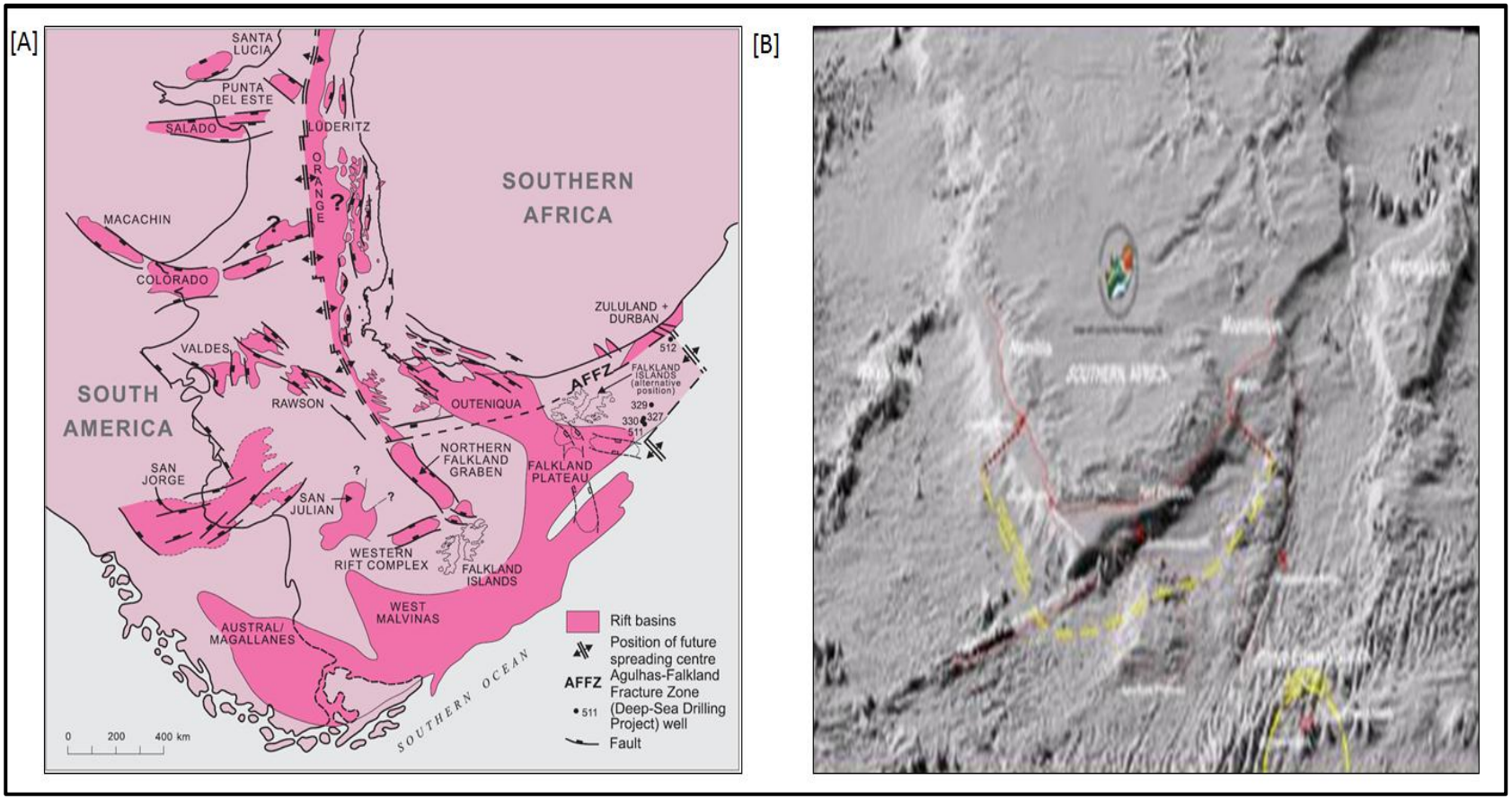

Figure 3.1: [A]-Plate tectonic reconstruction within southwest Gondwana, showing the likely breakup configuration of Late-Jurassic to Early Cretaceous rift basins (After Jungslager, 1999). [B]- Satellite altimetry derived image- showing the South African offshore topography with the extent of the sea floor and surrounding continental margin (After Broad, 2006).

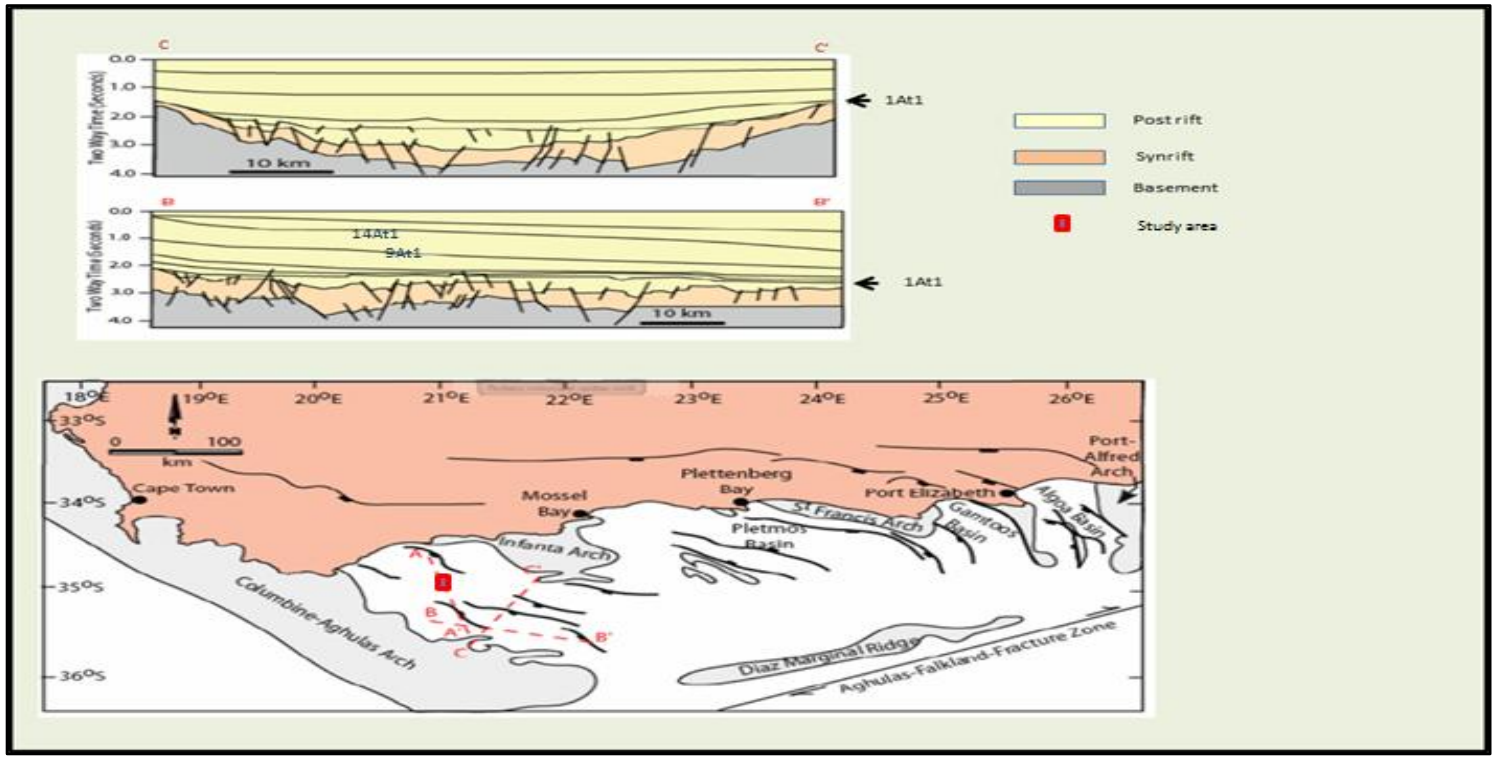

Figure 3.2: Schematic cross sections through the Bredasdorp Basin. Section B-B' and Section C-C' characterize an oblique and strike section of the basin with the extent of the post rift, synrift and basement (After Thomson, 1998). Red rectangular box marks study area.

3.4 Chronostratigraphy framework of the Bredasdorp sub-basin

Chronostratigraphic classification is regarded as the organization of rocks into units in accordance to their age or time of origin as proved as a valuable tool for time correlation and presenting geologic history in lieu of a record of events. In the Bredasdorp sub-basin, age assignments and correlations of the third–order sequences follow the studies of Brown et al. (1995) and the geological time framework adopts the time scale of Haq et al. (1988). Figure 3.3 displays the chronostratigraphic correlation chart.

3.5 Sequences 9At1 to 14At1

3.5.1 Albian and Aptian sandstone reservoir rocks

A reservoir is the rock plus void space contained in a trap while the reservoir rock is generally referred to as a coarse grained rock that possess adequate interconnected pores and permeability to allow oil and gas accumulation. The part of the rock that holds the accumulated oil or gas is termed the petroleum reservoir. Reservoir rocks are most commonly coarse-grained sandstones and carbonates. Exploration and drilling efforts to date in the Bredasdorp Basin has revealed some geological information that describe the presence of potential reservoir rocks containing oil and gas both in the Albian and Aptian sediments of sequence 13At1 and 14At1 (Fig 3.3). According to (Turner, 2000), sandstone reservoirs discovered within 9At1 and 14At1 sequences were recognized as deep marine in origin. The majority of sandstone reservoir rocks are characterized by a range of stacked and amalgamated channels and lobes considered to have derived from materials eroded from pre-existing high stand and shelf stand sandstones later transported to the central part of the basin by turbidity currents. The occurrences of numerous channelized reservoirs in the western section and south-western sections of the basin have emerged due to their proximity to the

base of the slope relative to the eastern area where fan lobes predominate (Petroleum Agency SA Brochure, 2008).

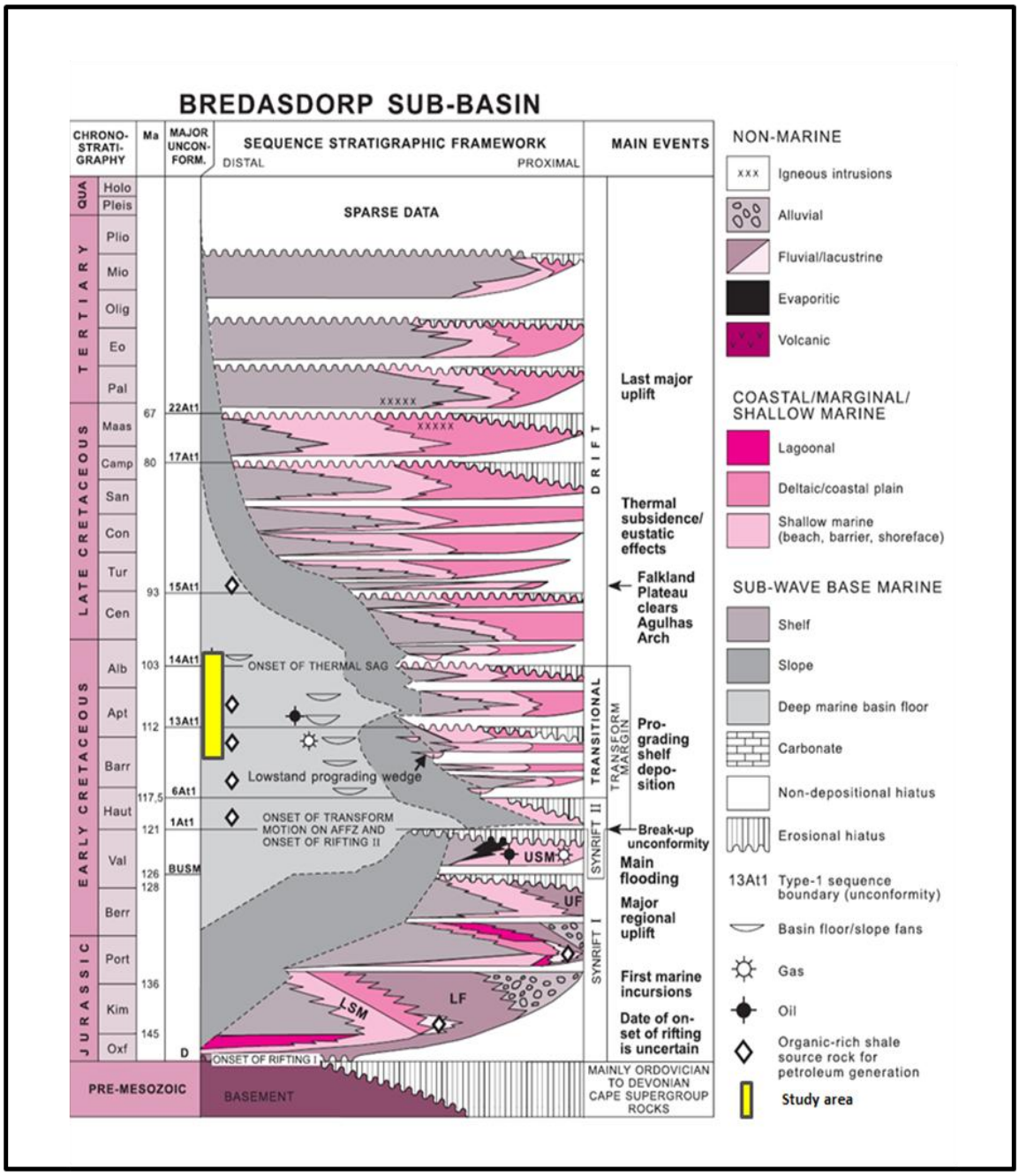

Fig 3.3: Generalized stratigraphic chart of the Bredasdorp Basin (After, Brown et al., 1996; Soekor 1994a, b). USM=upper shallow marine; UF= upper fluvial; LSM=lower shallow marine; LF= lower fluvial; BUSM=unconformity at base of upper shallow marine; Ma- age in millions of years using the time scale of Haq et al., 1988.

SECTION 2

CHAPTER FOUR

GEOLOGICAL MODELLING

4.1 Subsurface facies analysis

4.1.1 Reservoir definition

In selecting potential reservoir units of interest in the study area, a detailed study of stratigraphic sequence boundary interval (9A and 14A) in each selected well is performed. This result to the marking out of reservoir-sand sections from non-reservoir-shale sections based on log shape pattern analysis of (GR, SP and porosity logs), sediment stacking pattern, vertical facies succession, maximum grain size data, net to gross estimation and lithofacies correlation. In this instance, gamma ray values greater than 80 API and GR value equal or less than 30 API and less than 75 API are defined as non-reservoir rock-shale and reservoir rock-sand respectively (Dewan, 1983). A brief description of how gamma ray logs are used to define and quantify productive intervals is presented in APPENDIX D.

To this end, five lithofacies alongside four potential reservoir unit intervals are defined: lithofacies 1-clean sand, lithofacies 2-shaly sand, lithofacies 3-sandy-silt, lithofacies 4-shale and WBRED-A, WBRED-B, WBRED-C and WBRED-D respectively (Figs 4.1, 4.2, 4.3 and 4.4)

4.1.1.1 Log description: Well E-L1

The vertical grain size profile of well E-L1 based on gamma ray log is presented within the depth range of (1679-2500m) (Fig 4.1). Based on available data, the established stratigraphic formation tops in this well are (9At1, 13At1, 13Amfs and 14At1).

Facies description: A gradual transition of lithofacies 4 to 1 is evident and associated in 73-75m thick coarsening-upward successions characterized by substantial increase in net to gross (within log interval of 2220-2334m) (Fig 4.1). Also, from top to bottom of the studied interval six clean reservoir sand units with an average thickness of 44m each are measured. In the upper one third of the studied section (from 2220-2588m) there is an abrupt base fining-upwards blocky shaped gamma ray response followed by upward-coarsening successions, this is seen within log interval of (2558-2347m) the trend of fining-upward successions followed by coarsening-upward successions of low gamma ray values 67m below the 13Amfs stratigraphic marker (Fig 4.1). However, looking at the entire studied log section, 1700 to 2000m, lithofacies 4 to 1 form two coarsening–upward successions underlying a clean trend zone of shale into a cleaner sandy facies interbedded with silty sandstones.

4.1.1.2 Log description: Well E-AH1

The vertical facies interpretation and grain size profile of well E-AH1 based on gamma ray log is presented within the depth range of (1583-2784m) (Fig 4.2). Established stratigraphic formation tops (sequence boundary) in this well are (9At1 and 13At1, 14At1).

Facies description: Within (2009 to 2159m), a 150m thick coarsening upward succession is evident, corresponding with the upward transition from lithofacies 4 to 1 (shale to clean sand). Above the 2009m log depth, there is a gradual transition of lithofacies from shale to sandy-silt then shaly-sand and finally clean sand. A total of 344m of clean sandstone reservoirs interbedded with silt and shale are measured representing 28% of the studied log interval. The most prominent lithofacies are shale, representing approximately 44% of the studied log interval.

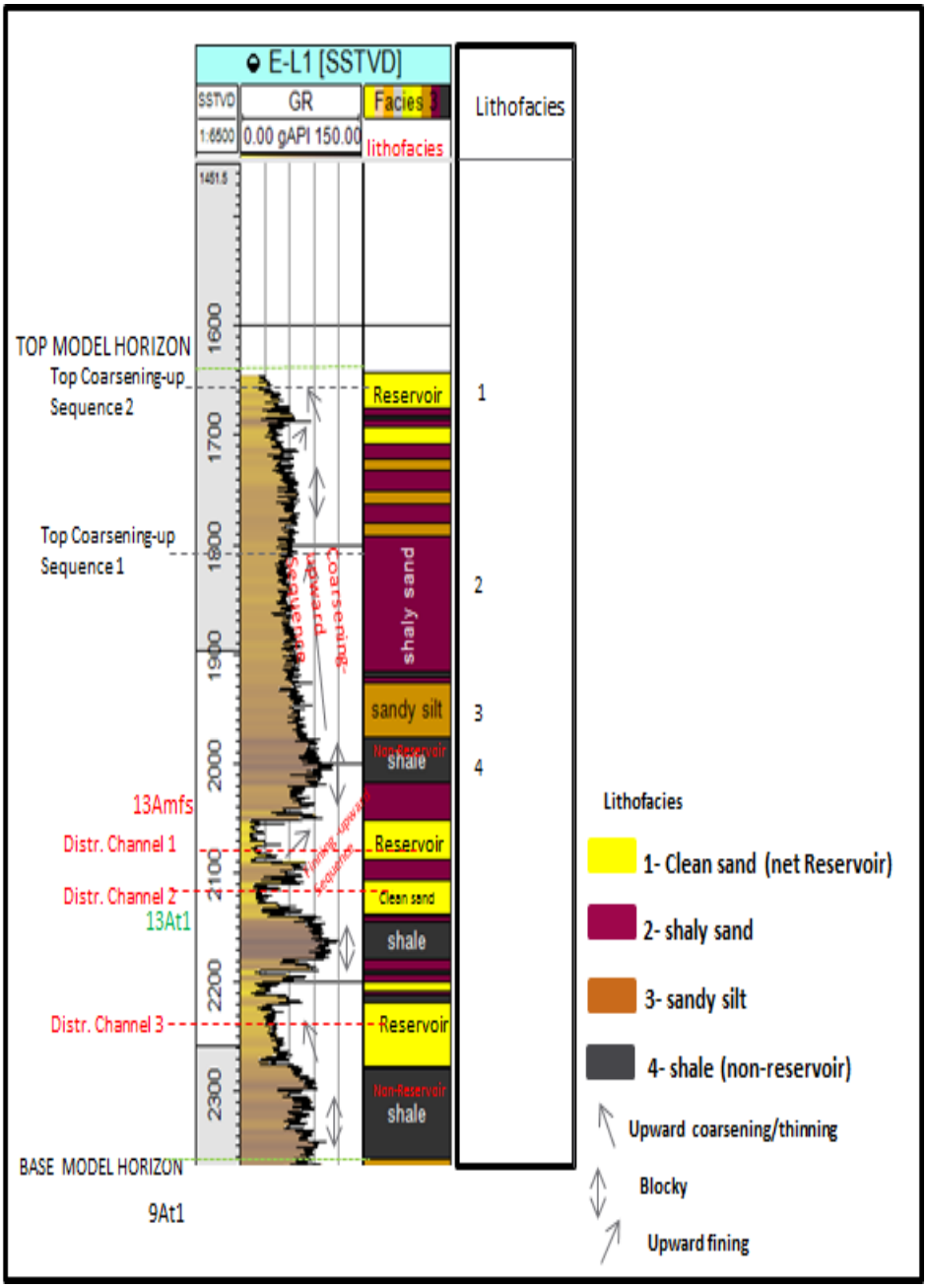

Figure 4.1: Log description of well E-L1 showing interpreted vertical facies successions and observed coarsening and fining upward sequences based on gamma ray log. More of the clean sand facies fall beneath and above the top of the fining-up sequences. (Note: GR ≤ 30-clean sand, GR>30≤8 0-shaly sand, GR>80≤120-sandy silt and GR>120-shale).

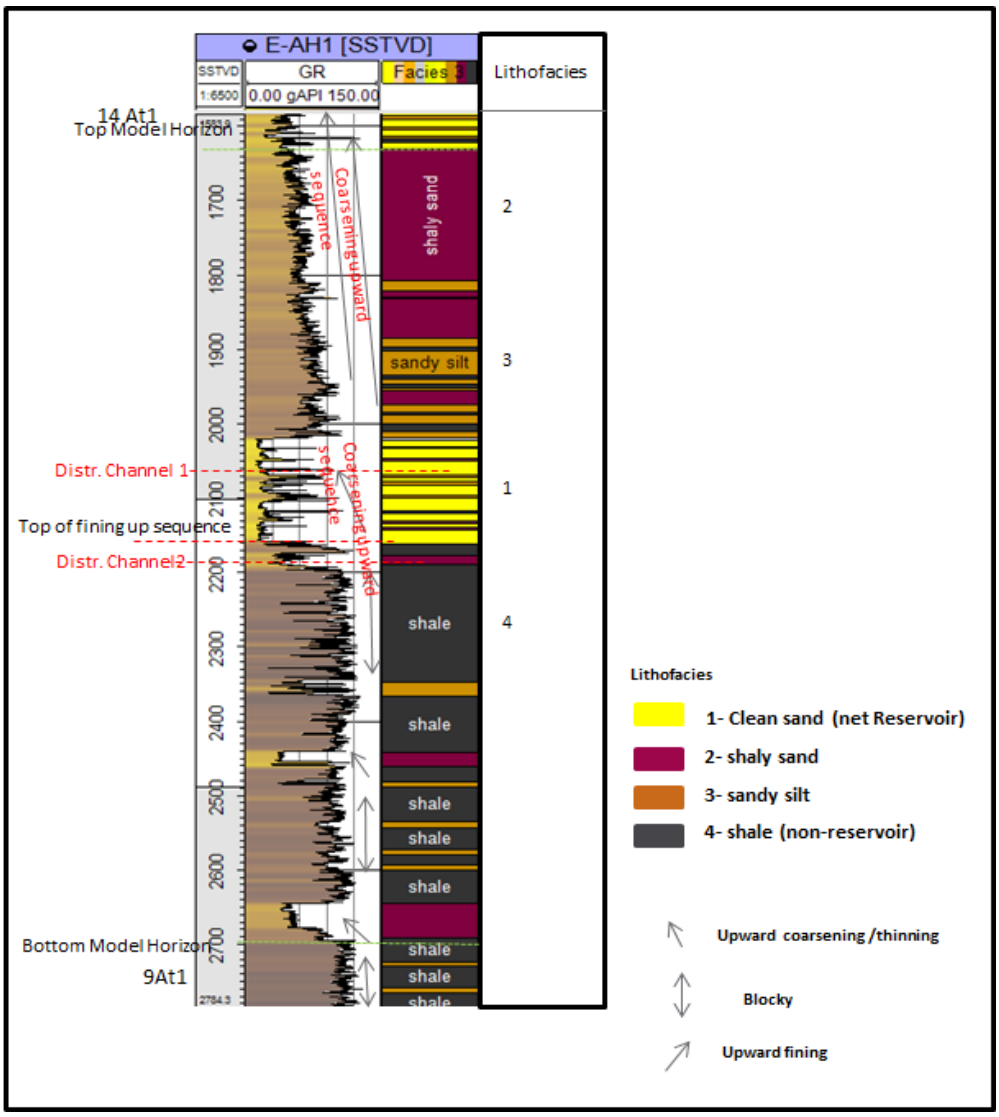

Figure 4.2: Log description of well E-AH1 showing interpreted vertical facies successions and observed coarsening and fining upward sequences based on gamma ray log. The clean sand facies fall just above the top of the upward fining-up sequences. (Note: GR ≤ 30-clean sand, GR>30≤80-shaly sand, GR>80≤120-sandy silt and GR>120-shale).

4.1.1.3 Log description: Well E-BD2

The log description of well E-BD2 based on gamma ray log is presented within depth range of (1633-2800m) (Fig 4.3).

Facies description: Lithofacies 2 (shaly sand facies) is the most prominent lithofacies in the studied log interval, increasing in thickness within log interval (1900 to 2550m). It represents approximately 60% of the log section. In the lower one third of the log section, a coarsening-up sequence characterized by low gamma ray value is evident between (2500-2600m). Five clean sandstone reservoir units are measured within the entire log section with the thickest unit measuring 226m.

4.1.1.4 Summary: Vertical grain size profile of the selected wells

The interpreted vertical facies succession of the selected wells is presented amongst related logs (i.e. synthetic seismogram) (Fig 4.4). The log shape pattern (i.e. gamma ray) characterization of the selected wells consists of four major distinct log patterns and there are more than one pattern present in each selected well. They are as follows:

1. Upward Coarsening: This log pattern is recognised in the selected wells mainly in the upper section of the logged interval, varying from 10-350m thick stacked cycles capped by glauconitic massive sandstones (up to 8m thick).

2. Upward fining: These are up to (10-170m) thick and are found mostly above block sand-silt to shaly sandstones.

3. Blocky sandstones: These vary from 5-60m thick are prevalent in the middle section to lower end of the logged interval. According to available geological reports they have been reported to corroborate and correspond with the ‘hydrocarbon fairways’ of the early progradation model by (Turner, 1991).

4. Interbedded (ratty) sandstones: These sandstones are interbedded with siltstones and claystones and rarely exceed 2m in thickness and form part of the interpreted shaly sand and sandy silt deposits that range within thickness of (10-80m).

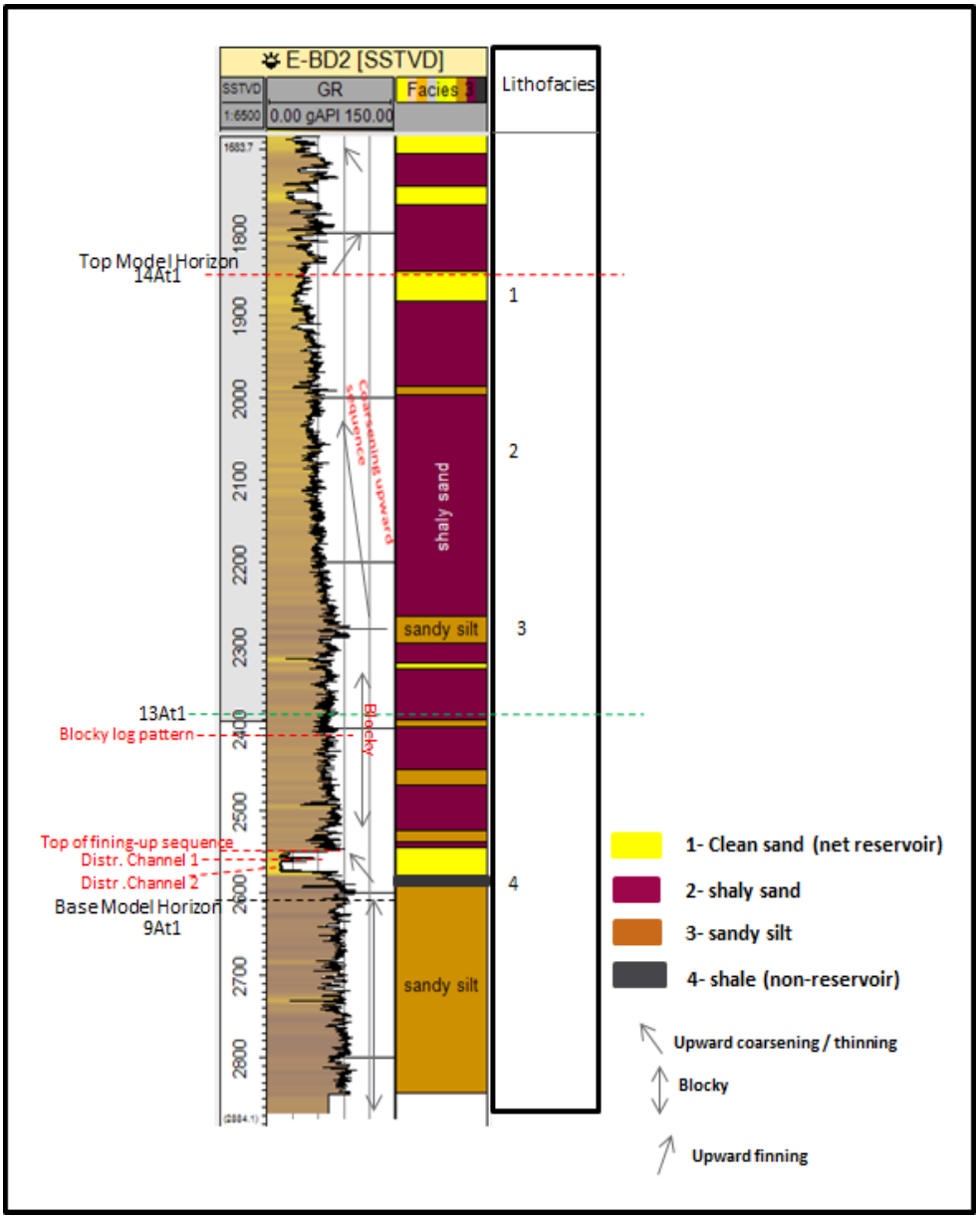

Figure 4.3: Log description of well E-BD2 showing interpreted vertical facies successions and observed coarsening and fining upward sequences based on gamma ray logs. Shaly sand is the more prominent facies in the logged interval. (Note: GR ≤ 30-clean sand, GR>30≤80-shaly sand, GR>80≤120-sandy silt and GR>120-shale).

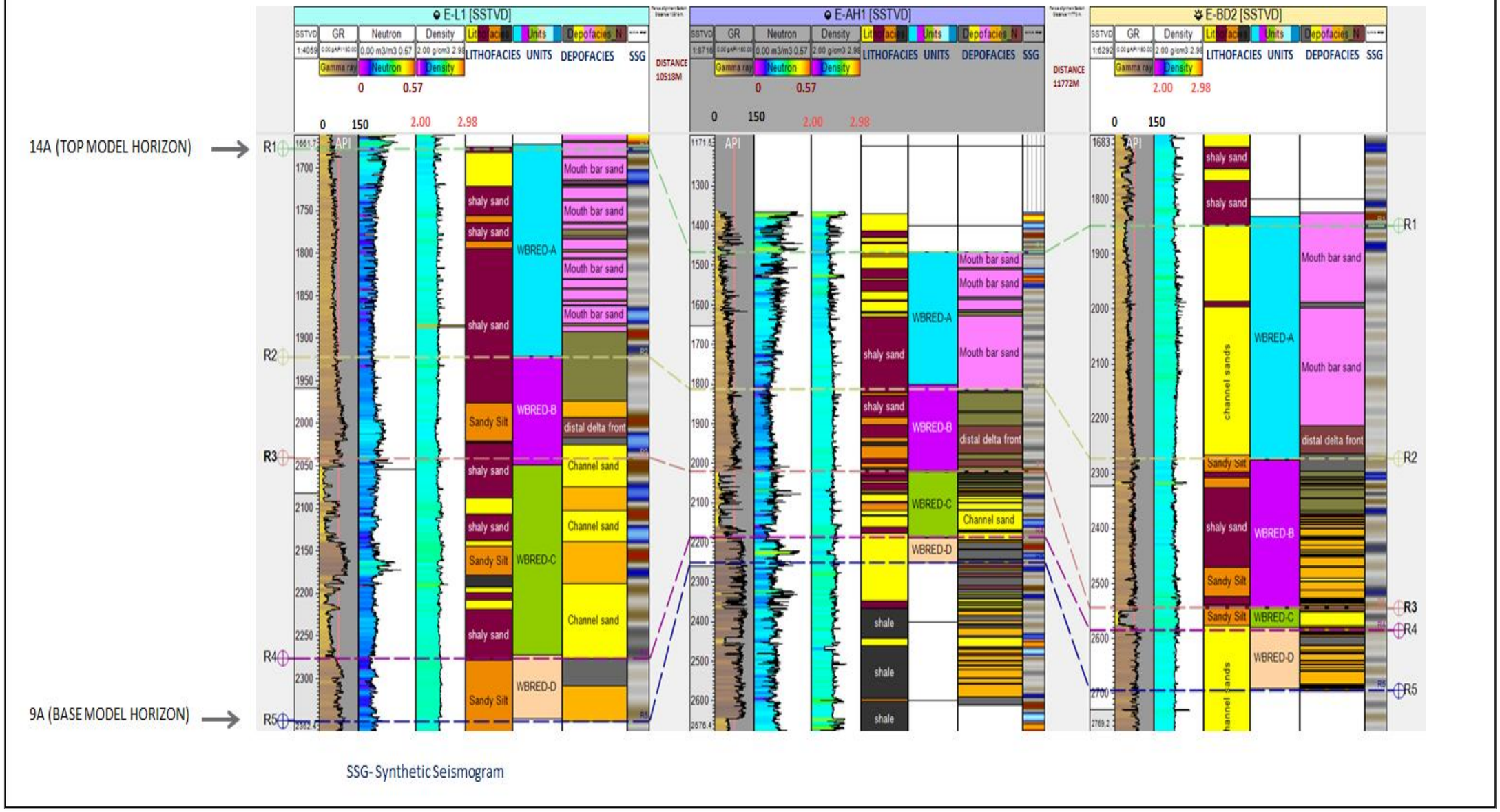

Figure 4.4: Interpreted vertical facies successions logs (i.e. lithofacies and depofacies) of selected wells showing established stratigraphic markers 14A-R1 and 9A- R5, marking top and base of the WBRED reservoir unit. R2, R3 and R4 are surfaces generated within 9A and 14A marking top and base for WREBD-B and WBRED-C reservoir units.

4.1.2 Sedimentological description and interpretation

The cores of the selected wells (E-L1, E-AH1, and E-BD2), located within and below the established stratigraphic log interval (9A and 14A) are physically -examined and described on the weight of inferring possible depositional environment. To these end, four lithofacies are identified based on colour, grain size, texture and sedimentary features. In addition, maximum grain size trends are investigated and used to better determine maximum energy conditions at the time of deposition (Figs 4.4, 4.5, 4.6 and 4.7). In the preceding section, interpreted lithofacies are described per cored well for the selected wells in the study area. Summarised descriptions of physical observations on all available cores in the selected wells are presented in APPENDIXES C and F.

4.1.2.1 WELL E-L1

In the well E-L1, four core plugs are available within the physical core samples examined. The core samples are obtained from a log depth range of (2798m-3300m). The descriptions of defined lithofacies are as follows:

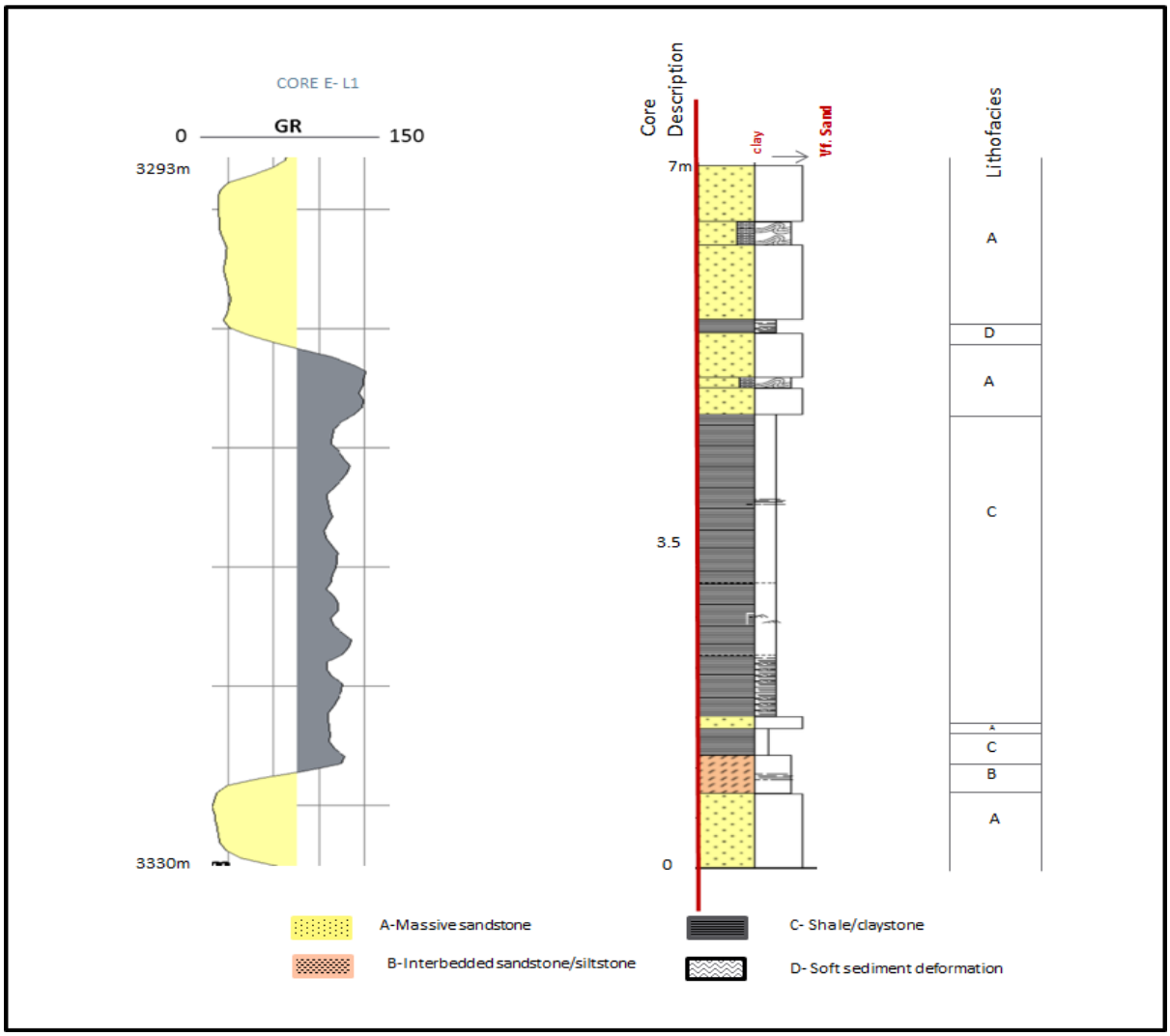

Figure 4.5: Illustration of massive claystone facies from generated sedimentary core log of well E-L1 with corresponding log pattern showing lithofacies C to A forming vertical coarsening upward successions. Gamma ray values decrease upwards from the 4m section of the cored interval.

Lithofacies A: Massive well sorted, fine to medium grained sandstones. The upper section of the examined core sample is 1.2m thick and characterised by massive sandstone. The lithofacies represents approximately 49 % of the examined core sample.

Lithofacies B: Interbedded shale/silt/sand with presence of wavy lamination, clay clast, sharp contacts and poorly developed flame structures. Measured sandstone to silt ratio is 1:3. The lithofacies described represent approximately 6% of facies described in the examined core.

Lithofacies C: Current ripple to planar laminated shale, interbedded with siltstone and sandstone; also minor deformation. Estimated sandstone to shale ratio is 1:7. The lithofacies represent approximately 44% of the facies described in the available core.

Lithofacies D: Extensive soft-sediment deformation, consist of silty sandstones with presence of flow structures and deformed clast with disrupted primary lamination. The lithofacies represent approximately 1% of the facies described in the available core sample.

4.1.2.2 WELL E-AH1

In the well E-AH1, nineteen core plugs are available within the examined core sample. The core samples are obtained from a log depth range of (2471m-3160m). It is observed that on correlation with geophysical logs that log depth is 2.5m deeper than driller's depth for the described core, so a depth match was done. The descriptions of defined lithofacies are as follows:

Lithofacies A: Well sorted, very fine to medium grained massive sandstone. The upper sandstone unit (7.5m thick) is generally massive. Massive sandstones of the lower section of the core are well sorted with a thickness of 2.61m. Presence of horizontal lamination is evident alongside distinguishable and defined high angle bedding towards the base, where it overlies observed claystones. The lithofacies represents the dominate feature in the cored interval and represent approximately 74.2% of the facies described.

Lithofacies B: It consist interbedded sandstone with clay clast and minor conglomerates. Preservation of sand and silt beds is visible. The lithofacies represents approximately 2.1% of the described facies in the examined core.

Lithofacies C: This consists of massive dark greyish black claystones with up to 10% minor thin siltstone interbeds. The 1.2m thick shale/claystone are characterised by near horizontal bedding near the contacts with the sandstones. The lithofacies represent approximately 8.5% of the entire facies described in the core sample of well E-AH1.

Lithofacies D: Soft-sediment deformation consisting of silty sandstones. Represent approximately 14% of the described facies in the examined core.

4.1.2.3 WELL E-BD2

In well E-BD2, eleven core plugs are available within the cored interval. The core samples are obtained from a log depth range of (2579m -2632m). The defined lithofacies are as follows:

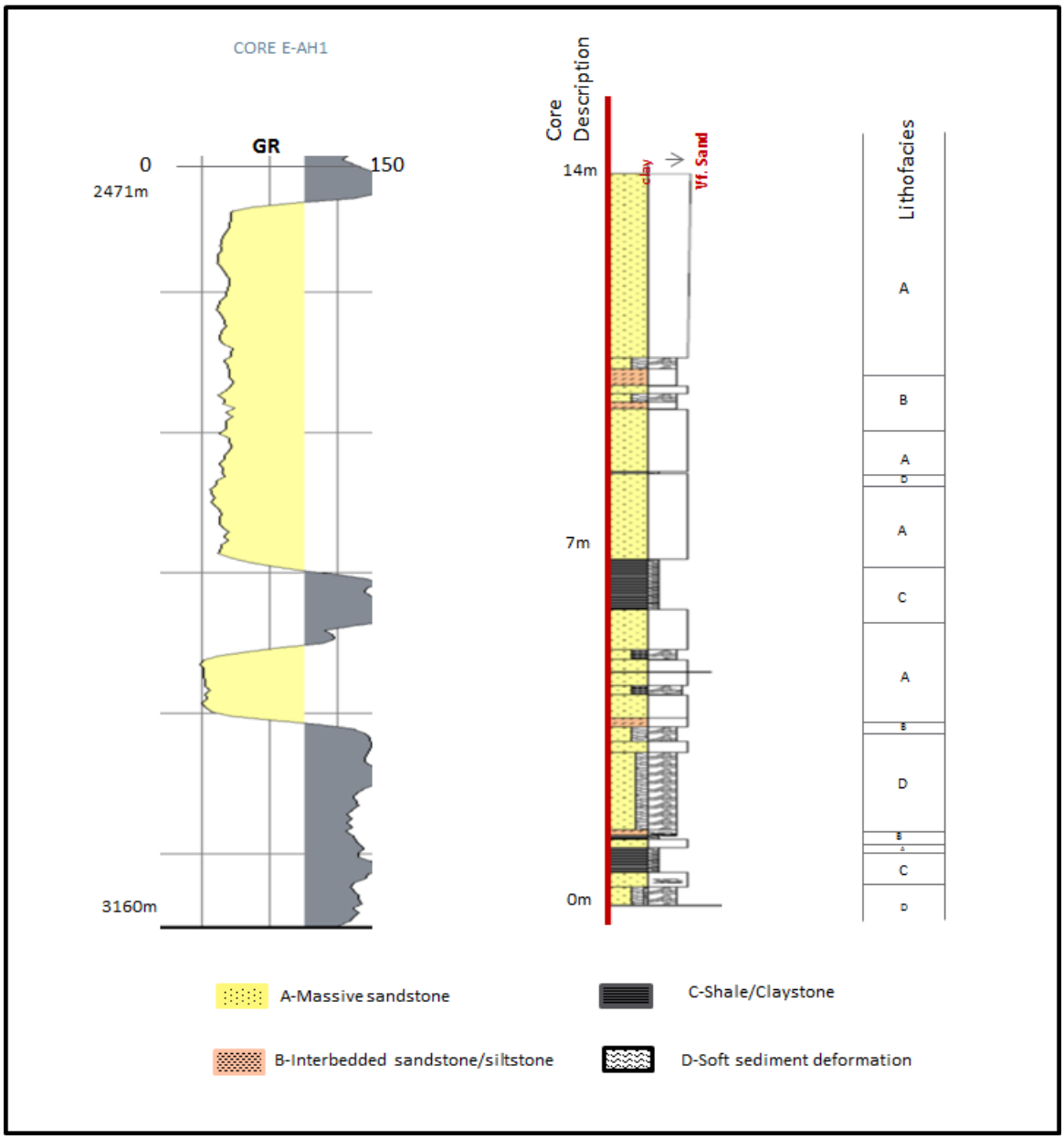

Figure 4.6: Illustration of massive sandstone facies from generated sedimentary core log of well E-AH1 and corresponding log pattern showing lithofacies C to A forming vertical coarsening upward successions, interbedded with silt and claystone sequences. Gamma ray values decrease upwards from the 7m section of the cored interval.

Lithofacies A: Well sorted, fine to medium-grained massive sandstones with occasional claystone clast in the thicker upper amalgamated sandstone unit. The amalgamated sandstones units are up to 4.5 meters thick with the thinnest individual bed 10cm thick. In the middle section, the evident massive sandstone unit has poorly developed low angle cross-stratification and occasional concentration of argillaceous material. These massive sandstones are more dominant in the cored interval, representing approximately 63.4% of the facies described.

Lithofacies B: Interbedded sand/siltstone with minor deformation and conglomerate. Preservation of parallel lamination towards the base of contact is evident.

Lithofacies C: Uniform dark grey to dark grey claystone, 2-14 centimetres thick massive structureless shale/claystone with minor horizontal lamination and sand lenses towards the base. At the upper section of this facies, minor soft-sediment deformation of the claystones is visible.

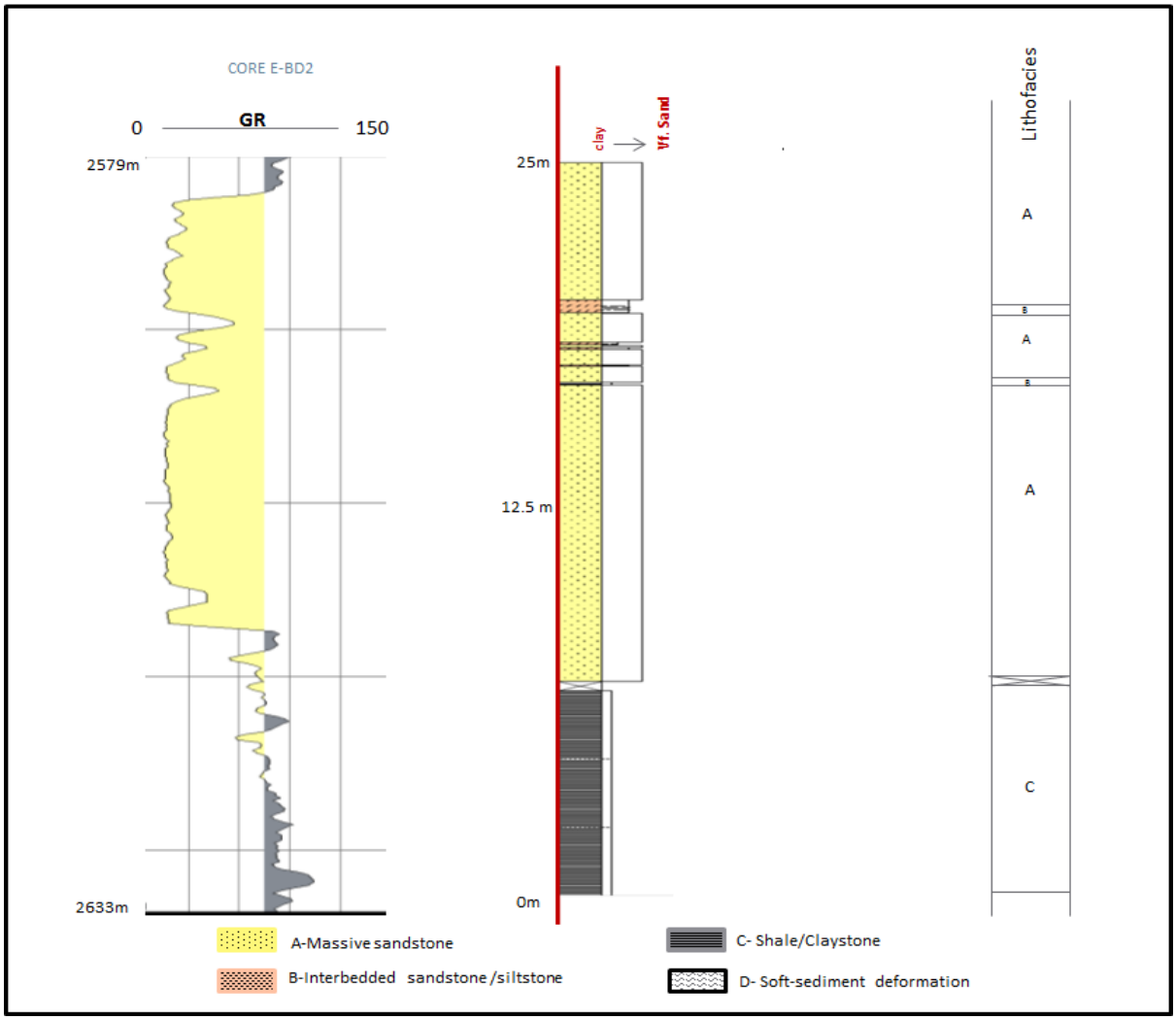

Figure 4.7: Illustration of a massive sandstone facies and corresponding log pattern showing lithofacies C to A forming an even block with sharp top and base underlying successions interbedded with silt and claystone sequences. Gamma ray values decrease upwards from the 5m section of the cored interval. This demonstrates a log through a distributary channel-fill deposit.

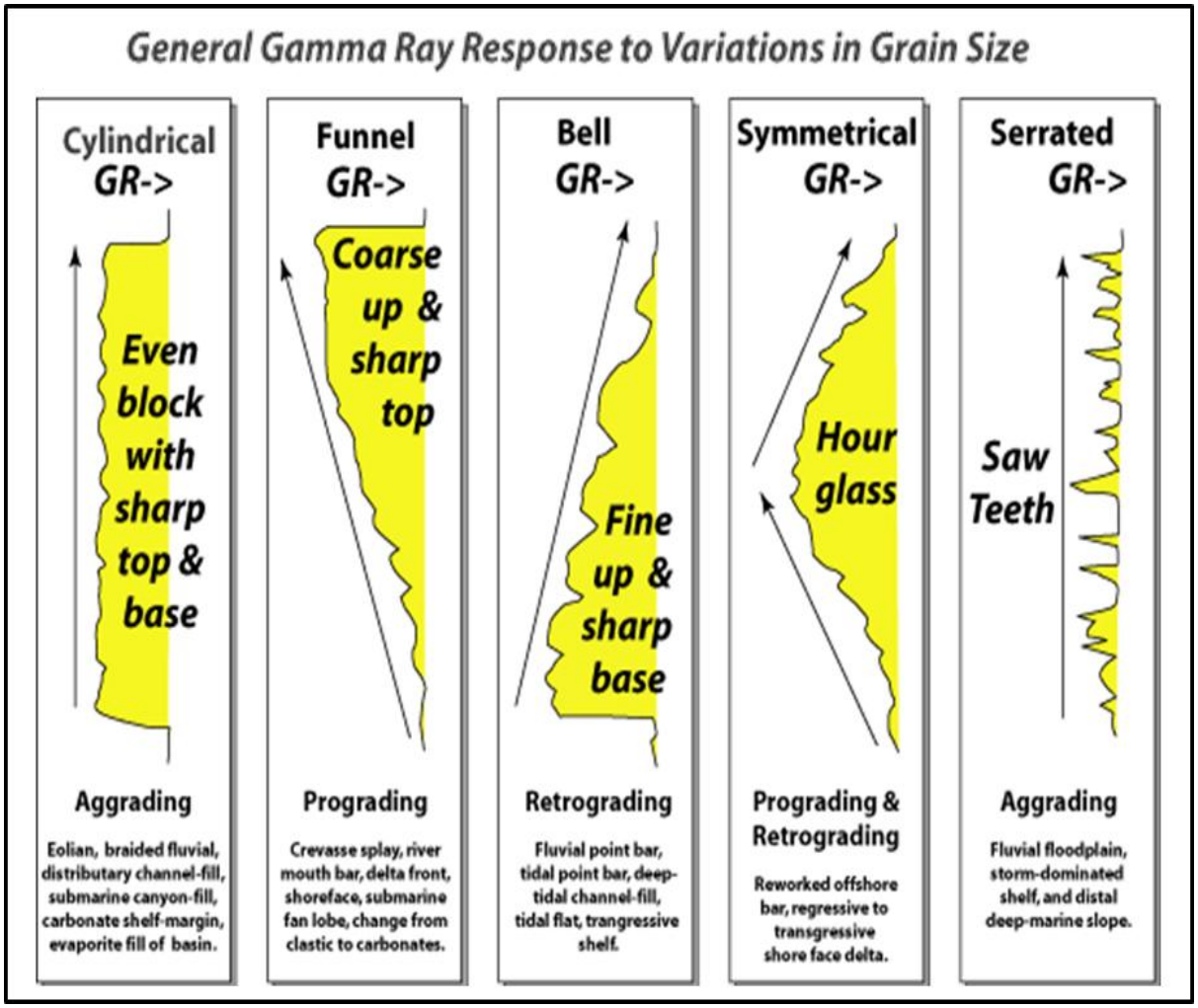

Figure 4.8: Gamma ray log response pattern with typical grain size profile and possible associated vertical facies associations. Note- similar facies associations can occur in more than one environment and log sections range from tens to hundreds of metres (After Galloway and Hobday, 1996).

4.2. Reservoir stratigraphic framework and architectural elements

4.2.1 Sedimentological interpretation

Based on core observations and associated log shape pattern, analyses of stacked lithofacies, interpreted vertical facies successions and possible depositional processes, sedimentary bodies are interpreted in the studied area (Figs 4.4, 4.5, 4.6, 4.7 4.9 and 4.10). A generalised gamma ray log responses pattern, showing vertical grain profiles and associated vertical facies associations is presented in Figure 4.8.

[A] <u>Mouth bar sandbodies</u>

Considering the studied intervals in the selected wells, there is an evident coarsening-upward succession in the upper section (i.e. WBRED-A) of the stratigraphic log interval (9A to 14A) (Figs 4.1, 4.2 and 4.3). This transmits to the gradual transition of lithofacies 4 to 1 and lithofacies C to A; forming heterolithic coarsening-upward–successions characterized by a funnel gamma ray log shape (Figs 4.1, 4.2, 4.5 4.9 and 4.10). This observed coarsening-upward–succession corresponds to mouth bar on comparison to the log shape models/electrofacies models of Schlumberger (1991) and those described by (Turner, 1991; Adedokun 1981). Also, according to (Readings, 1981), mouth bar reservoirs are shaped in regions where fluvial sediment load enters a basin and dispersed while interacting with basinal processes. These events are mainly characterised by upward decreasing gamma ray values (Morse, 1994; Labourdette et al., 2008). To these ends, the upward-coarsening successions are interpreted as low to high energy mouth bar sandbodies (Morse, 1994; Olairu and Bhattacharya, 2006).

[B] Delta front deposits

There is a gradual change of lithofacies D to A as well as the forming of coarsening upward heterolithic successions. Homogenous fine silty sand (lithofacies D) passes on to massive clean sand (lithofacies C to A) and (lithofacies 4 to 1) (Figs 4.1, 4.6, 4.7, 4.9 and 4.10). The successions are interpreted as delta front deposits (Allen, 1987). In electric logs, these deposits are characterised by funnel shaped gamma ray log response (Fig 4.8).

[C] Distributary channel-fill deposits

In the lower section of the logged interval for well E-L1, lithofacies 1 to 4 form two fining-up sequences whose base erupts sharply into underlying silty sand and shale sequences. Also in the middle and lower section of well E-AH1 and E-BD2 respectively, log shapes and sediment pattern are both characterized by sharp basal contact and gradational upper contacts to give a blocky shape that corresponds to distributary channel characterization as described in Schlumberger (1985) classifications of electrofacies for sedimentary environments (Figs 4.1-4.10). This trend is also visible within the lower section of the cored interval of well E-L1; where (Lithofacies C to A) are associated with a 3.7m thick fining up sequence whose base erodes sharply into and underlying interbedded sand/siltstone (Figs 4.5 and 4.9). According to (Labourdette et al., 2008), blocky to fining upward gamma ray responses in well logs are generally associated with channel fills, and, these facies are interpreted as distributary channel associations 1 and 2. The two channels are laid down within a slope to shallow-water setting but separated by an over bank /inter-channel deposit.

Inter-channel deposits

In the middle to lower section of the cored interval of the selected wells, lithofacies A to B form heterolithic mud dominated successions one to six meters thick (Figs 4.5 and 4.6). These thin bedded units fringing the interpreted channelized deposits above are interpreted as inter-channel deposits/over bank deposits. Consisting primarily of alternating parallel and laminated interbedded sandstone/siltstones (lithofacies 3 and B) (Figs 4.1, 4.6, 4.9 and 4.10). Evident from well log patterns, inter-channel/overbank deposits appear to be frequently eroded by channel-fills as seen in well E-L1 from log depth range (2100-2150m), well E-AH1 from (2100-2140m) and E-BD2 from (2200-2240m) (Figs 4.1, 4.2, and 4.3).

[E] Flood plain deposits

Flood plain deposits can be found in all regions of the pro-delta and predominantly associated with massive and structureless claystone (lithofacies C). They are usually cut-off from channel fill complexes and are considered products of continuous background deposition. Towards the lower section of the studied cored interval for well E-L1, E-BD2 and E-AH1, lithofacies C and 4 are associated with serrated GRlog pattern and high gamma ray values (Figs 4.4, 4.7, 4.9 and 4.10). They are interpreted as flood plain deposits (Allen, 1987; Dalrymple et al 2003; Brown, 1996).

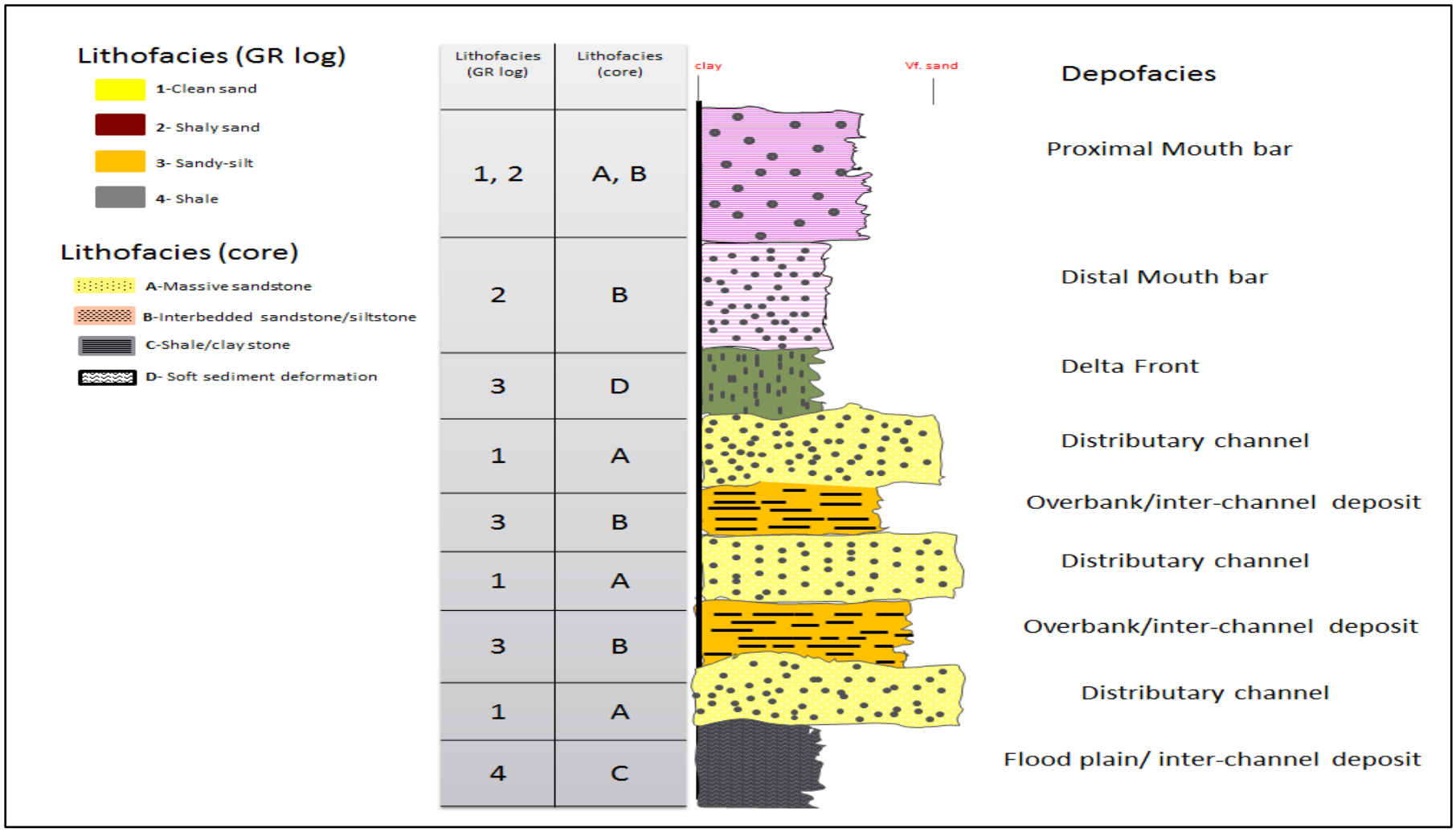

Figure 4.9: Interpreted vertical depofacies succession based on organization of GR log pattern, vertical grain size profile and core description of the selected cored wells in the study area.

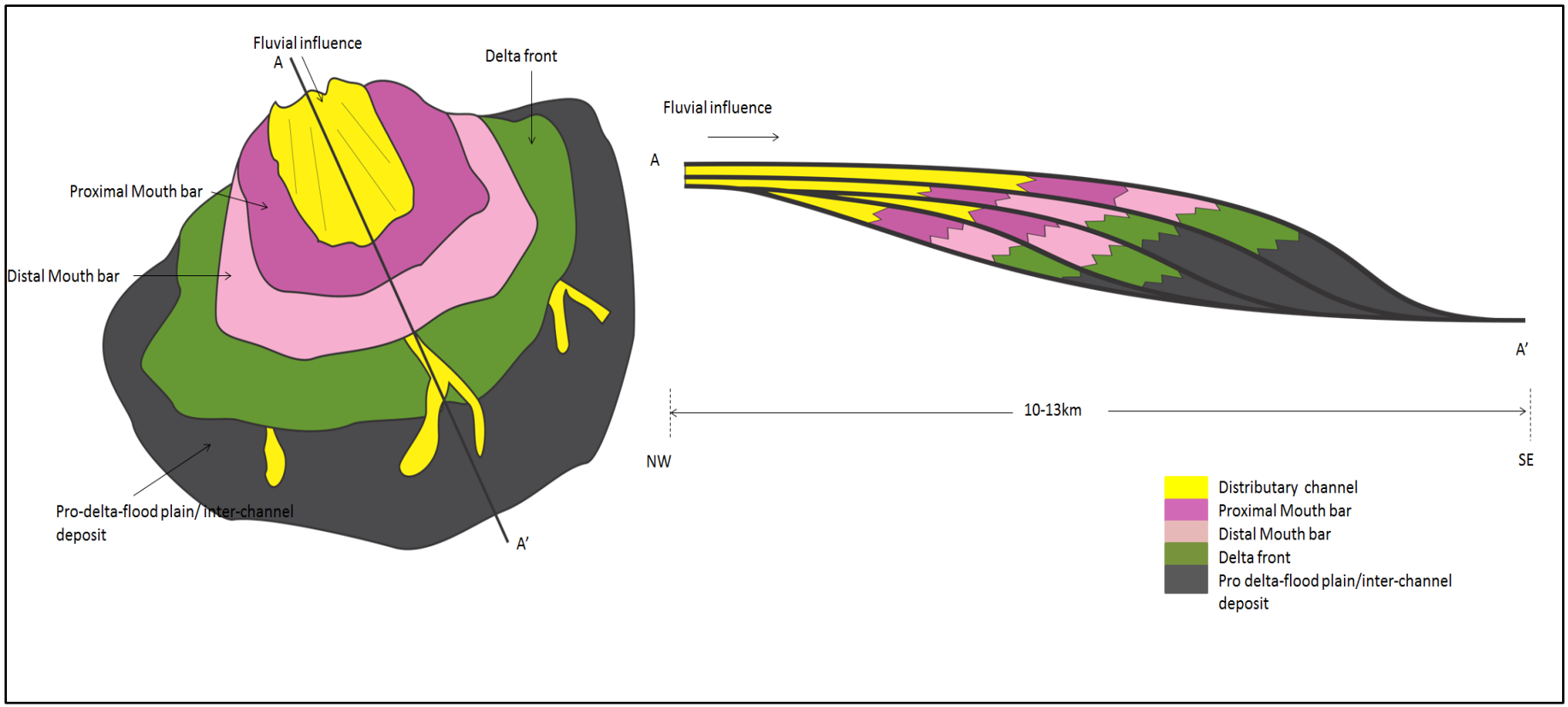

Figure 4.10: Geometry of a channel mouth bar showing the plane symmetry position (A-A') (modified from Labourdette et al., 2008; Sonibare et al., 2011).

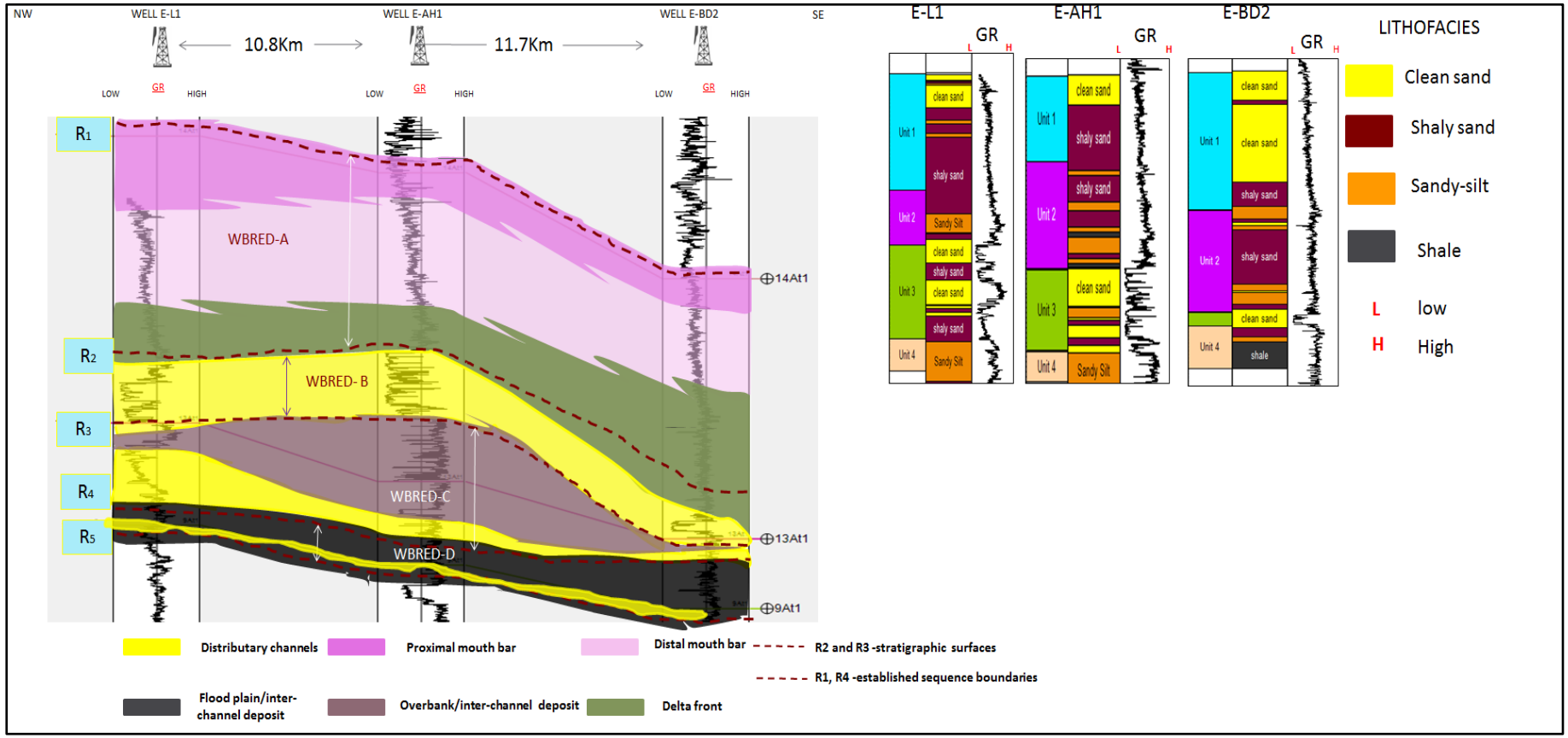

Figure 4.11: 2-D sedimentological model or geological vertical cross section of identified reservoir zones showing defined stratigraphic reservoir unit intervals; derived from well log analysis and interpreted vertical facies successions of the selected wells (E-L1, E-AH1 and E-BD2). A cross section profile of the selected wells is presented in Figure 1.3. Unit 1-4 represents WBRED [A-D] respectively.

4.2.2. 3-D grids and stratigraphic framework

Combining seismic horizon interpretation, well to well correlation and stratigraphic modelling in PETREL, a 3-D grid stratigraphic frame work of the 2-D sedimentological model shown in Figure 4.12 is created.

To this end, five reservoir stratigraphic horizons that match well ties are mapped and afterwards surfaces are generated (R_1, R_2, R_3, R_4, and R_5) (Fig 4.13A). Results of seismic horizon interpretation are shown in Figure 4.13. Based on these 3-D reservoir grids of selected stratigraphic reservoir units are generated (Figures 4.12, 4.13B and 4.13C).

3-D grid cell thicknesses in each of the respective stratigraphic units are constant, where the base of each unit is used to construct the grid upwards. This leaves room for the possibility that grid cells at the top of a unit may be truncated by the unit above (visible in WBRED-B) (Fig 4.13B).

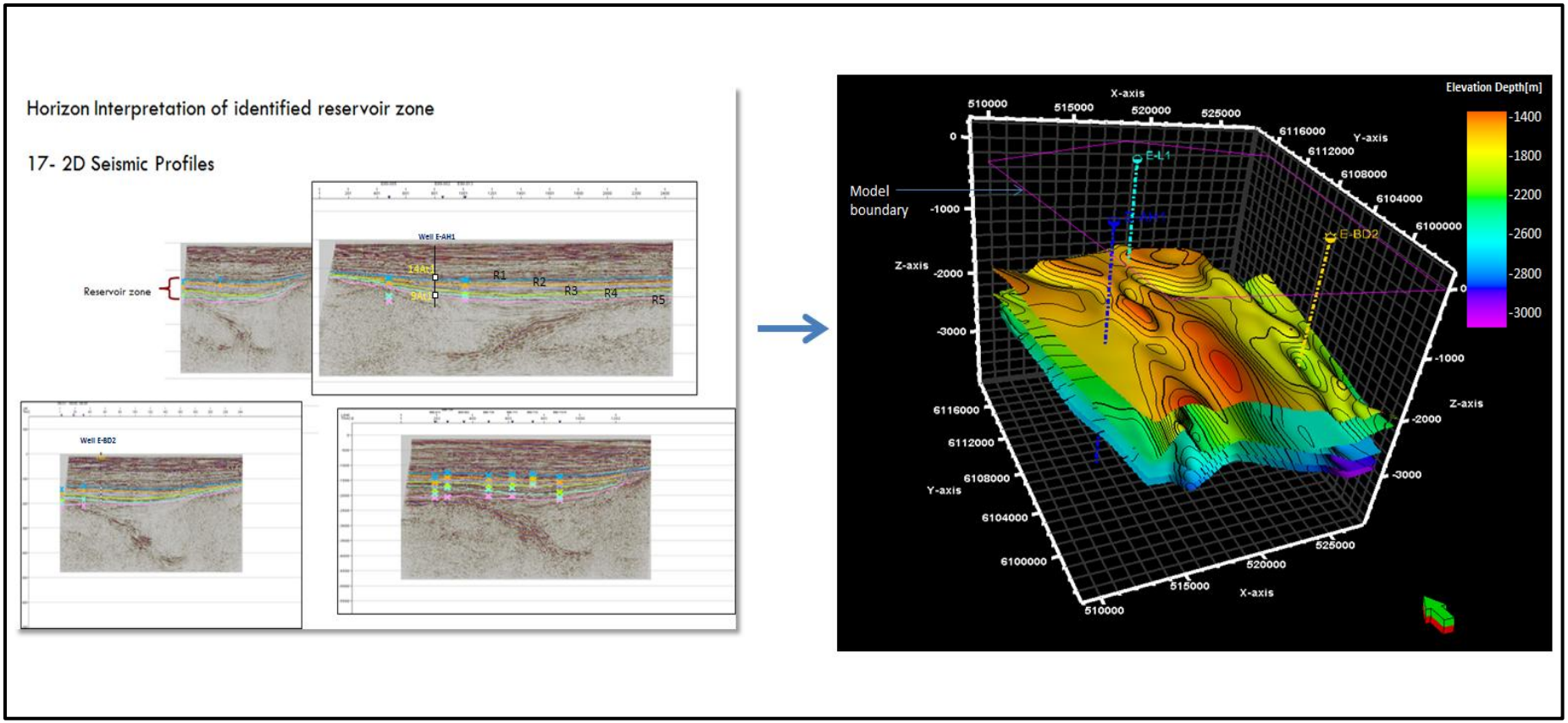

Figure 4.12: Seismic horizon interpretation of the study area based on seventeen 2-D seismic profiles, showing selected seismic sections cutting across the model boundary in vertical and horizontal positions. Results generated five seismic stratigraphic horizons/surfaces R1, R2, R3, R4 and R5. The picking of these horizons were guided by formation top data of 9At1, 13At1 and 14At1 in each of the selected wells.

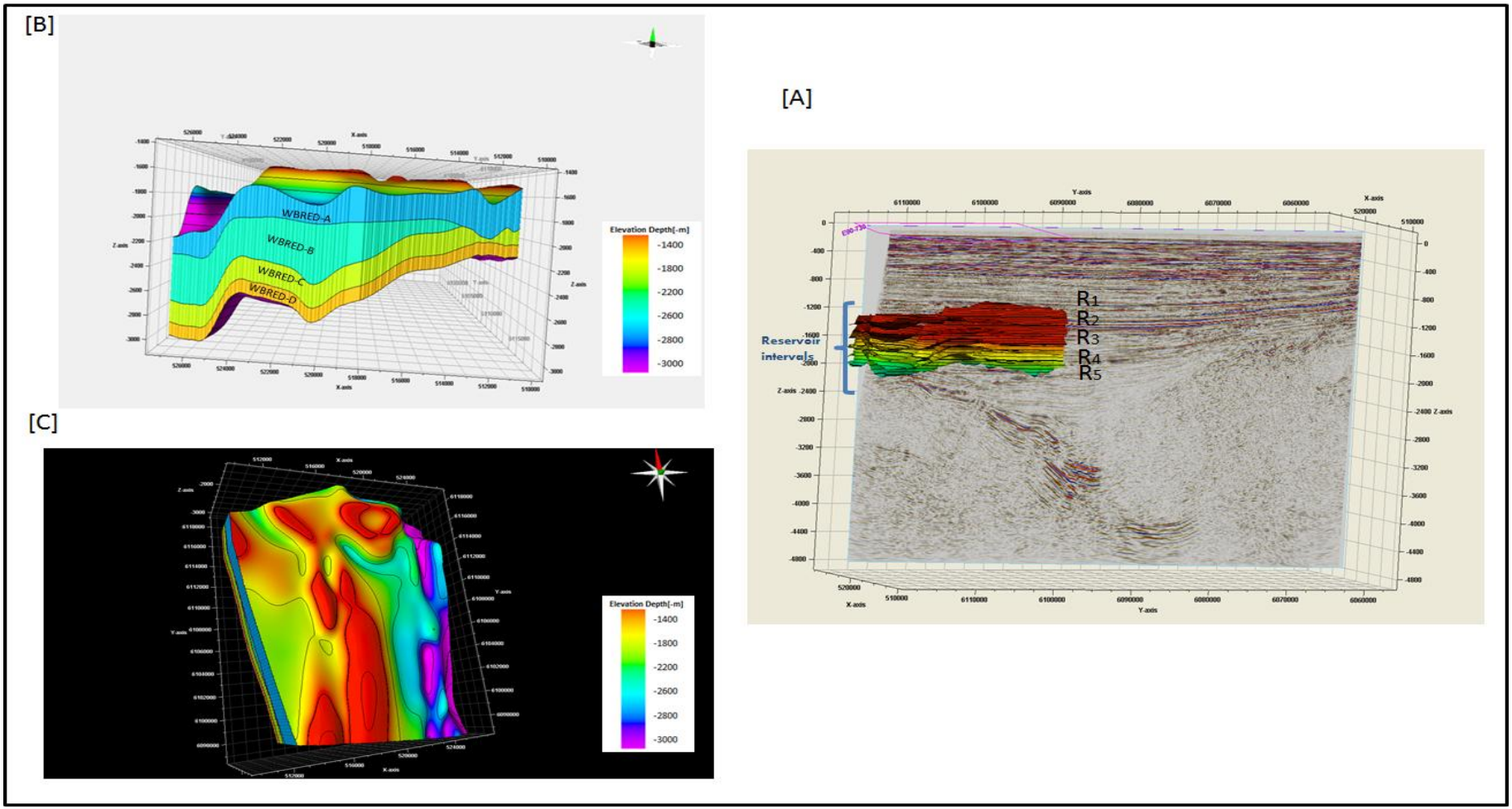

Figure 4.13: (A) Five stratigraphic horizon surfaces generated in PETREL. (B) & (C) The 3-D stratigraphic framework for the WBRED reservoir units (WBRED-A, WBRED-B, WBRED-C, and WBRED-D) generated in PETREL showing north and south orientation.

Table 4.1 Dimensions of simulated objects as deduced from well analyses and sedimentological outcrop studies (e.g. Lowry and Jacobsen, 1993).

	Channel parameters			Sinuosity		
	Width (m)	**Thickness (m)**	**Branching (m)**	**Wavelength (m)**	**Amplitude (m)**	**Channel routing number**
Minimum	400	5	1500	1000	600	0.7
Mean	650	15	2300	1500	1000	0.7
Maximum	800	25	3500	2000	2500	0.7

4.3 Modelling of stratigraphic reservoir units

The 3-D facies model of the identified reservoir units characterizes the distribution of the upscaled log facies into the created 3-D grid using both the hierarchical object and truncated gaussian simulation (TGS) algorithm in PETREL. Five depofacies types are modelled: Mouth bar sand, distributary channel sand, proximal delta front, distal delta front, over bank deposits and flood plain. The simulated depofacies objects are deduced from well analyses and outcrop analogue studies (e.g. Corbeanu et al., 2004; Olariu and Bhattacharya, 2006) (Table 4.1). The modelled facies distribution and pattern show northwest southeast trend (Figs 4.14 to 4.18).

4.3.1 3-D facies model of WBRED (all units)

The depofacies models of the WBRED reservoir units are displayed in 3-D window with grid lines and the axis (Figures 4.14 to 4.18).

4.4 Discussion

Based on studied seismic sections and log interval (9At1 to14At1), four distinct reservoir units are identified and interpreted. Seismic sections show no active fault systems, perhaps due to the studied interval being within post-rift successions with no evidence of fault re-activation (Sonibare et al., 2014; in press). The WBRED reservoir sandbodies are interpreted to be composed of stacked deltaic sequences, implying the need to honour and model the mouth bar sandbodies, distributary channels and inter-channel deposits relationships according to a defined conceptual sedimentological stratigraphic frame work. From a geological point of view it sounds straightforward, but during modelling it posed a lot of challenge.

Moreover, typical depo-settings of this nature are shaped by mainly river and wave forces in creating a particular architecture of reservoir sands, hence the distribution of vertical and lateral heterogeneity. In this instance the finest materials are dispersed at the mouth of the delta with local actions of mud flooding events being eroded by distributary channels. Consequently, creating spatial relationships between the relative locations of mouth bar sandbodies and distributary channel fills. Knowledge of these spatial relationships when harnessed can aid in delineating reservoir flow barriers, hence enhancing the fluid flow reservoir characterisation process.

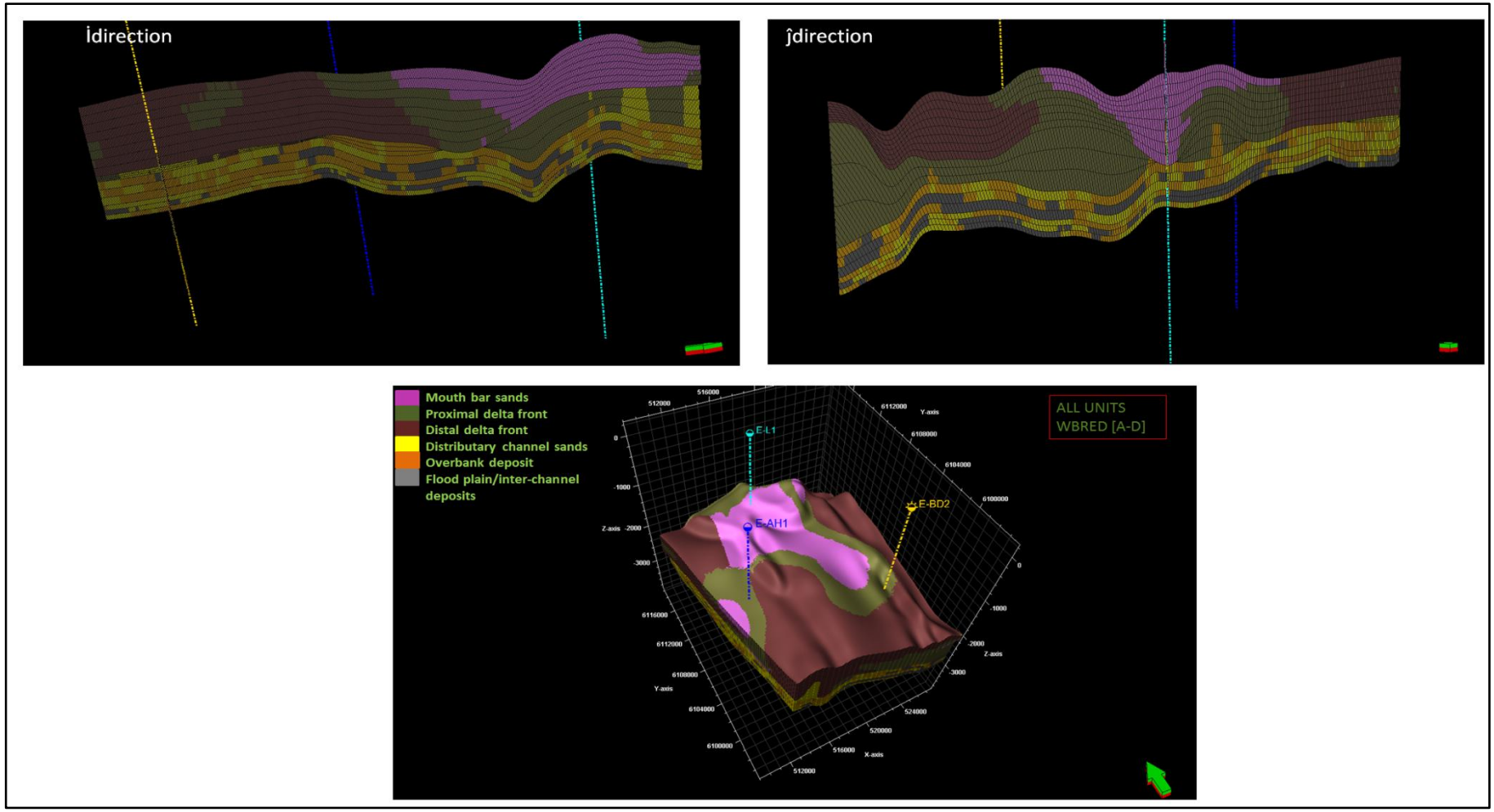

Figure 4.14: Depofacies model of the WBRED reservoir (all units), the longitudinal and transverse sections (i and j direction) are also displayed.

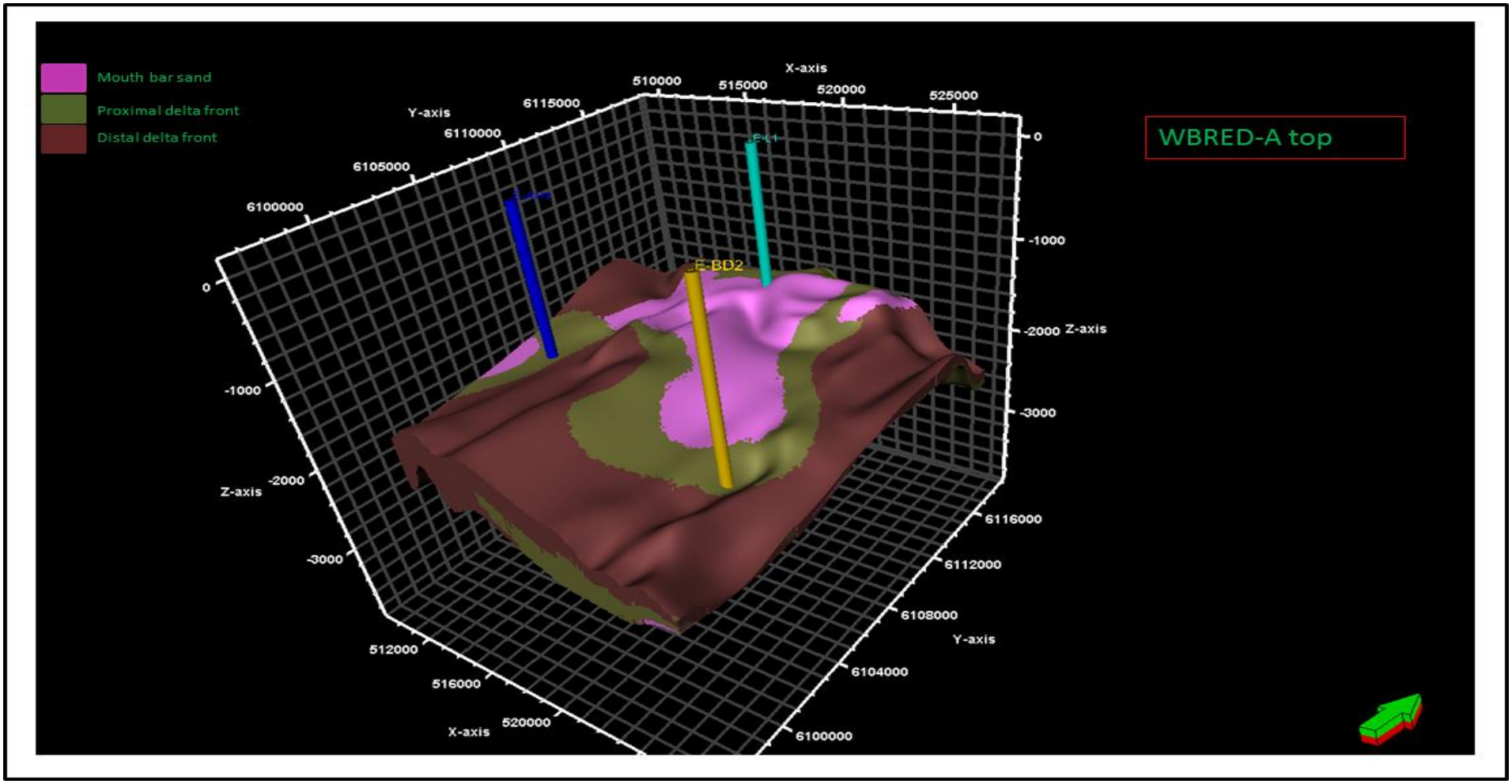

Figure 4.15: Depofacies model of WBRED-A showing the distributions of mouth bar sands with an extension of the proximal and distal delta front deposits (WBRED-A-top).

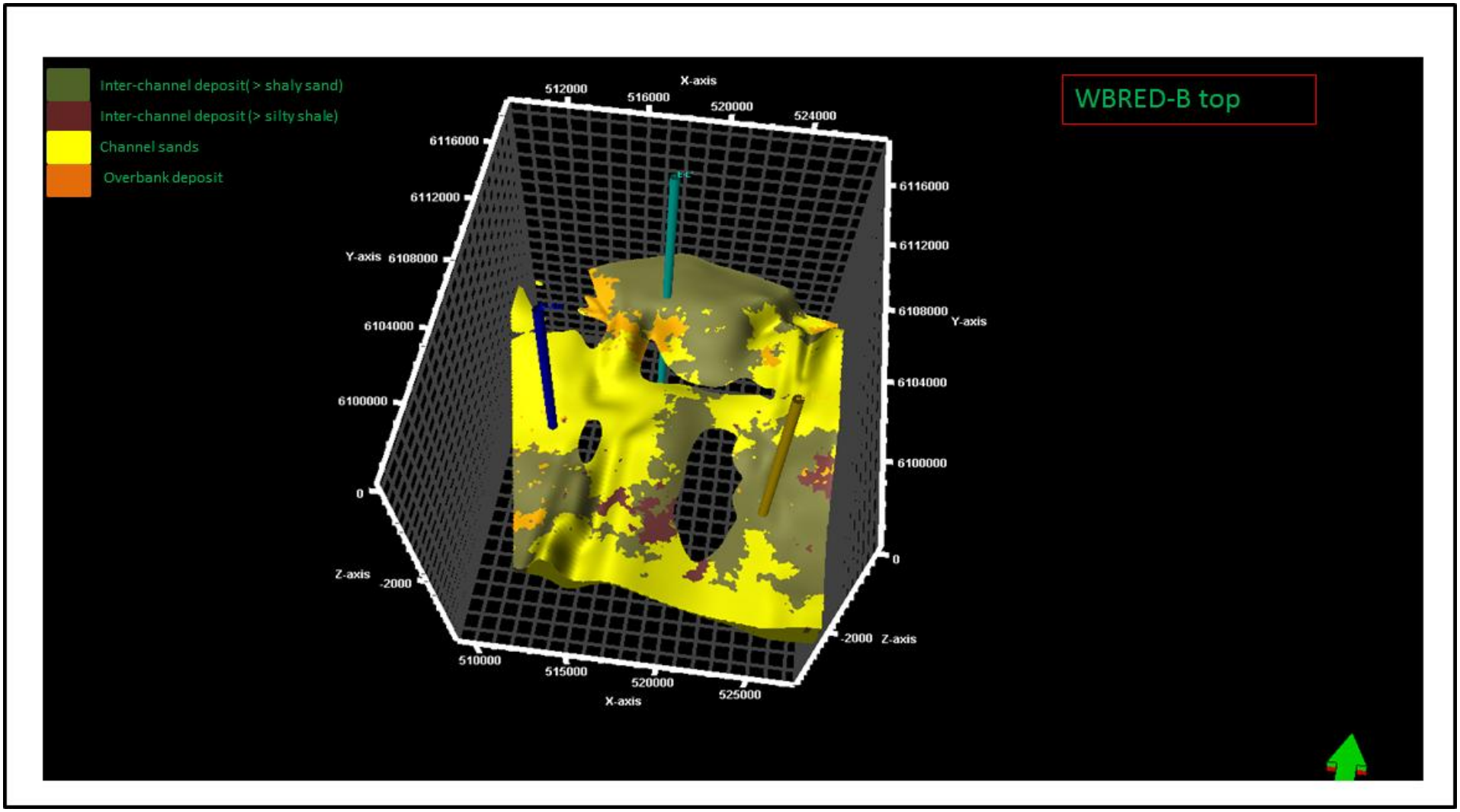

Figure 4.16: Depofacies model of the WBRED-B characterized mainly by channel-fill deposits.

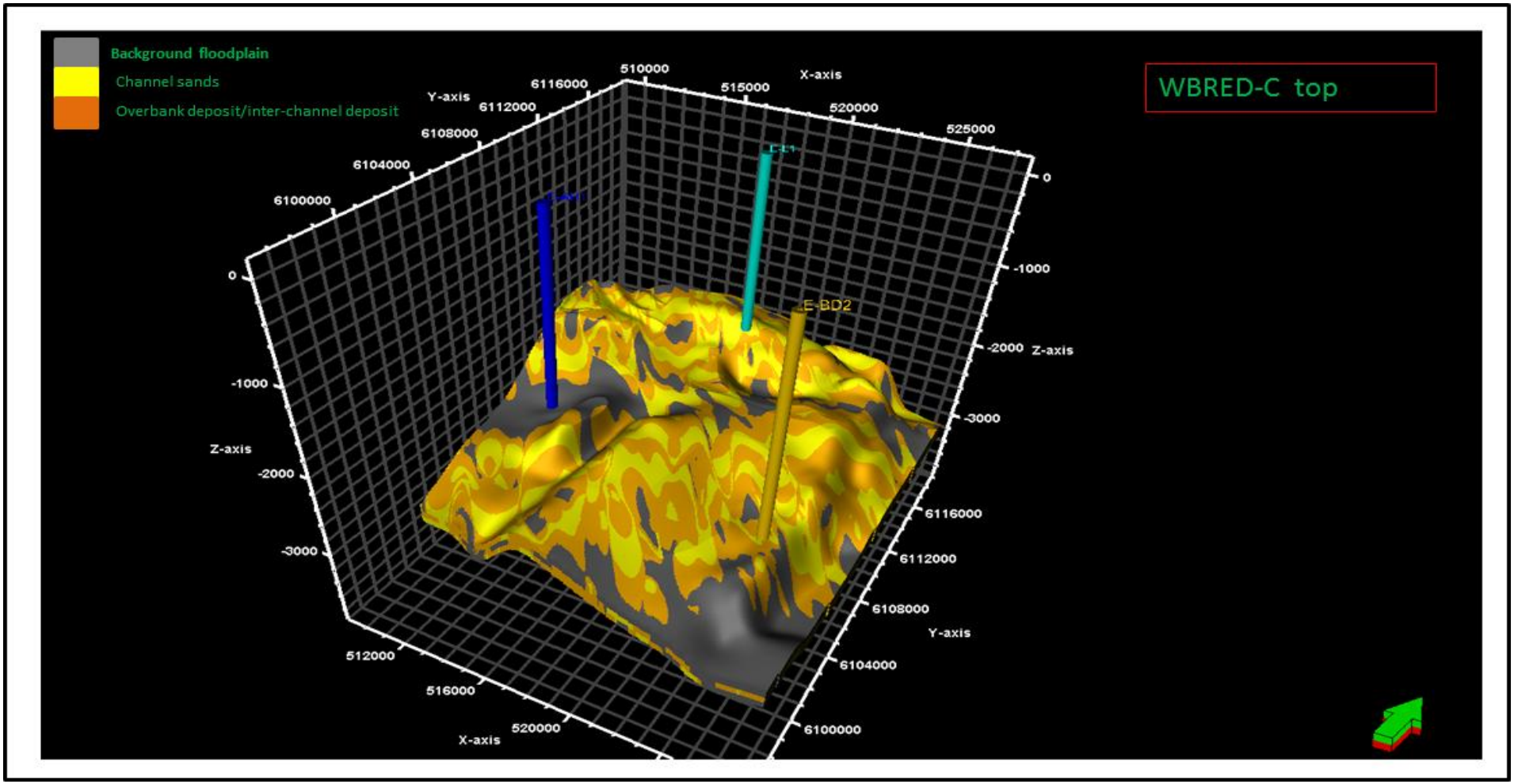

Figure 4.17: Depofacies model of WBRED-C characterized mainly by channel and overbank /inter-channel deposits.

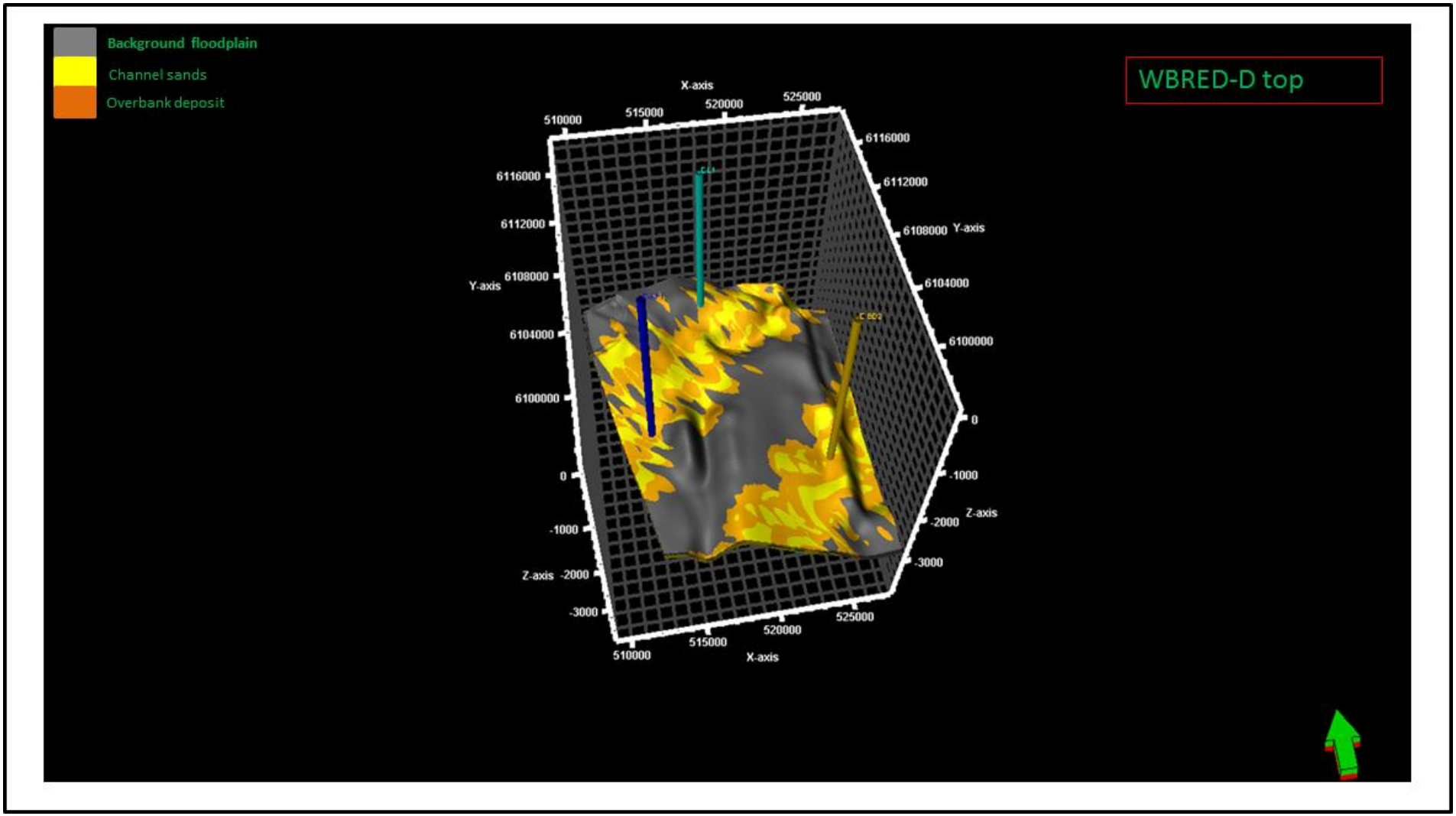

Figure 4.18: Depofacies model of WBRED-D characterized mainly by channel and over bank deposits.

CHAPTER FIVE

PETROPHYSICAL CHARACTERIZATION AND MODELLING

5.1 Introduction

This chapter highlights the petrophysical evaluation and modelling of the identified potential reservoir units in the selected study area, the Western Bredasdorp Basin based on established 3-D facies models of the respective reservoir units (i.e. WBRED-A, WBRED-B, WBRED-C and WBRED-D). The chapter presents firstly, a brief overview of each log derived petrophysical property together with detailed petrophysical evaluation (i.e. qualitative and quantitative analysis) of identified reservoir units in each selected well. This is followed by definition of stratigraphic (depth) distributions of flow units for each reservoir unit and lastly, the analysis and discussion of generated 3-D petrophysical models of each reservoir unit as performed in PETREL.

5.2 Petrophysical characterization

5.2.1 Log derived petrophysical properties

The following log derived petrophysical rock properties are evaluated in the studied reservoir unit intervals:

1) Volume of Shale or Vshale (V_{sh})
2) Total Porosity (F_{tot})
3) Effective Porosity (F_{eff})
4) Water saturation (S_w)
5) Hydrocarbon Saturation (S_{hc})
6) Irreducible Water Saturation (S_{wirr})
7) Bulk Volume of Water (V_B)

8) Permeability (K)
9) Reflection Coefficient (RC)
10) Synthetic Seismogram (SSG)

In evaluating the above stated log derived petrophysical properties the following digitized geophysical wire-line log data were loaded from both las and asci format into the PETREL database. A list of the data loaded includes the following:

1) Measured Depth referenced to Kelly bushing
2) Gamma ray log (GR)
3) Spontaneous Potential (SP)
4) Density Log (RHOB)
5) Neutron log (NPHI)
6) Sonic log (DT)
7) Caliper log
8) Deep Laterolog (LLD
9) Shallow Laterolog (LLS)
10) Deep Induction Log (ILD)
11) Micro-spherically Focussed Log (MSFL)
12) Bit size
13) Integrated Volume (IHV)
14) Check shot Time (CHK)

The listed digitized wire-line log data on loading in PETREL are firstly corrected for depth with reference to KB (i.e. Kelly bushing- the height of the drilling floor above the ground level) and then displayed as log signatures in the WSW (i.e. well section window). The use of the histogram tab for the individual wire-line log data in the input panel function in PETREL allowed quick and proper estimation of maximum and minimum values for each log, in addition to a combined display of NPHI-RHOB, ILD, SFLU-MSFL and LLD-LLM-MSFL log signatures, possible through the use of the group panel function tab. Using the PETREL calculator function and syntax to run appropriate equations, quantitative operations are run on a combination of different input data listed above and results displayed as curves with distinctive colour fillings under assigned wells (i.e. E-L1, E-AH1, and E-BD2) in the Well Section Window. Detailed steps taken in calculating the listed log derived petrophysical properties and associated formulas are shown with a flow chart in Fig 5.1 and in Table 5.1. A more elaborate discussion is subsequently given showing clear descriptions of symbols and their respective units.

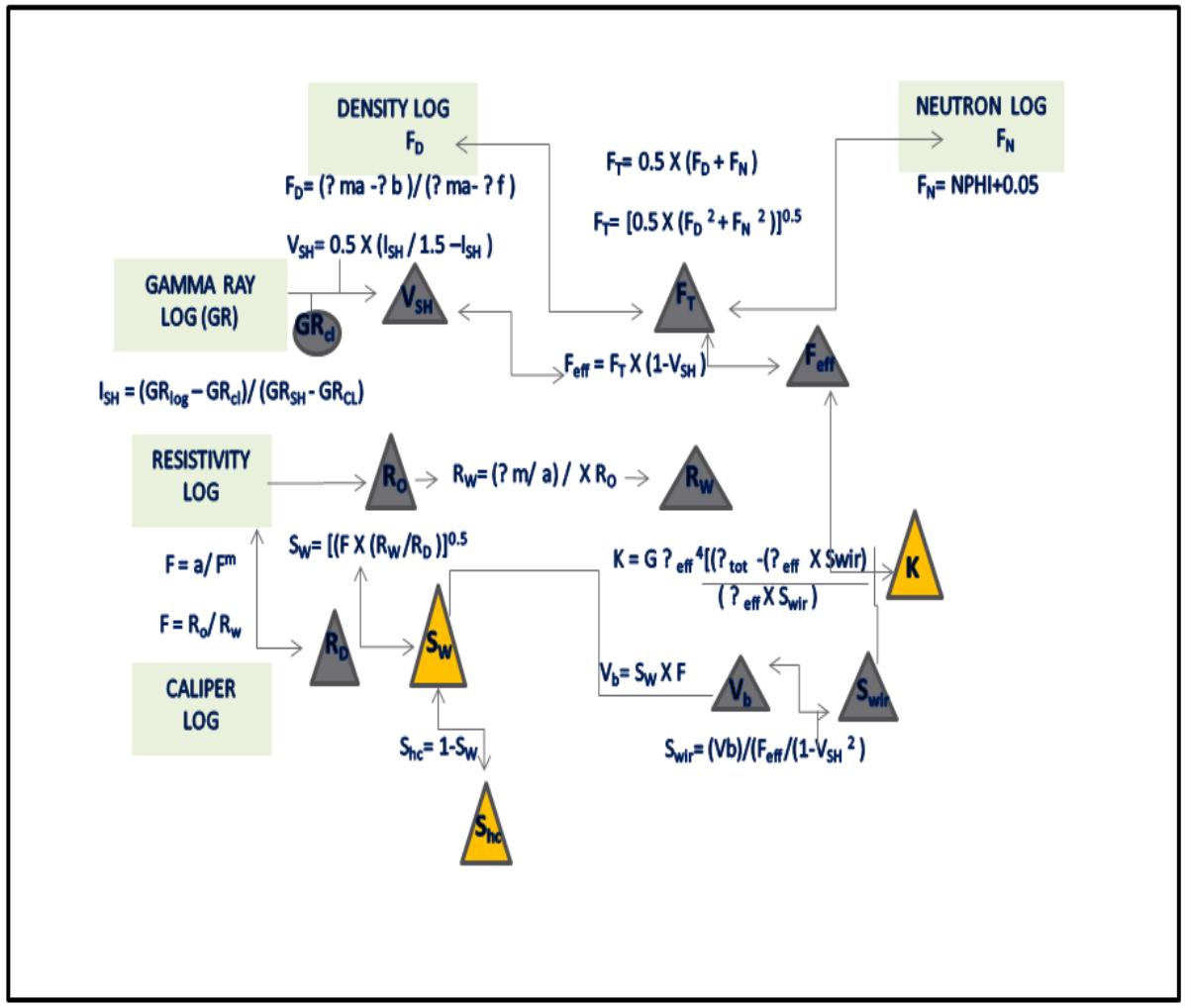

Symbol	Description	Unit
a	Saturation Exponent	constant
m	Porosity Exponent	constant
F	Formation Factor	constant
NPHI	Neutron Porosity	% or fraction
RHOB	Density Log	g /cm^3
F_D	Density Porosity	% or fraction
F_N	Neutron Porosity	% or fraction
F_T/F_{tot}	Total Porosity	% or fraction
F_{eff}	Effective Porosity	millidarcies
K	Permeability	millidarcies
G	Permeability Scale Factor	constant
?ma	Matrix/Grain Density	g /cm3
?b	Bulk Density	g /cm3
?f	Fluid Density	g /cm3
V_{SH}	Shale Volumne	fraction
I_{SH}	Gamma ray index	API
GR_{log}	GR value in zone of interest	API
GR_{cl}	GR value for sand basline	API
GR_{SH}	GR value for shale baseline	API
R_0	Resistivity of Brine-filled rock	OHM-M
R_W	Formation water resistivity	OHM-M
R_D	True formation resistivity	OHM-M
S_W	Water saturation	% or fraction
S_{HC}	Hydrocarbon saturation	% or fraction
S_{wirr}	Irreducible water saturation	% or fraction
V_b	Bulk volume of water	fraction

Figure 5.1: The petrophysical analysis flow chart and associated nomenclatures generated for this study.

Table 5.1: Calculated log derived petrophysical properties and corresponding formulas.

Derived parameters	Discussion	Formula
Volume of Shale V_{sh} or Vshale	This provides an estimate of the shale volume within the WBRED reservoir and it is derived from the (GR) log of the selected cored wells. The Steiber method is chosen among the few equations available for calculating the V_{sh} mainly to its advantage of suppressing high responses of (GR) log to little amount of shale.	V_{sh}= Ish/3-(2I_{sh})
Gamma-ray index I_{sh}	Its offers the first step into determining the volume of shale within the WBRED reservoir interval and also expresses the linear scaling of the (GR) log between the (GR) max and (GR) min values. It ranges from 0 to 1.	I_{sh}=(GR_{log}- GR_{cl})/(GR_{sh}- GR_{cl}) GR_{cl}- Gamma ray value of clean sand GR_{sh}-Gamma ray value of shale
Porosity	The porosity within the WBRED reservoir formation interval is obtained from recorded porosity logs in calibration with core porosity of the selected cored wells. The porosity logs are density and neutron logs.	Density porosity F_D= (? ma- ?b)/(?ma -?f) ?=density Neutron porosity F_N = NPHI +0.05 Total porosity is estimated by $F_T = 0.5 x(F_D + F_N)$ or $F_T = [0.5 x(F_D^2 + F_N^2)]^{0.5}$ in gas zones Effective porosity (F_{eff}) based on use of Steiber method $F_{eff} = F_T x (1-V_{sh})$ Where NPHI is the Neutron Porosity Hydrogen Index ?ma= Matrix (or grain) density ?b=Bulk density ?f = fluid density Fresh water mud, ?f =1.0g/cm^3 Saltwater mud, ?f =1.1g/cm^3 Gas mud, ?f =0.7g/cm3 With 10% porosity Sandstone ?ma= 2.65g/cm^3 Limestone ?ma= 2.71g/cm^3 Dolomite ?ma=2.87g/cm^3
Formation Resistivity (R_D, R_S)	There are quite a number of methods for computing formation water resistivity but for this study, Rw was analysed using a water zone approach and verified with the calculated Rw given in the SCAL data. This involved back calculation of R_w@FT from log data of selected wells within the WBRED reservoir formation interval in a non shaly zone using the relationship between the formation factor and shale free, water filled rock. Using R_w method (FT – formation temperature)	F= R_o/R_w **F**= a/F^m F= Formation factor R_o= Resistivity of the formation @100% formation water saturation a= Saturation exponent m=porosity exponent **F**= porosity a = 0.81 for tight sandstones (F < 15%), 0.62 for porous sandstones (F > 15%). m = 2.00 for tight sandstones (F < 15%), 2.15 for porous sandstones (F > 15%) For carbonates, ‘a’ and ‘m’ values are 1.00 and 2.00 respectively.
Water Saturation S_w	Kamel and Mabrouk (2002) expressed that in a typical hydrocarbon bearing reservoir rock, 100% hydrocarbon saturation is not possible. Often reservoir rock pores contain formation water and hydrocarbons. In estimating water saturation within the WBRED reservoir formation a number of available empirical formulations for water saturation (i.e. Archie, Indonesia and Simandoux equation) was calculated and compared in order to compensate for the shaly formation evident within each reservoir unit interval. Besides, each method was overlaid upon available core derived water saturation values to see best fit. The Indonesian equation is selected as it provided better characterization of the water saturation. In order to examine and determine accurately m and n exponents for water saturation calculations the Pickett plot was applied. Pickett plot-resistivity vs. porosity.	Archie= (0.81*Rw/ILD)/ Feff Modified Simandoux =(0.5*Rw/Feff ^ m)*((4*Feff ^ m)/(Rw*ILD)+(Vsh /Rsh)^ 2)^(1/n)-Vsh/Rsh Rsh=Shale resistivity (ohm-m) Indonesia=√(1/RT)/(Vsh^(1-0.5*Vsh)/√(Rsh)+√Feff^ m/(a*Rw)))
Net pay	Defined as the thickness of a rock, contributing significantly to economic viable production based on today’s technology, today’s prices and today costs (Crain petrophysical handbook , 2008) A porosity cuttoff of 10% was used with a shale volume cut off 40% to define the quality of the reservoir rock. In addition a cuttoff value of 65% for S_w was used to define pay.	Cuttoffs Applied: 1: If (V_{sh} <= V_{sh}max) *F_{eff} >= F_{eff} min) * (S_w <= S_w max) * (K>= Kmin) = 1 2: Then Pay flag = 1 3: Else Pay flag = 0 4: Hnet = Sum (Pay flag * Thick) Range : Vshmax = 0.25 – 0.40 F_T min = 0.03 – 0.19 S_w max = 0.30 – 0.70 Kmin = 0.1 – 5.0 md

Table 5.1: Calculated log derived petrophysical properties and corresponding formulas (continued from page 86).

Derived parameters	Discussion	Formula
Hydrocarbon Saturation S_{hc}	This express the fraction of pore volume filled with hydrocarbons (oil or gas)	$S_{HC}= 1-S_w$
Bulk Volume of water (BVW)	This is the percentage of the total rock volume that is occupied by water. A critical component used in estimating fluid mobility in the reservoir.	BVW= Sw x F
Irreducible Water Saturation S_{wir}	This is the percentage of the total rock volume that is occupied by water that is bound to the rock matrix by capillary forces. Critical input in the calculation/estimation of permeability.	$S_{wirr}=(V_b)/(Feff/(1-Vsh^2))$
Permeability (K)	Estimations permeability of selected reservoir rocks are calculated using Coates simplified method and calibrated with core derived permeability model. This method works much better in shaly sands (Crain, 2004).	$K=G?\ eff^4\ [(? tot – (? eff X Swir))]^2 / (? eff X Swir)$
Reflection coefficient	Reflection coefficient is considered synonymous with reflectivity; however, it is defined as the ratio of amplitude of the reflected wave to the incident.	R= (?2V2-?V1)/(?2V2+?1V1) R=reflection coefficient ?1= density of medium 1 ?2= density of medium 2 V1=Velocity of medium 1, V2= Velocity of medium 2
Synthetic Seismogram (SSG)	This illustrate a one dimensional acoustic energy profile travelling through layers of the earth, however, generated for the sole reasoning of improving interpretation by comparing and correlating picked marker beds on well logs to major observed reflections on seismic. For this study, convolving the reflectivity derived from digitized acoustics and density logs with extracted representative wavelet obtained from seismic data generates the synthetic seismogram in each selected well.	R(t) * W(t) = S(t) S(t) = seismic trace W(t)= wavelet R(t)=reflectivity (Reflection coefficient) * = convolution

5.2.2 Log derived petrophysical properties of (WBRED reservoir) in well E-L1

The calculated petrophysical properties of the identified reservoir units in well E-L1 are displayed as composite logs in the Well section window panel offered in PETREL (Fig 5.2). In addition, sampled data values are presented in (Table 5.2).

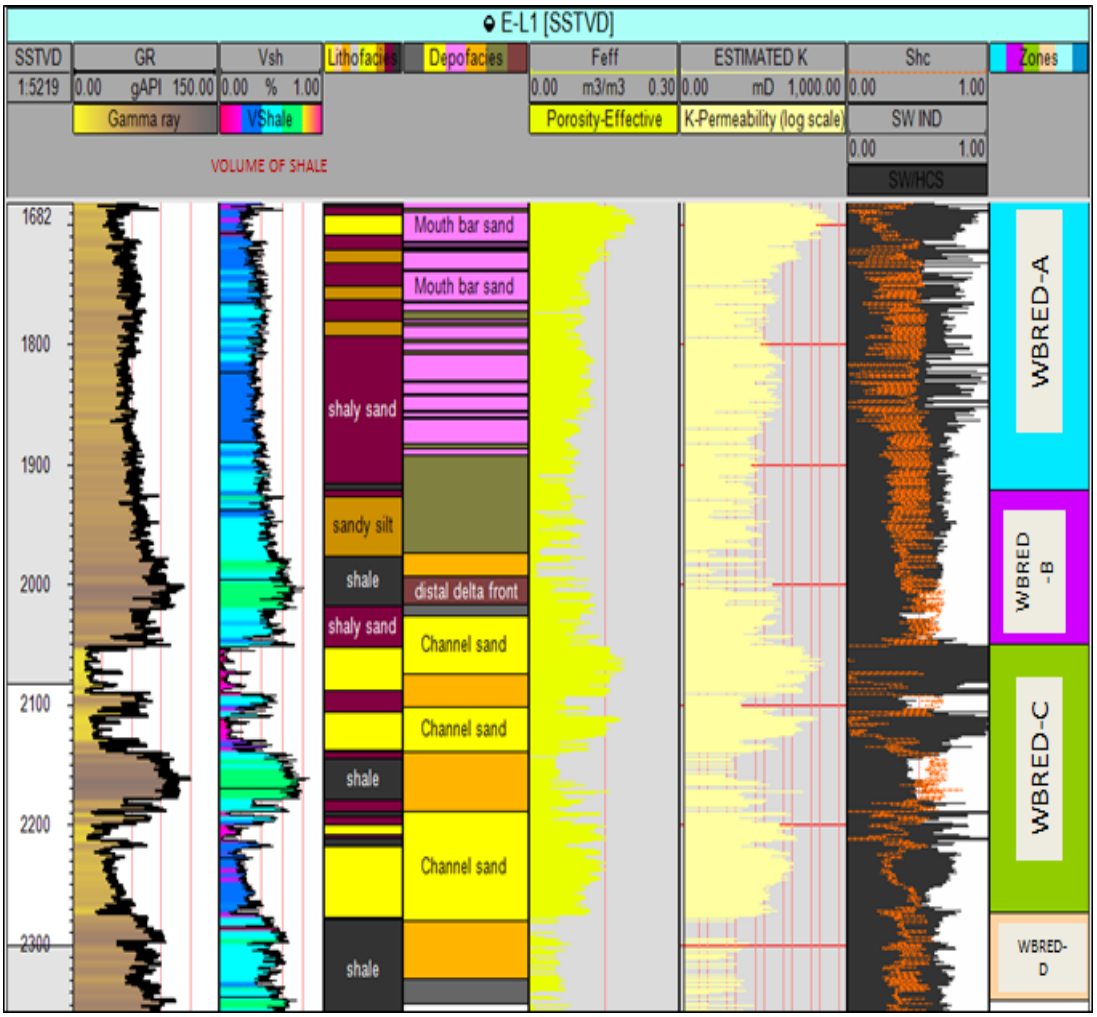

Figure 5.2: Logs of derived petrophysical properties within the defined stratigraphic reservoir unit intervals in well E-L1 as generated in PETREL.

5.2.3 Log derived petrophysical properties of (WBRED reservoir) in well E-AH1

The identified stratigraphic reservoir units in well E-AH1 together with calculated petrophysical properties are displayed as composite logs in the Well section window panel offered in PETREL (Fig 5.3). In addition, sampled data values of log derived petrophysical are presented in (Table 5.3 and Table 5.4).

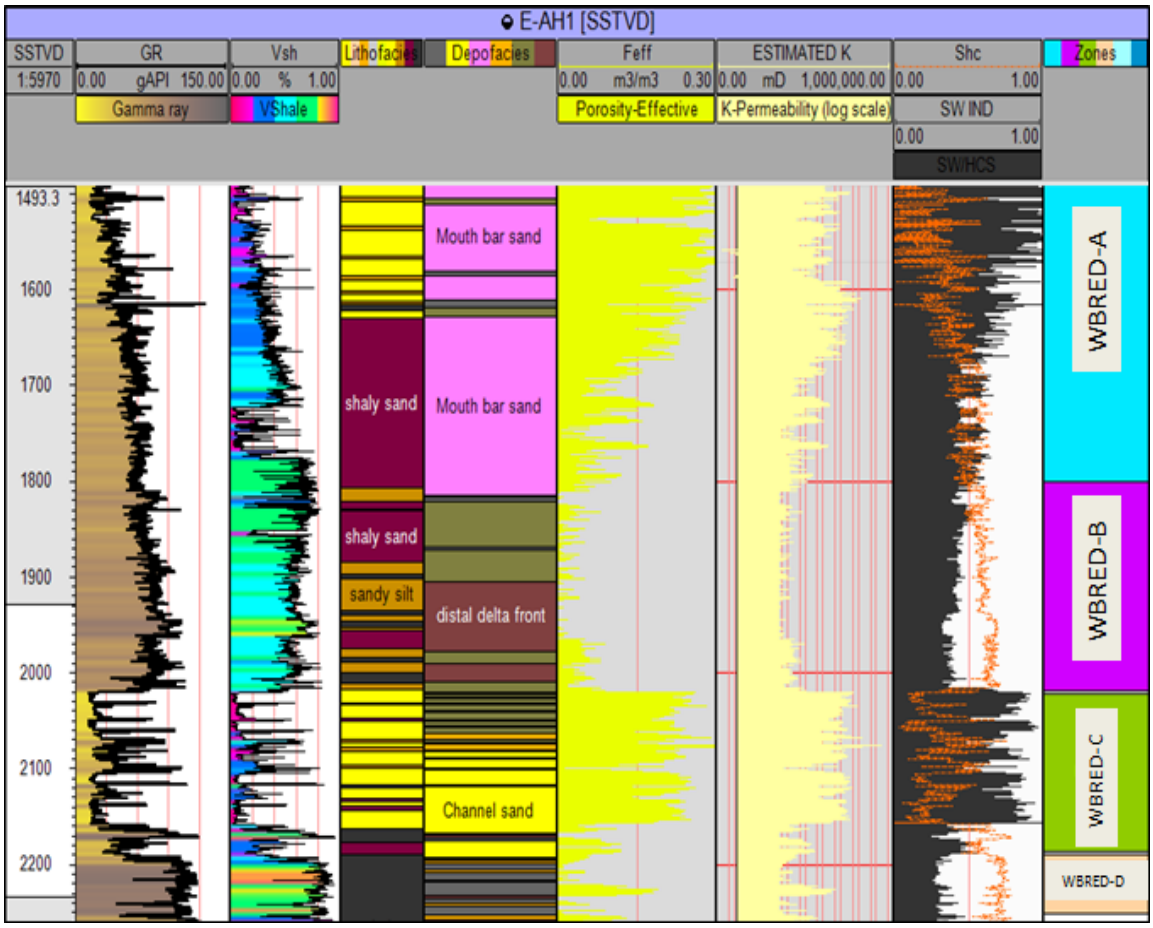

Figure 5.3: Logs of derived petrophysical properties within the defined stratigraphic reservoir unit intervals in well E-AH1 as generated in PETREL.

5.2.4 Log derived petrophysical properties of (WBRED reservoir) in well E-BD2

The calculated petrophysical properties of identified reservoir units in well E-BD2 are displayed as composite logs in the Well section window panel offered in PETREL (Fig 5.4) Sampled log data values of selected petrophysical properties (i.e. effective porosity, permeability and hydrocarbon saturation) (Tables 5.5 and 5.6).

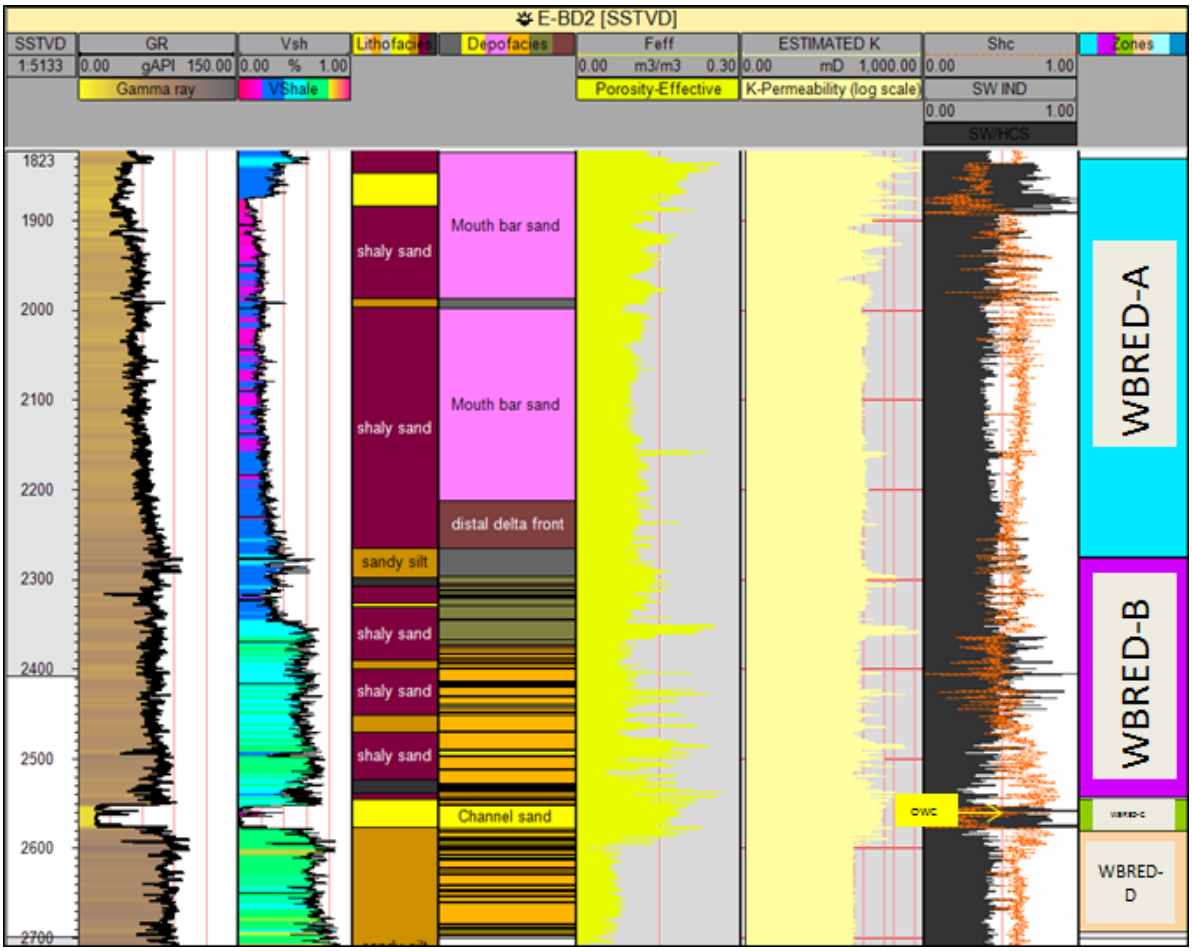

Figure 5.4: Logs of derived petrophysical properties within the defined stratigraphic reservoir unit intervals in well E-BD2 as generated in PETREL. Marked by the yellow arrow is the oil water contact (OWC) for the WBRED-C unit.

5.2.5 Porosity-permeability relationship of reservoir units

The proof of a quantitative log analysis is the degree of core-log data match. For this study, after matching core-log depth, a multi-well cross-plot of (core porosity and core permeability) of the three cored wells is prepared. The data are obtained from special and routine core analysis laboratory results.

The data results are sorted based on each selected well and used to establish poro-perm relationships for the individual facies created within the respective reservoir units in determining the perfect regression line to correct log derived petrophysical results (i.e., porosity, permeability and water saturation) against RCAL (routine core analysis data) for the studied log interval (Figs 5.5 and 5.6). In addition, quantify associated uncertainties attached to log derived petrophysical properties. Results obtained generate correlation coefficient values showing good relationship of core porosity and permeability, suggesting reservoir units are permeable and have porosities that are in communication. Examples of an overlay of core porosity, permeability and water saturation to log derived porosity and permeability is shown in (Fig 5.7). A linear plot of core porosity versus corresponding log porosity is shown in (Figure 5.8). All core data values associated with (Figs 5.7 and 5.8) and poro-perm plot per well is presented in APPENDIX E.

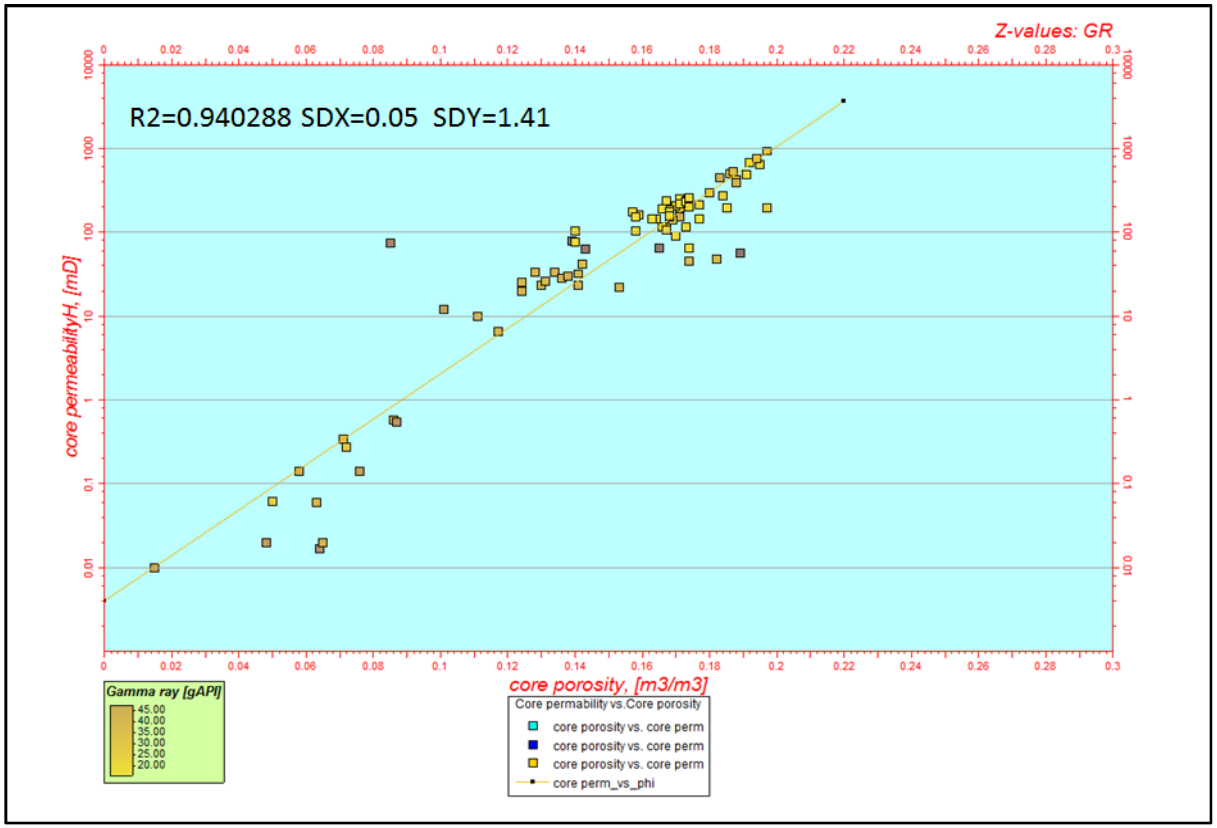

Figure 5.5: Multi-well cross plot for core porosity, core permeability and gamma ray values for well (E-L1, E-AH1, and E-BD2).

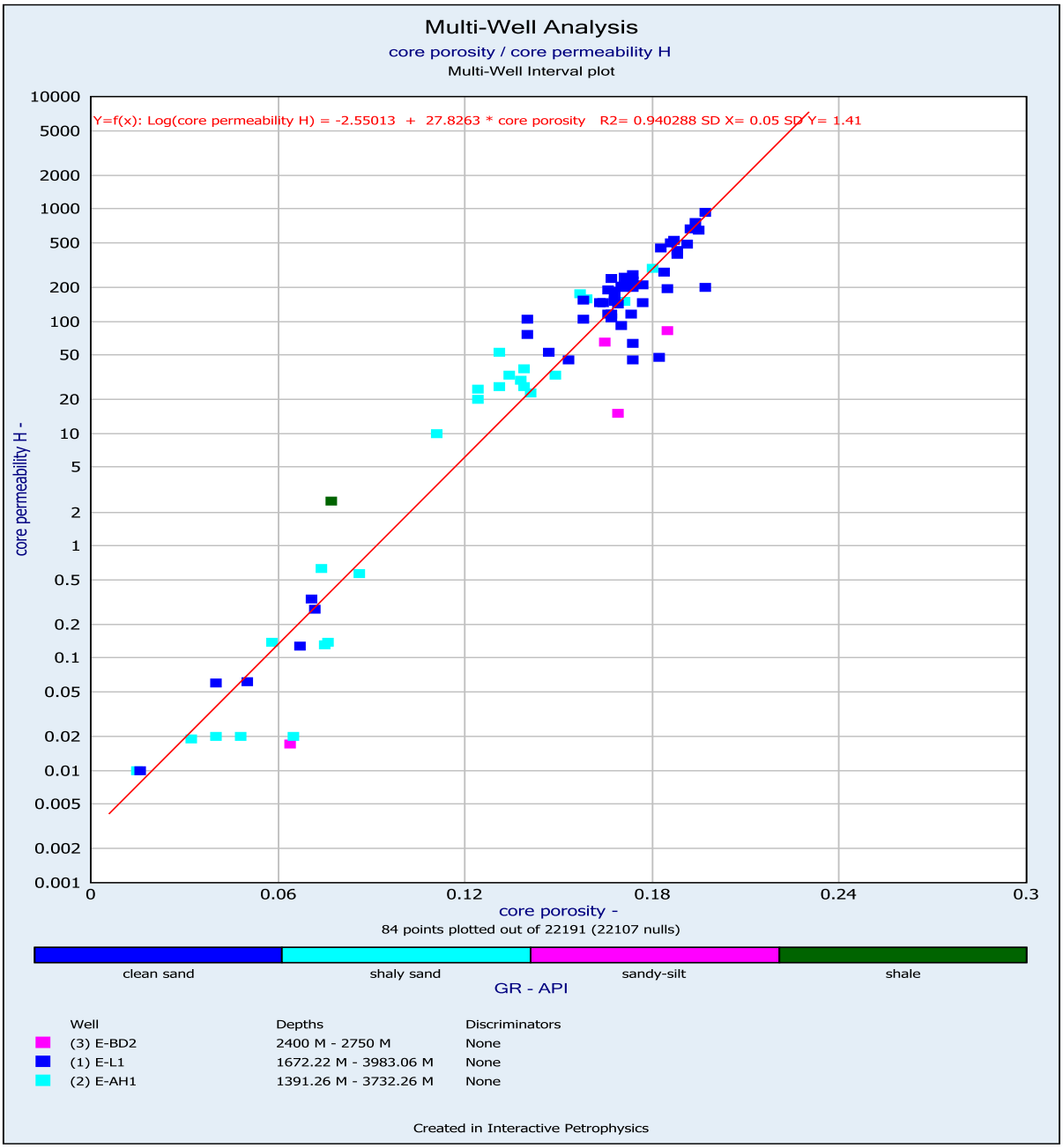

Figure 5.6: Multi-well cross plot for core porosity, core permeability and lithofacies for the selected wells (E-L1, E-AH1, and E-BD2). Excellent relationship is observed between both core porosity and core permeability, indicating very good reservoir quality.

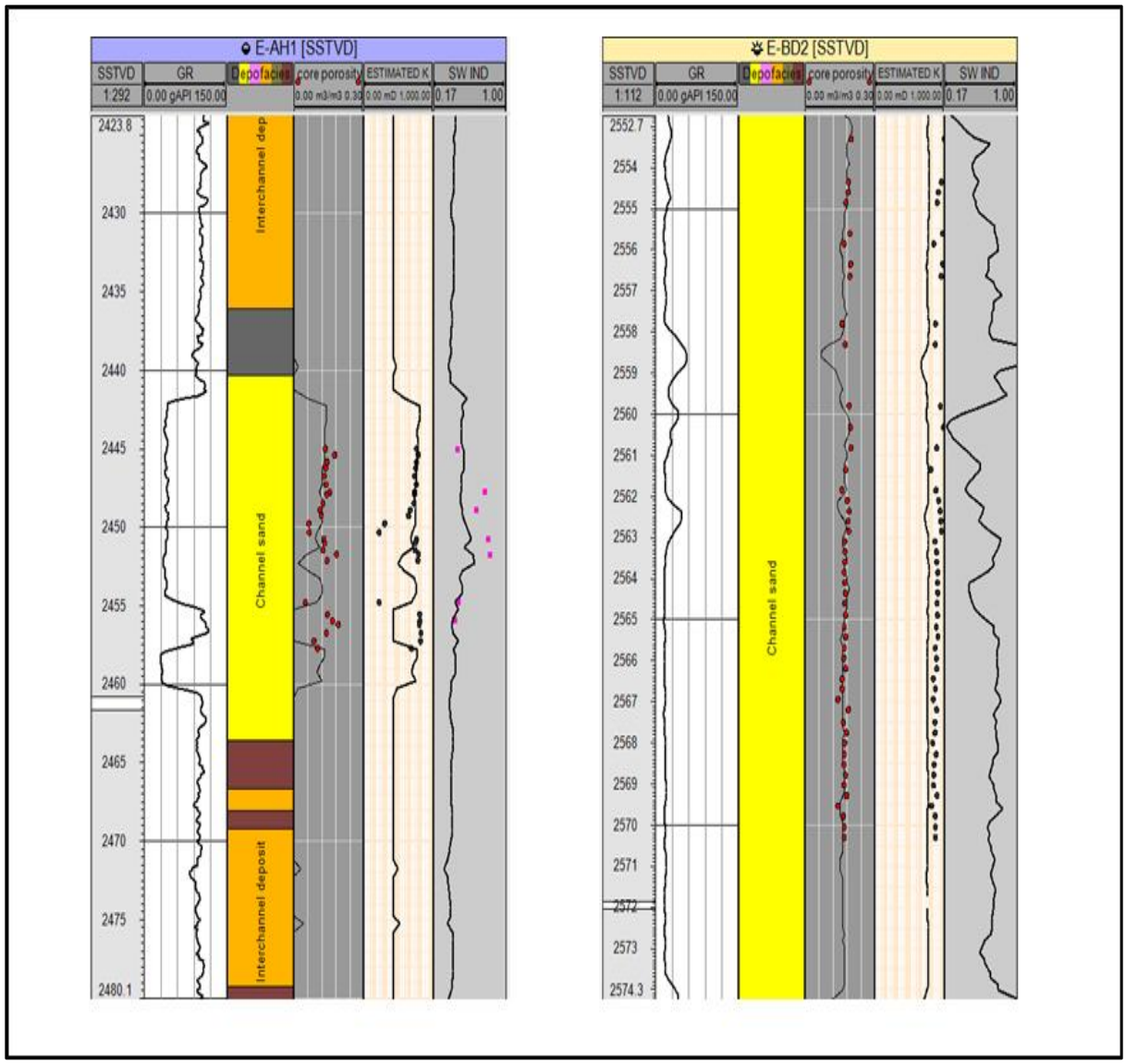

Figure 5.7: Example of log overlays of core analysis petrophysical properties (porosity, permeability and water saturation) against log derived petrophysical properties (effective porosity, permeability and water saturation) for wells E-AH1 and E-BD2. A good match to near fit of (core porosity/calculated log porosity) and (core permeability and estimated log permeability) is observed. The red, black and pink dots represent core analysis values of porosity, permeability and water saturation respectively.

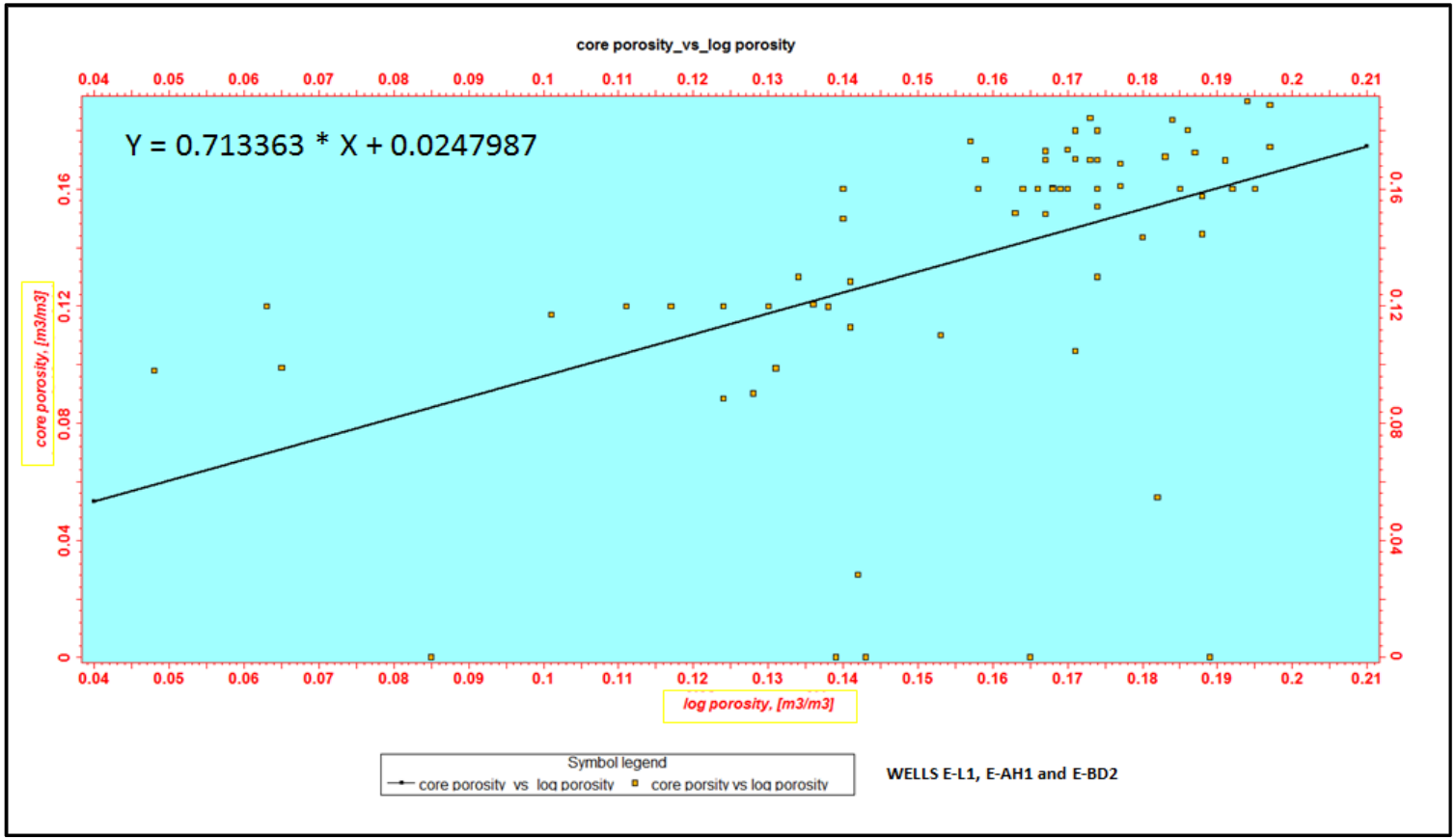

Figure 5.8: Core porosity data vs. log derived porosity, a strong linear relationship is evident between the two variables, confirming better constrain of log derived data to core data throughout the studied log intervals.

Table 5.2: SAMPLED DATA OF LOG DERIVED PETROPHYSICAL PROPERTIES OF IDENTIFIED RESERVOIR UNITS IN WELL E-L1.

MD (m)	F_{tot} (fraction)	F_{eff} (fraction)	S_{hc} (fraction)	K (md)
1672.22	0.0464	0.0462	0.5617	0.0023
1687.45	0.0533	0.0531	0.9811	0.0033
1702.68	0.3816	0.3799	0.4086	71.3329
1717.91	0.3891	0.3876	0.1858	39.2982
1733.14	0.39	0.3885	0.3812	34.0088
1748.37	0.3843	0.3829	0.5042	20.0356
1763.6	0.3894	0.388	0.5633	21.0148
1778.83	0.2767	0.2758	0.6216	2.6216
1794.06	0.3598	0.3586	0.5906	12.6364
1809.29	0.3518	0.3506	0.628	10.8643
1824.52	0.3492	0.348	0.6239	10.3434
1839.75	0.3707	0.3694	0.551	15.4324
1854.98	0.3628	0.3616	0.5715	13.3752
1870.21	0.3562	0.355	0.5366	12.1089
1885.44	0.104	0.1039	0.6998	0.5439
1900.67	0.3221	0.321	0.6793	6.25
1915.9	0.3658	0.3638	0.6754	0.5618
1931.13	0.362	0.3607	0.6662	12.7911
1946.36	0.3174	0.3163	0.6783	5.6944
1961.59	0.2826	0.2816	0.6879	2.9029
1976.82	0.3204	0.3193	0.6383	6.1217
1992.05	0.3146	0.3135	0.6912	5.398
2007.28	0.2889	0.2879	0.6822	3.2848
2022.51	0.386	0.3844	0.6746	41.6447
2037.74	0.3835	0.3819	0.6627	51.3106
2052.97	0.2734	0.2725	0.6838	2.4213
2068.2	0.2096	0.209	0.6973	1.3017
2083.43	0.3013	0.3003	0.1025	5.0229
2098.66	0.3141	0.313	0.3552	6.1585
2113.89	0.2999	0.2989	0.1993	4.7571
2129.12	0.2117	0.2111	0.6089	0.6178
2144.35	0.2959	0.295	0.1994	4.4056
2159.58	0.2326	0.2318	0.5078	1.0482
2174.81	0.1771	0.1765	0.7839	0.2491
2190.04	0.3358	0.3346	0.6695	8.0489
2205.27	0.2324	0.2316	0.6874	0.9842
2220.5	0.2464	0.2456	0.6872	1.3598
2235.73	0.2924	0.2914	0.3853	3.8631
2250.96	0.2822	0.2813	0.4282	3.1238
2266.19	0.3292	0.3281	0.4204	7.6861
2281.42	0.2704	0.2695	0.5846	2.3328
2296.65	0.2422	0.2414	0.618	1.2677
2311.88	0.1949	0.1942	0.7103	0.4039
2327.11	0.2368	0.236	0.6811	1.095
2342.34	0.2434	0.2426	0.688	1.2732
2357.57	0.2081	0.2074	0.676	0.5631
2372.8	0.3264	0.3253	0.6651	6.7584
2388.03	0.2662	0.2653	0.6347	2.1055

Table 5.3: SAMPLED DATA OF LOG DERIVED PETROPHYSICAL PROPERTIES OF IDENTIFIED RESERVOIR UNITS IN WELL E-AH1.

MD (m)	F_{tot} (fraction)	F_{eff} (fraction)	S_{hc} (fraction)	K (md)
1699.761	0.1749	0.1653	0.5542	33.9613
1700.261	0.129	0.1194	0.5714	20.7553
1708.761	0.1302	0.1204	0.574	20.6375
1717.261	0.0584	0.0458	0.5585	43.4423
1725.761	0.1305	0.1206	0.5007	45.0158
1734.261	0.0911	0.0829	0.5615	9.222
1742.761	0.13	0.121	0.4433	32.4956
1751.261	0.0132	0.0001	0.5216	5.3545
1759.761	0.1067	0.0966	0.5686	24.9026
1768.261	0.0583	0.0469	0.5573	19.2474
1776.761	0.0803	0.069	0.6019	29.4982
1785.261	0.0497	0.0378	0.585	22.3814
1793.761	0.0828	0.072	0.6155	9.1046
1802.261	0.0907	0.0808	0.5929	20.1729
1810.761	0.0451	0.0328	0.6053	22.4772
1819.261	0.0804	0.0714	0.6029	15.7479
1827.761	0.0496	0.0389	0.5445	16.7656
1836.261	0.0586	0.0484	0.5562	7.8632
1844.761	0.0129	0.0001	0.6239	5.6601
1853.261	0.0362	0.0264	0.588	4.9162
1861.761	0.034	0.0257	0.6161	2.4513
1870.261	0.0192	0.0061	0.5871	13.0137
1878.761	0.0315	0.0198	0.6121	10.9394
1887.261	0.0253	0.0129	0.6226	7.7853
1895.761	0.0499	0.0374	0.5995	6.2708
1904.261	0.0157	0.0001	0.6156	9.1566
1912.761	0.0136	0.0001	0.6139	7.5992
1921.261	0.017	0.0001	0.6063	6.5537
1929.761	0.016	0.0001	0.6189	11.4492
1938.261	0.0145	0.0001	0.5897	8.4793
1946.761	0.0157	0.0001	0.5819	8.7489
1955.261	0.0143	0.0001	0.5898	8.5034
1963.761	0.0155	0.0001	0.5622	7.5131
1972.261	0.018	0.0001	0.5834	4.2339
1980.761	0.0167	0.0001	0.4504	6.1559
1989.261	0.0151	0.0001	0.523	6.8104
1997.761	0.0521	0.0412	0.5232	3.6462
2006.261	0.044	0.0337	0.5183	2.8182
2014.761	0.0441	0.0312	0.5882	3.277
2023.261	0.0175	0.0001	0.5703	3.559
2031.761	0.0831	0.0694	0.478	1.205
2040.261	0.0182	0.0001	0.4994	1.5523
2048.762	0.2473	0.2455	0.4744	272.8044
2057.262	0.238	0.2371	0.4788	165.5411
2065.762	0.2069	0.2055	0.55	108.941
2074.262	0.1925	0.1861	0.5449	86.018
2082.762	0.2233	0.222	0.5944	209.0602
2091.262	0.231	0.2294	0.5981	218.1795
2099.762	0.0155	0.0001	0.624	2.1969
2108.262	0.0549	0.0425	0.5729	19.4955
2116.762	0.1764	0.1742	0.4999	62.3597
2125.262	0.1421	0.1356	0.5346	74.5014
2133.762	0.2272	0.226	0.5858	189.237
2142.262	0.2435	0.2414	0.5357	399.4822
2150.762	0.2368	0.2343	0.5431	333.4272

Table 5.4: SAMPLED DATA OF LOG DERIVED PETROPHYSICAL PROPERTIES OF IDENTIFIED RESERVOIR UNITS IN WELL E-AH1.

MD (m)	F_{tot} (fraction)	F_{eff} (fraction)	S_{hc} (fraction)	K (md)
2159.262	0.2334	0.2318	0.5155	249.765
2167.762	0.2157	0.2141	0.496	163.9001
2176.262	0.23	0.2281	0.5273	182.8827
2184.762	0.0533	0.0485	0.5334	2.7469
2193.262	0.0155	0.0001	0.5345	6.3879
2201.762	0.0844	0.0795	0.5461	11.1914
2210.262	0.0679	0.0593	0.5672	7.4493
2218.762	0.0444	0.0328	0.6135	2.0113
2227.262	0.02	0.0001	0.4678	1.2865
2235.762	0.0223	0.0001	0.6251	1.0129
2244.262	0.0218	0.0001	0.5569	3.8106
2252.762	0.1507	0.1336	0.5041	132.02
2261.262	0.0195	0.0001	0.5012	35.2917
2269.762	0.018	0.0001	0.5478	1.8946
2278.262	0.0207	0.0001	0.5408	40.2288
2286.762	0.0239	0.0001	0.5067	26.1
2295.262	0.0214	0.0001	0.5454	1.1595
2303.762	0.017	0.0001	0.5249	1.0115
2312.262	0.022	0.0001	0.5223	1.083
2320.762	0.0189	0.0001	0.5252	18.6807
2329.262	0.0152	0.0001	0.5194	3.2538
2337.762	0.0174	0.0001	0.5247	2.0056
2346.262	0.0222	0.0001	0.5022	1.0095
2354.762	0.1037	0.0998	0.5794	10.9706
2363.262	0.0197	0.0001	0.5401	1.0095
2371.762	0.021	0.0001	0.5424	2.2732
2380.262	0.1067	0.0945	0.5806	23.1921
2388.762	0.1458	0.1424	0.5637	31.4491
2397.262	0.0212	0.0001	0.625	1.0095
2405.762	0.0237	0.0001	0.6044	25.8045
2414.262	0.0242	0.0001	0.6116	4.7919
2422.762	0.0221	0.0001	0.5888	1.5088
2431.262	0.0208	0.0001	0.6197	1.0496
2439.762	0.0203	0.0001	0.61	2.0635
2448.262	0.0277	0.0084	0.6525	85.53
2456.762	0.0196	0.0001	0.6632	6.6571
2465.262	0.018	0.0001	0.6468	2.2157
2473.762	0.1193	0.1125	0.6519	20.433
2482.262	0.0227	0.0001	0.6553	2.9875
2490.762	0.0192	0.0001	0.6633	1.9942
2499.262	0.0194	0.0001	0.5956	2.043
2507.762	0.0202	0.0001	0.6719	2.9748
2516.262	0.0193	0.0001	0.6572	2.0842
2524.762	0.0234	0.0072	0.6513	1.9027
2533.262	0.0234	0.0072	0.6639	1.5261
2541.762	0.0234	0.0072	0.6508	3.1134
2550.262	0.0234	0.0072	0.6126	1.9885
2558.762	0.0234	0.0072	0.5499	1.8103

Table 5.5: SAMPLED DATA OF LOG DERIVED PETROPHYSICAL PROPERTIES OF IDENTIFIED RESERVOIR UNITS IN WELL E-BD2.

MD (m)	F_{tot} (fraction)	F_{eff} (fraction)	S_{hc} (fraction)	K (md)
1842.0966	0.2043	0.1997	0.1983	49.1072
1842.2491	0.2082	0.2031	0.2316	50.4522
1849.8741	0.1331	0.1209	0.6845	14.1169
1857.4991	0.1786	0.161	0.6908	19.467
1865.1241	0.2174	0.2072	0.3153	43.5659
1872.7491	0.2051	0.1943	0.3815	36.5759
1880.3741	0.1943	0.1844	0.3786	33.6053
1887.9991	0.1862	0.176	0.4142	29.9594
1895.6241	0.2007	0.1909	0.4135	37.0141
1903.2491	0.1138	0.108	0.0641	14.5927
1910.8741	0.1451	0.1361	0.2917	18.5135
1918.4991	0.1822	0.1759	0.2228	33.9731
1926.1241	0.1426	0.1314	0.6251	16.7542
1933.7491	0.101	0.0896	0.6364	9.4711
1941.3741	0.1352	0.1262	0.4412	16.431
1948.9991	0.1756	0.16	0.5724	20.0978
1956.6241	0.1441	0.1305	0.6802	15.2146
1964.2491	0.1381	0.1232	0.6925	13.0856
1971.8741	0.1587	0.1463	0.6333	19.484
1979.4991	0.1317	0.1189	0.712	13.4681
1987.1241	0.1202	0.1044	0.6839	9.7685
1994.7491	0.1108	0.0973	0.7088	9.8484
2002.3741	0.1571	0.1412	0.6839	16.0325
2009.9991	0.1495	0.1382	0.5538	18.0238
2017.6241	0.1272	0.1099	0.7684	10.135
2025.2491	0.0823	0.0671	0.7952	6.1967
2032.8741	0.1346	0.1212	0.7194	13.6192
2040.4991	0.1293	0.1145	0.7293	11.8586
2048.124	0.0972	0.0851	0.7662	8.927
2055.749	0.0783	0.0666	0.7375	6.9928
2063.374	0.0881	0.0775	0.7324	8.4756
2070.999	0.1034	0.089	0.7568	8.5289
2078.624	0.124	0.1095	0.7384	11.2134
2086.249	0.0645	0.0536	0.7907	6.0971
2093.874	0.0856	0.073	0.7994	7.4395
2101.499	0.0945	0.0839	0.7701	9.3017
2109.124	0.0704	0.0583	0.7862	6.2252
2116.749	0.0942	0.0807	0.7705	7.9326
2124.374	0.0909	0.0782	0.7266	7.8558
2131.999	0.1002	0.0868	0.7539	8.6528
2139.624	0.1108	0.0968	0.7473	9.6408
2147.249	0.0972	0.0827	0.7511	7.8184
2154.874	0.1019	0.0871	0.7675	8.2377
2162.499	0.0864	0.0741	0.7237	7.5586
2170.124	0.1348	0.1174	0.7961	11.2864
2177.749	0.1034	0.0894	0.6851	8.6329
2185.374	0.108	0.0959	0.7249	10.2614
2192.999	0.1025	0.0892	0.72	8.9222
2200.624	0.1121	0.097	0.7175	9.2446
2208.249	0.1289	0.113	0.7096	11.0595
2215.874	0.1166	0.1026	0.6594	10.2208
2223.499	0.1265	0.1094	0.7311	10.1257
2231.124	0.0834	0.0702	0.6499	6.9095
2238.749	0.1307	0.114	0.7254	10.9333
2246.374	0.0967	0.0816	0.6598	7.4181
2253.999	0.1168	0.1024	0.6606	10.0892
2261.624	0.0819	0.0651	0.6653	5.6581
2269.249	0.1079	0.09	0.6697	7.4366
2276.874	0.0916	0.073	0.6794	5.8579
2284.499	0.0952	0.0749	0.7109	6.39
2292.124	0.1028	0.0843	0.6926	6.7569
2299.749	0.0991	0.0793	0.7371	6.0647

Table 5.6: SAMPLED DATA OF LOG DERIVED PETROPHYSICAL PROPERTIES OF IDENTIFIED RESERVOIR UNITS IN WELL E-BD2.

MD (m)	F_{tot} (fraction)	F_{eff} (fraction)	S_{hc} (fraction)	K (md)
2307.374	0.0765	0.0586	0.6322	4.9964
2314.999	0.0524	0.0303	0.7036	9.2348
2322.624	0.1254	0.1096	0.6788	10.5511
2330.249	0.0965	0.0762	0.6169	14.8444
2337.874	0.0746	0.0536	0.653	12.1644
2345.499	0.1281	0.1087	0.769	11.0483
2353.124	0.1196	0.1051	0.7054	10.5039
2360.749	0.1158	0.0961	0.6529	10.8929
2368.374	0.0922	0.0718	0.6935	6.4729
2375.999	0.0872	0.0702	0.7214	5.9845
2383.624	0.1035	0.0835	0.583	29.9784
2391.249	0.0875	0.0669	0.5381	9.818
2398.874	0.0753	0.0563	0.565	4.6651
2406.499	0.0582	0.0365	0.6307	4.7225
2414.124	0.0826	0.0656	0.5925	5.656
2421.749	0.0852	0.069	0.6062	6.0696
2429.374	0.0997	0.0827	0.5387	6.9888
2436.999	0.083	0.0623	0.6748	5.7684
2444.624	0.1185	0.099	0.612	7.8517
2452.249	0.0164	0.0001	0.5355	4.6651
2459.874	0.0858	0.0697	0.6226	6.1671
2467.499	0.1008	0.0822	0.7132	6.5874
2475.124	0.0758	0.0598	0.5898	5.4566
2482.749	0.0928	0.0757	0.6937	6.4059
2490.374	0.176	0.1579	0.7576	20.8989
2497.999	0.0645	0.0471	0.677	4.6651
2505.624	0.1237	0.1042	0.7633	14.0759
2513.249	0.0468	0.0244	0.5699	152.9003
2520.874	0.1011	0.0913	0.5329	10.2914
2528.499	0.0671	0.0458	0.8111	4.6651
2536.124	0.0367	0.0159	0.7871	4.6651
2543.749	0.0612	0.0404	0.8212	4.6651
2551.374	0.1143	0.0971	0.9043	8.5017
2558.999	0.0805	0.0633	0.8851	5.593
2566.624	0.088	0.0747	0.9039	7.3644
2574.249	0.1967	0.1793	0.8487	52.8735
2581.874	0.1704	0.1692	0.2596	39.1851
2589.499	0.1695	0.1674	0.233	36.7244
2597.124	0.1502	0.1476	0.3137	28.2158
2604.749	0.1865	0.1687	0.8493	61.5083
2612.374	0.0433	0.0206	0.812	5.9823
2619.999	0.0505	0.0283	0.8967	8.7226
2627.624	0.0285	0.0001	0.3	4.6651
2635.249	0.0374	0.0184	0.8538	4.6651
2642.874	0.0401	0.0171	0.7688	4.6651
2650.499	0.0639	0.045	0.7542	4.6651
2658.124	0.0698	0.0495	0.8131	4.6651
2665.749	0.0422	0.0194	0.8393	4.6651
2673.374	0.0424	0.0197	0.831	4.6651
2680.999	0.042	0.0192	0.7928	4.6651
2688.624	0.0344	0.0107	0.7579	5.0714
2696.249	0.0354	0.0119	0.787	4.6651

5.2.6 Petrophysics reservoir summary

Tables 5.7 to 5.10 present a tabulated summary of calculated reservoir petrophysical properties for each identified reservoir unit for this study.

WELL-E-L1

Table 5.7: Calculated petrophysical values for each identified reservoir unit in well-E-L1.

WBRED reservoir units	Top (m)	Bottom (m)	Gross thickness (m)	Net pay (m)	Average effective porosity (%)	Average permeability (mD)
WBRED-A	1672	1877	205	14	14	22
WBRED-B	1877	2017	140	0	0	0.2
WBRED-C	2017	2218	201	1.22	12	6
WBRED-D	2218	2339	121	0	0	2

WELL E-AH1

Table 5.8: Calculated petrophysical values for each identified reservoir unit in well-E-AH1.

WBRED reservoir units	Top (m)	Bottom (m)	Gross thickness (m)	Net Pay (m)	Average effective porosity (%)	Average permeability (mD)
WBRED-A	1620	2061	441	182	17	249
WBRED-B	2061	2245	184	115	20	689
WBRED-C	2245	2445	200	11	13	565
WBRED-C	2445	2564	119	14	13	5

WELL-E-BD2

Table 5.9: Calculated petrophysical values for each identified reservoir unit in well-E-BD2.

WBRED reservoir units	Top (m)	Bottom (m)	Gross thickness (m)	Net Pay (m)	Average effective porosity (%)	Average permeability (mD)
WBRED-A	1900	2294	394	42	13	15
WBRED-B	2294	2372	78	9	15	1117
WBRED-C	2372	2573	201	1	17	18
WBRED-D	2573	2700	127	3	20	11

All Wells- (E-L1, E-AH1, and E-BD2)

Table 5.10: Average poro-perm values for each identified reservoir unit (WBRED-A, WBRED-B, WBRED-C and WBRED-D).

WBRED reservoir units	Average effective porosity (%)	Average permeability (mD)
(WBRED-A)	15	95
(WBRED-B)	12	602
(WBRED-C)	14	196
(WBRED-D)	11	6

Table 5.11: Flow unit type description of the different identified reservoir units in the study area (Figures 5.9 and 5.10).

WBRED RESERVOIR UNITS	FLOW UNIT TYPE	NUMBER OF GEOLOGICAL LAYERS
WBRED-A	1,2,3	3
WBRED-B	4, 5, 6	3
WBRED-C	7,8,9	3
WBRED- D	10	1

5.3. Flow unit characterization of WBRED reservoir units

The significance of mapping portions or zoning a reservoir into flow units is aligned towards capturing consistent and predictable geological and petrophysical properties that affect the flow of fluids in different neighbouring reservoir rock volumes (Ebanks et al., 1992). To this end, the combination of qualitative geological facies and log derived petrophysical properties (porosity and permeability) are used as the basis for identifying and quantitatively characterizing flow unit types (Ebanks et al., 1992; Gunter et al., 1997). The flow unit types aid proper assignment of geological layering during the modelling of depositional lithofacies units.

For this study, the flow unit characterization of each reservoir unit involved the subdivision of log/core petrophysical data samples into units having similar predictable flow characteristics by combining porosity, permeability and bed thickness using simple cross-plotting techniques (i.e. SML plot). The SML plot is a cross plot of cumulative flow capacity (i.e. defined as the product of average permeability and thickness of an interval (Kh) versus cumulative flow storage (i.e. defined as the product of the average porosity and thickness of the same interval (φh).

5.3.1 Flow unit description for well E-L1, E-AH1 and E-BD2

Based on the SML plot together with interpreted geologic facies, ten flow unit types are defined in well E-L1, named from 1 to 10 (Figs 5.9A and 5.9B). Using this information, the defined flow units are correlated to the other two selected wells (E-AH1 and E-BD2) in the study area (Table 5.11). Also, considering the plot of cumulative flow storage versus cumulative flow capacity of the cored well E-L1, it is observed that shaly intervals plot low-angle to horizontal trending flowing units (i.e. flow unit 2, 3, 5, 6, 8 and 10), whereas, the defined flow units of the sandy intervals contribute significantly to the overall cumulative

flow storage and cumulative flow capacity as well as exhibiting steeper gradient-slope (Fig 5.9A; particularly flow units 1, 7 and 9).

5.4 Petrophysical models of WBRED reservoir units

The 3-D petrophysical models of the identified reservoir unit displays the distribution of selected upscaled petrophysical logs conditioned to existing 3-D facies model in the 3-D grid using the inbuilt sequential gaussian simulation method available in PETREL. Three petrophysical rock properties are modelled (i.e. effective porosity (F_{eff}), permeability (K) and water saturation (S_w).

Below in Figures 5.12 to 5.15 are the petrophysical models of WBRED reservoir units.

5.5 Discussion of petrophysical reservoir description results

Based on the respective petrophysical analysis of the reservoir units, it is observed that the WBRED-D presents the lowest average poro-perm results. The key control of effective porosity and permeability is the continuity and connectivity of the channel sands and inter-channel deposits. Effective porosity for the reservoir units ranges from (0.14-0.35) indicating moderate to very good reservoir quality, while permeability values ranges from (6mD - 602mD) attributing to well sorted sands. According to poro-perm results of the various reservoirs units it is determined that where there are increasing porosity values, permeabilities are equally high. Average water saturation values also range from 12% - 69%. Considering these end results and calculated reservoir units oil movability index (MHI) values suggest fairly to strong hydrocarbon potential and a reservoir system considered satisfactory for hydrocarbon production.

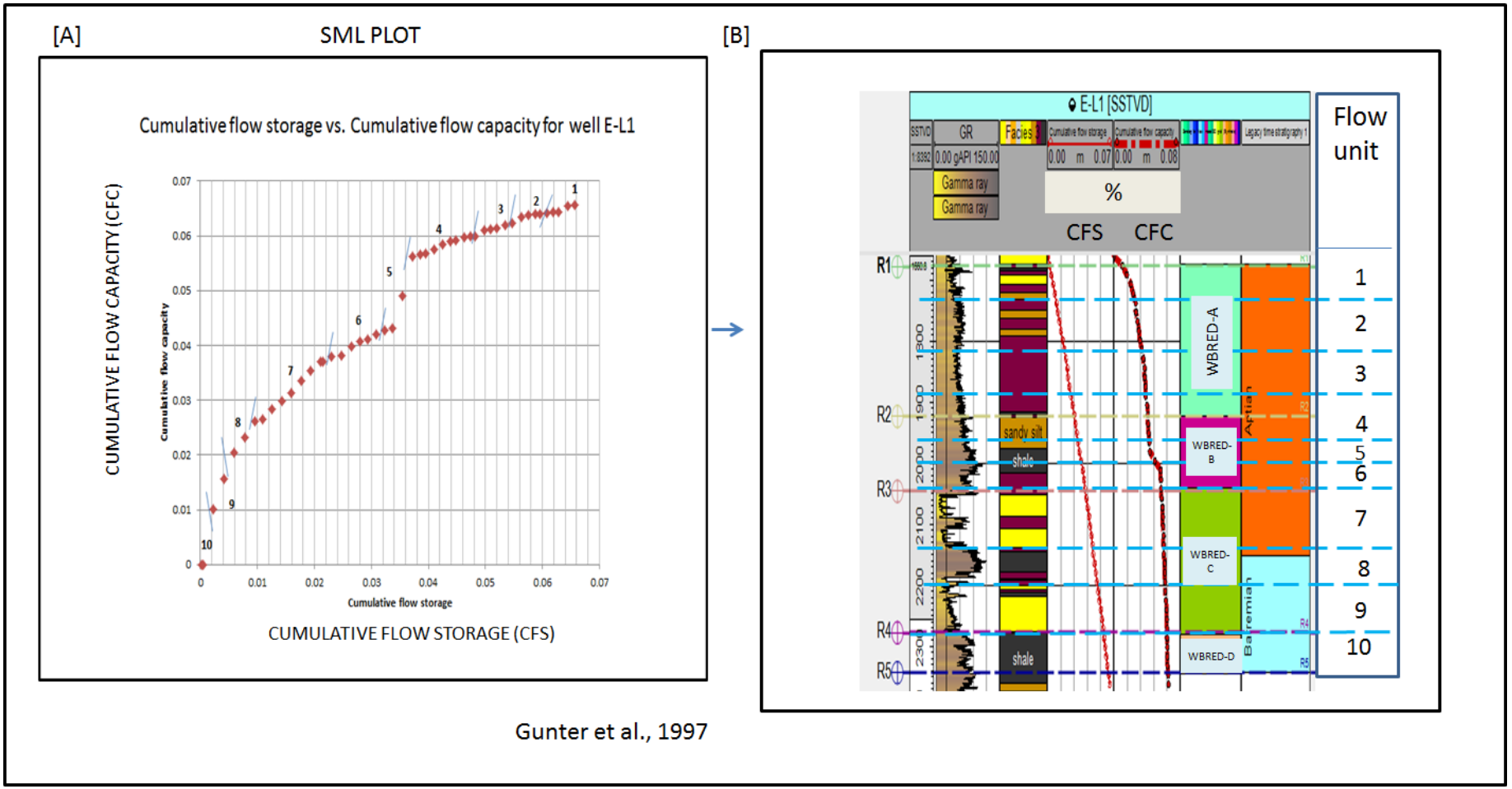

Figure 5.9: [A] - SML plots of cumulative flow capacity versus cumulative flow storage for well E-L1. Ten flow units are defined for the identified reservoir stratigraphic intervals on the basis of a combination geologic and petrophysical (i.e. porosity and permeability) values. [B] -Depth plot of gamma ray log, interpreted facies, cumulative flow storage log, cumulative flow capacity log and zone log for the WBRED stratigraphic reservoir unit intervals for well E-L1.

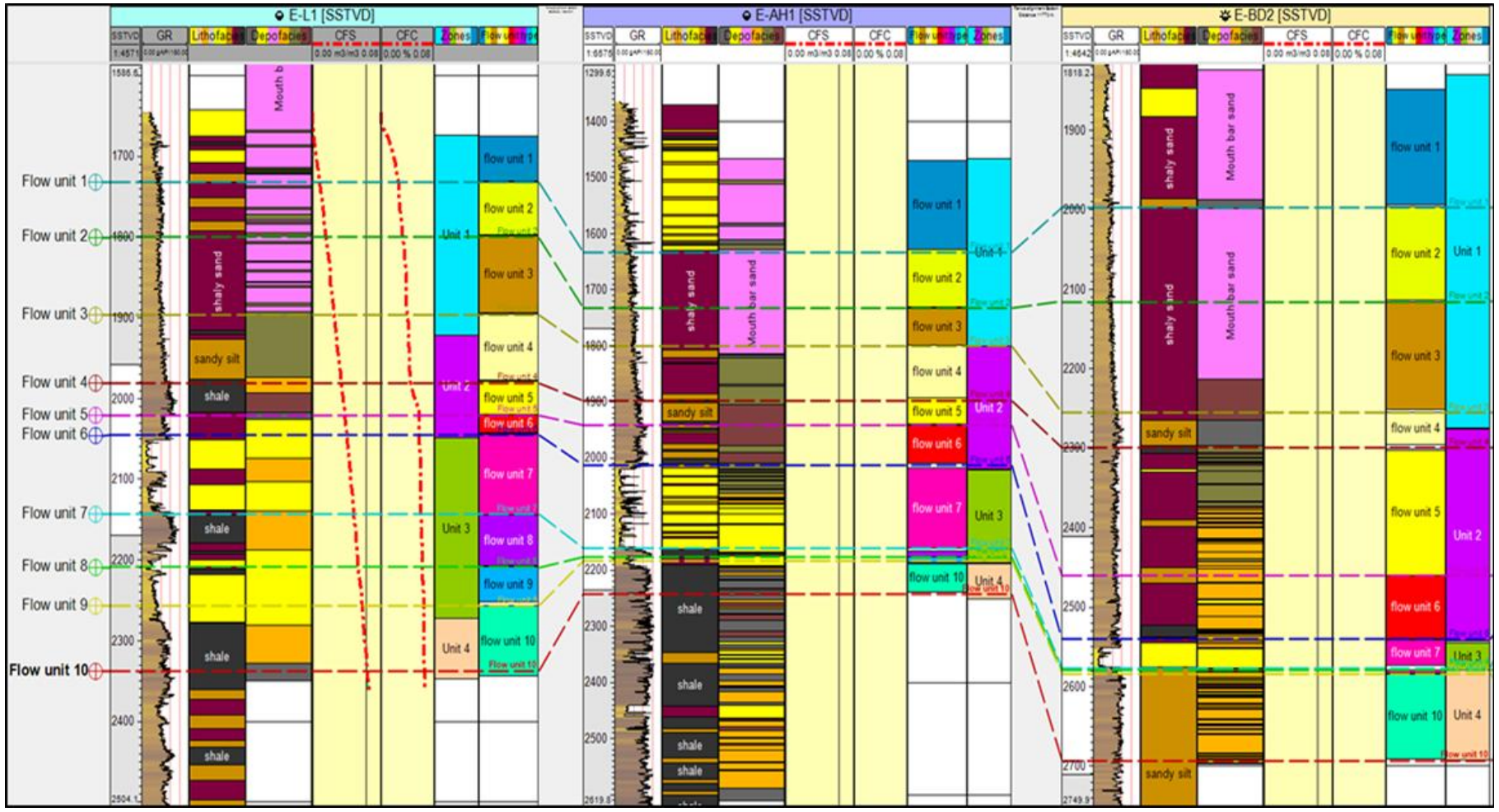

Figure 5.10: Flow unit characterizations of identified reservoir units showing depth- gamma ray log, facies log, cumulative flow storage log (CFS) and cumulative storage flow capacity log (CFC) of well E-L1 correlated with well E-AH1 and E-BD2. The ten defined flow units (1-10) in (Fig 5.9A and Fig 5.9B) are shown. Unit 1-4 refers to WBRED [A-D] respectively.

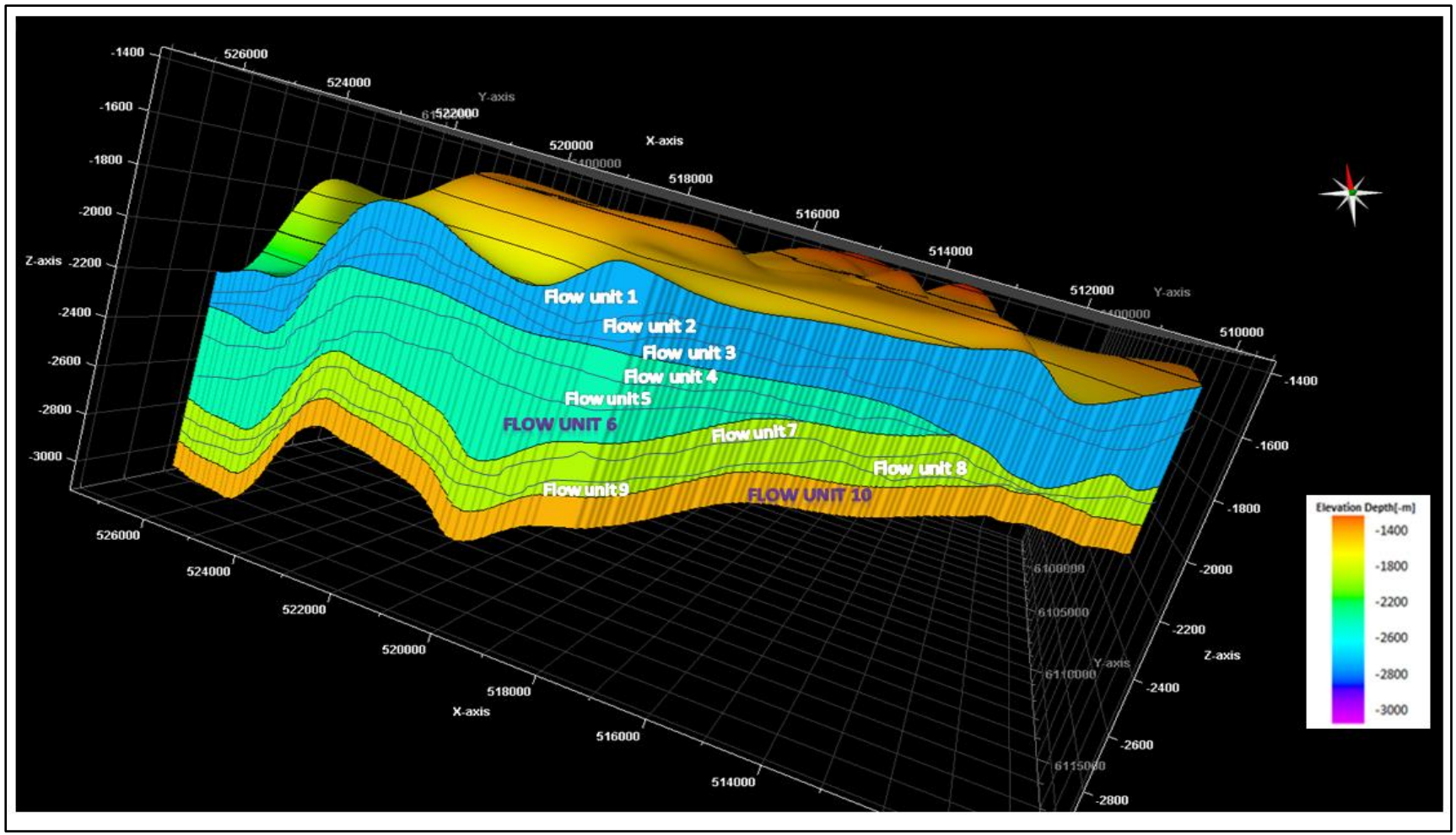

Figure 5.11:3-D distributions of flow units based on a combination of geologic and petrophysical properties (porosity and permeability) within the modelled area. Flow units 6 and 10 show very poor flow characteristics and identified as flow barriers.

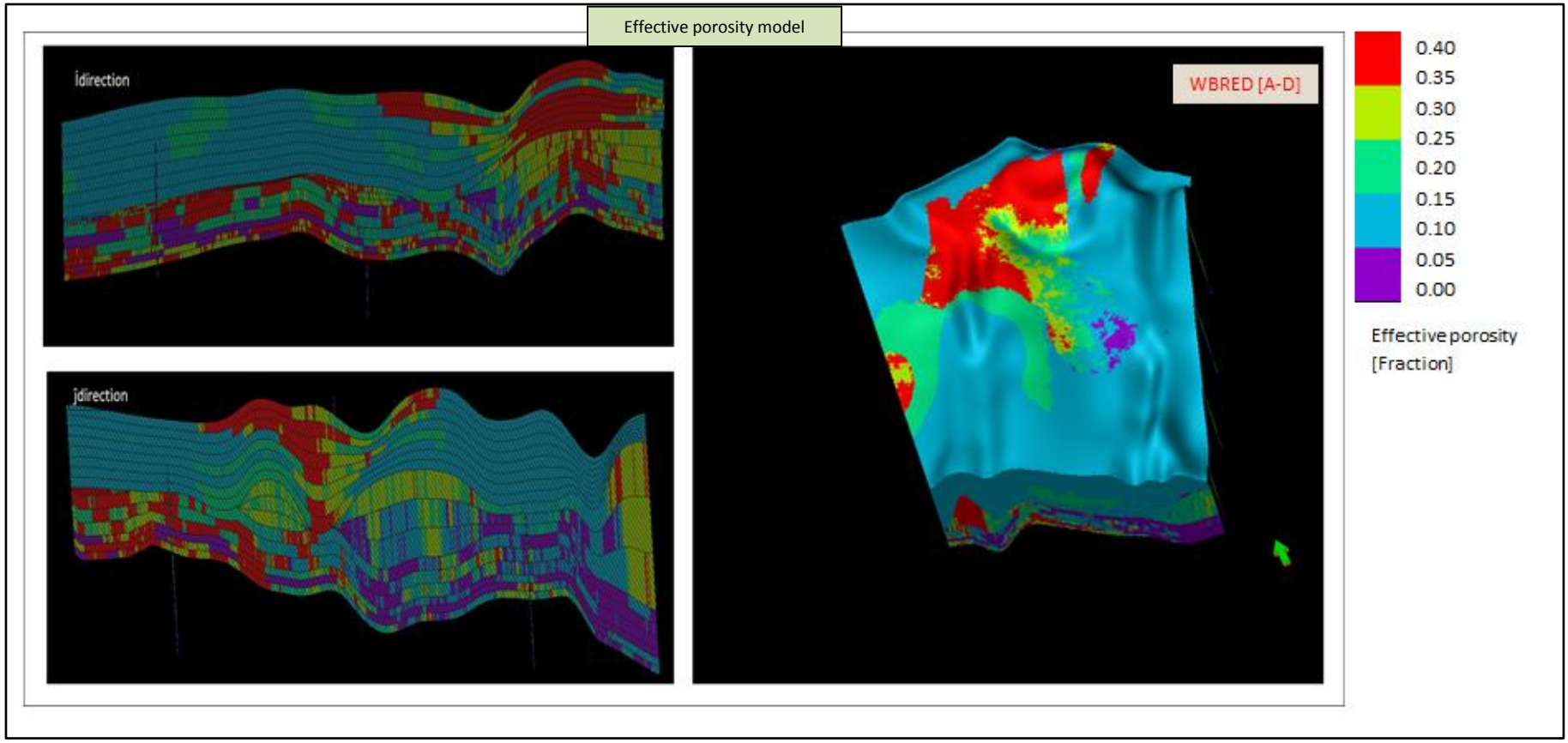

Figure 5.12: Effective porosity distribution models of the WBRED reservoir (all units), the longitudinal and transverse sections mark position of I and j directions.

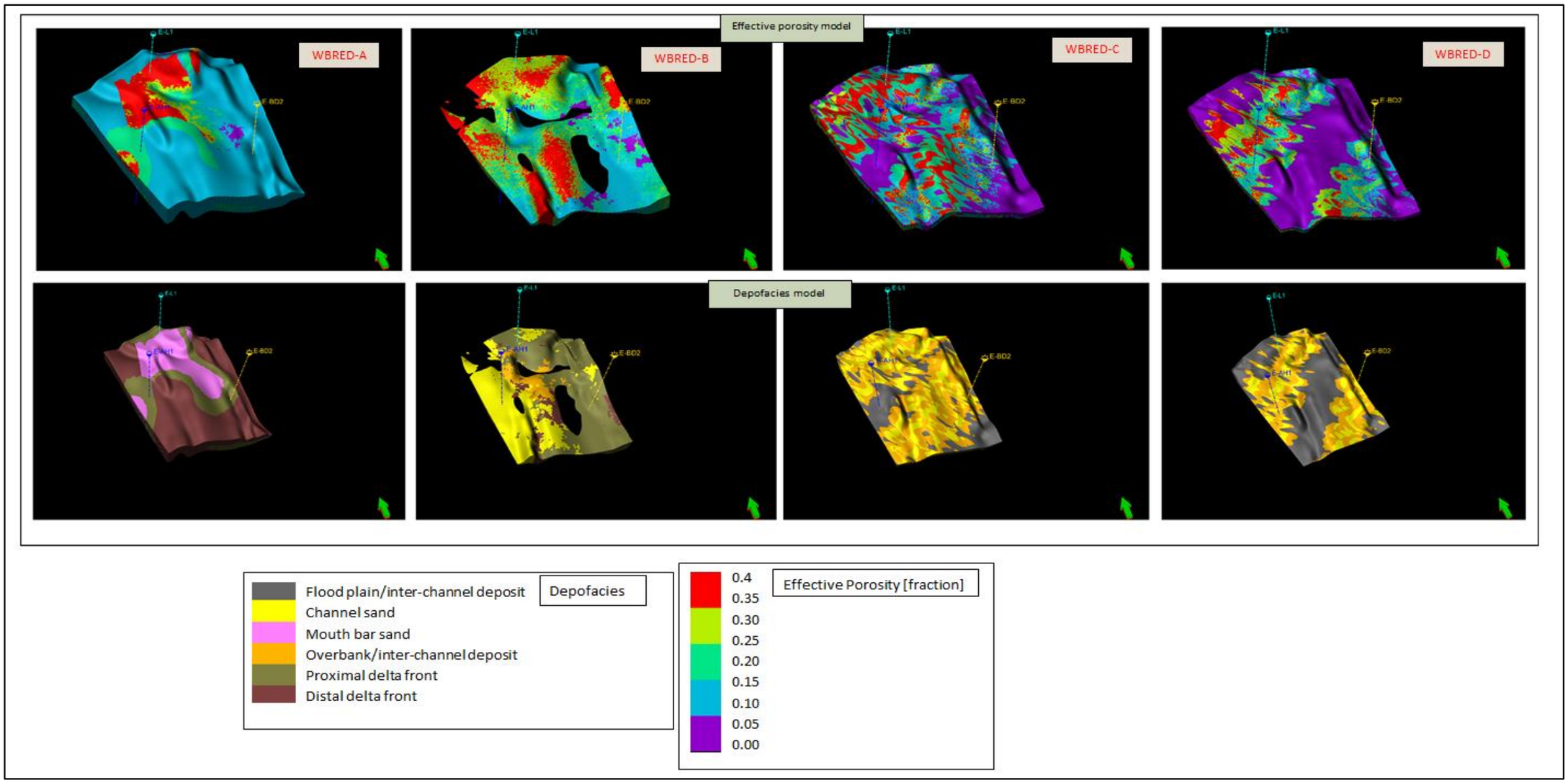

Figure 5.13: Porosity distribution models, showing all reservoir units [WBRED A-D] and corresponding depofacies models. Porosity values are high in the channel sands and low in the flood plain deposits.

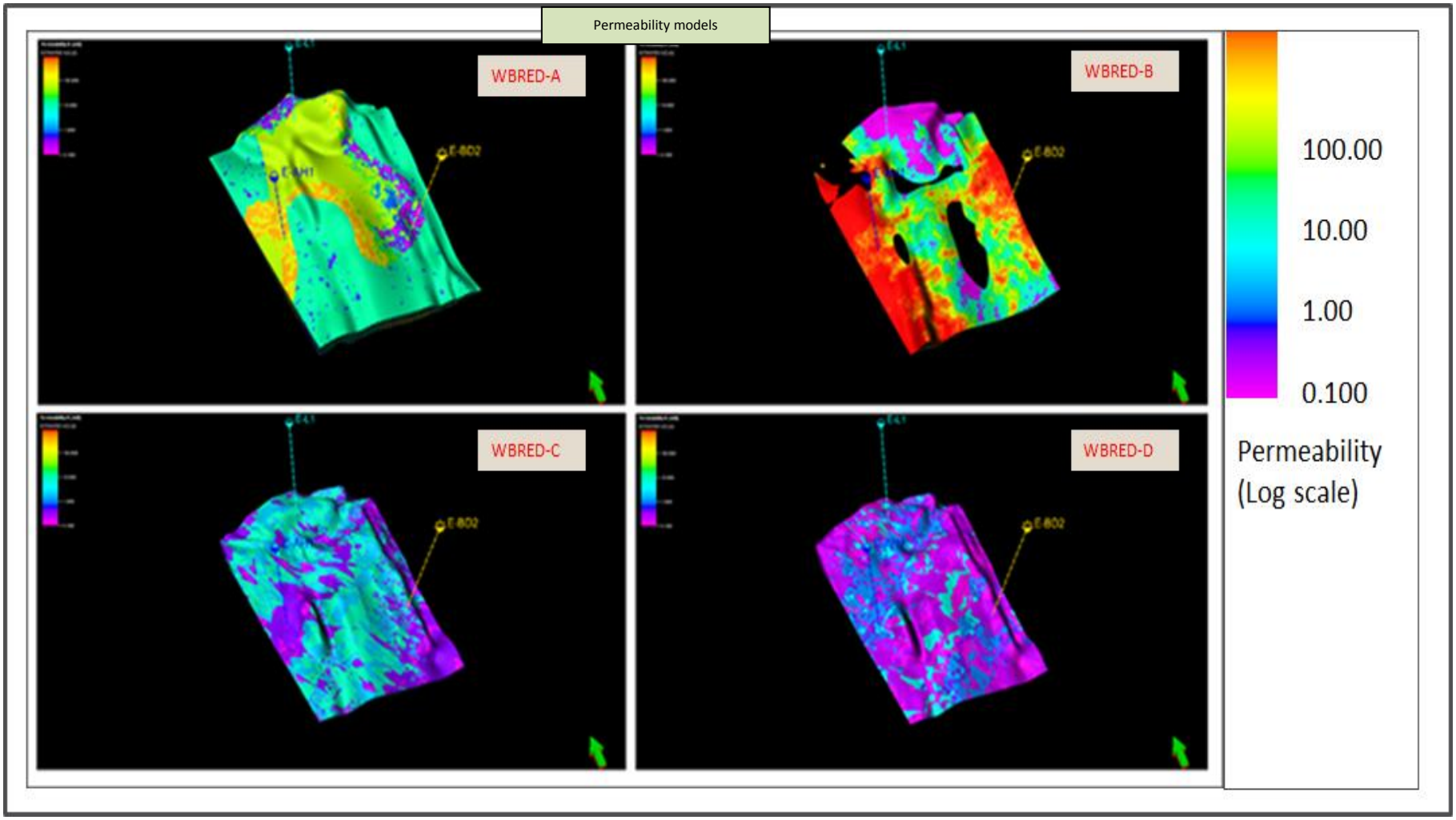

Figure 5.14 Permeability distribution models showing [WBRED A-D]. In the various units, porosity and permeability values increase correspondingly suggesting a good balance in connectivity of reservoir rock pore structures.

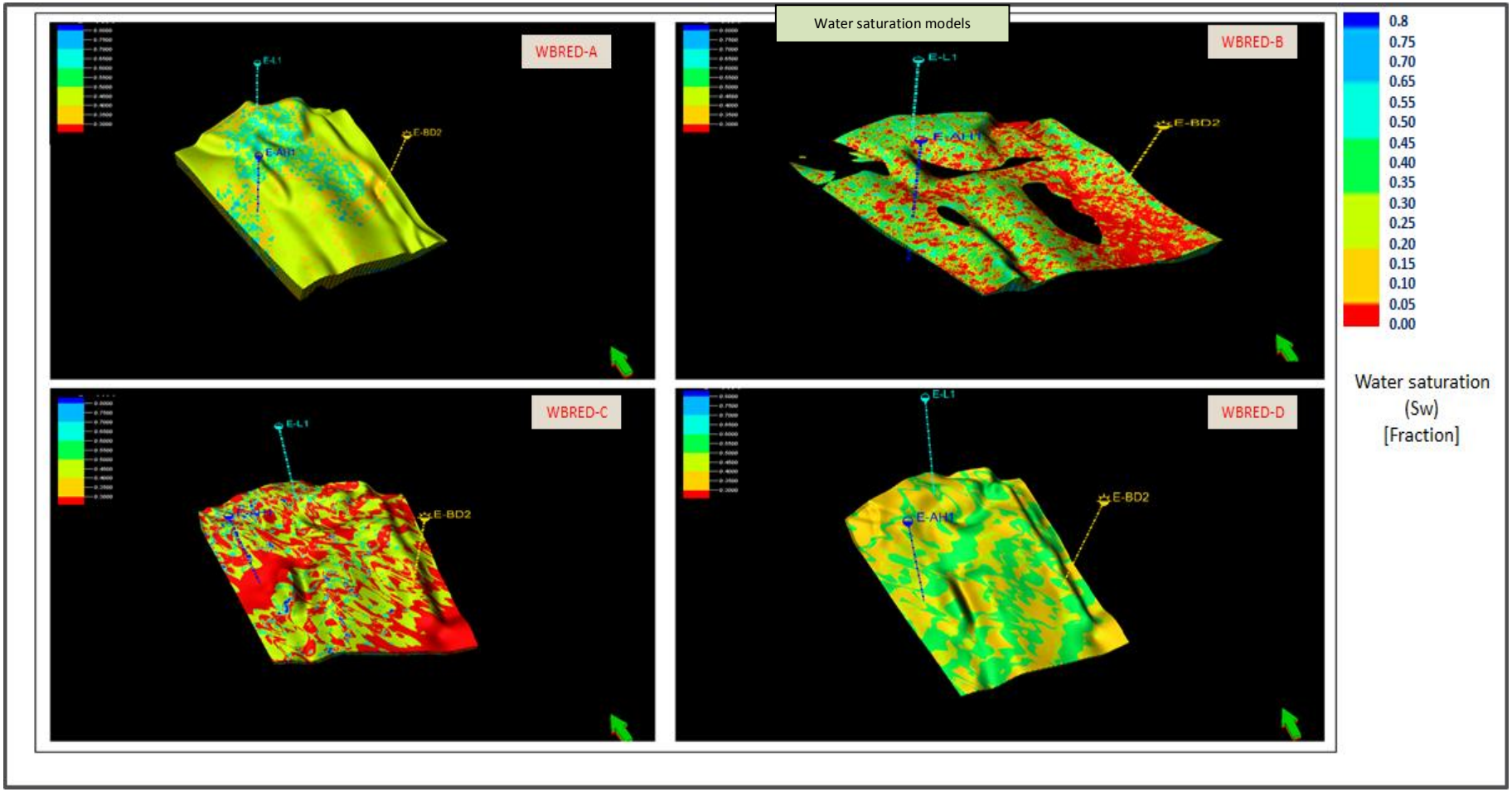

Figure 5.15: Water saturation distribution models showing all reservoir units [WBRED A-D]. Water saturation values within the reservoir units generally range between (0.12-0.69), suggesting reservoir system within acceptable levels for hydrocarbon production.

SECTION 3

CHAPTER SIX

RESERVOIR FLOW SIMULATION MODELLING

6.1 Introduction

This chapter discusses upscaling and flow simulation of the WBRED-C reservoir unit. The discussion starts with factors weighed prior to commencing upscaling, the adopted two-stage upscaling workflow, upscaling results and the fluid-flow simulation of the WBRED-C unit. The two-stage upscaling workflow describes the synthesis of all aspects of the upscaling procedure as it relates to both the static and dynamic modelling stage in this study. The first stage describes upscaling of selected well logs into defined 3-D geological grids, while the second stage defines a two-step upscaling of the fine grid WBRED-C geological reservoir model. The steps include upscaling of the 3-D grid structure and properties into defined simulation grid cells. A demonstration to the concept of upscaling is shown in Figure 1.6. The WBRED-C unit is selected based on the availability of more well control data (i.e. drill stem test (DST), permeability, porosity and effective water saturation) for wells (E-L1, E-AH1 and E-BD2) when compared to the other units.

6.2 Upscaling approach and special concerns

The fact that multi-scale reservoir heterogeneities occur with a wide range of lengthy scales which includes their interaction with various transport mechanisms requires the need for an upscaling approach which can sufficiently reproduce the detailed geological description of the identified reservoir units at all levels of modelling for this study (Leung and Srinivasan, 2008).

The following considerations stated below guided the execution of the upscaling process.

Consideration 1

The first consideration is adequate preservation of defined flow features in the different reservoir units, especially as it relates to handling the complexity of the channelized reservoir units as created in the conceptual depofacies architecture framework. As a result, a rigorous scheme that involved testing various upscaling methods together with statistical quality checks is designed to reproduce desired upscaling results in PETREL.

Consideration 2

The second consideration is finding the right balance for the WBRED-fine grid model resolution-(areal and vertical) in order to capture the heterogeneity and associated spatial distribution of reservoir facies properties. To these, the geological layering of the WBRED grid model is proportioned based on the characterization of defined flow units set in each reservoir unit (Table 5.11).

Consideration 3

The final consideration is determining the model size against available computational resources and accuracy of simulation results. To these, one of the identified reservoir units is set to a master model for flow simulation. In this case, the WBRED-C model is selected as been optimal to fast track rapid reservoir engineering solutions for fluid-flow characterization. Upscaling of the model grid structure and properties is carried out before commencing fluid flow simulation. Highlights of this are discussed in section 6.3.2 and 6.3.3.

6.3 Upscaling workflow, results and discussions

6.3.1 First stage-upscaling of selected well logs

Four well logs in each selected well are upscaled (i.e. discrete log–depofacies and continuous logs- porosity, water saturation, permeability). The averaging (most methods) proved effective in reproducing depofacies log characteristics, representing the highest occurring log values. For the porosity and water saturation log, the (arithmetic mean) and combination of arithmetic mean and mid-point pick are found optimal for use in the different reservoir units. The combination of the geometric and harmonic proved effective in the case of the permeability log due to the log normal distribution exhibited by the log values. Well upscaling results are summarized in Table 6.1. Examples of validation for raw and upscaled well logs for wells E-L1 and E-AH1 are shown in Figs 6.1. Based on the respective histogram analyses presented in (Figure 6.2), 91 % match of upscaled data and raw log data is evident.

6.3.2 Second stage-model upscaling

6.3.2.1 Upscaling of model grid

Upscaling the WBRED-C fine grid model structure is part of a pre-process which involves coarsening of the grid cell structure to meet the compatibility criteria of the selected flow simulator. A coarsening of the fine grid by a factor 4 in the x- direction and 4 in the y-direction is selected. Vertical upscaling is set to a minimum in turn exercising more flexibility to areal upscaling. These prudent adjustments measures up to compensating for well spacing, target model size, geological layering, depofacies architecture and uncertainty of property distribution between the inter-well volumes. The WBRED-C fine grid model and upscaled model grid dimensions are shown in Table 6.2.

6.3.2.2 Upscaling of model properties

Upscaling of model properties involves the transfer of properties from the fine to simulation grid model cells. To preserve reservoir connectivity during upscaling, conditioning of the WBRED-C fine grid model properties is carried out (e.g. cut-offs were introduced to differentiate reservoir from non-reservoirs). Net to gross is used as a weighting factor for porosity, permeability and saturation upscaling. Upscaled permeabilities, porosity and water-saturation are validated by performing water-flood streamline simulations of the fine grid and coarse grid. Results show a very good agreement between water saturations of the fine and grid model. Comparison of the WBRED-C fine grid model against the generated upscaled model is shown in Figs 6.3, 6.4 and 6.5. Also, pore volume calculations of the WBRED-C fine and upscaled grid model are generated and compared. The results show an overall difference of 0.98%.

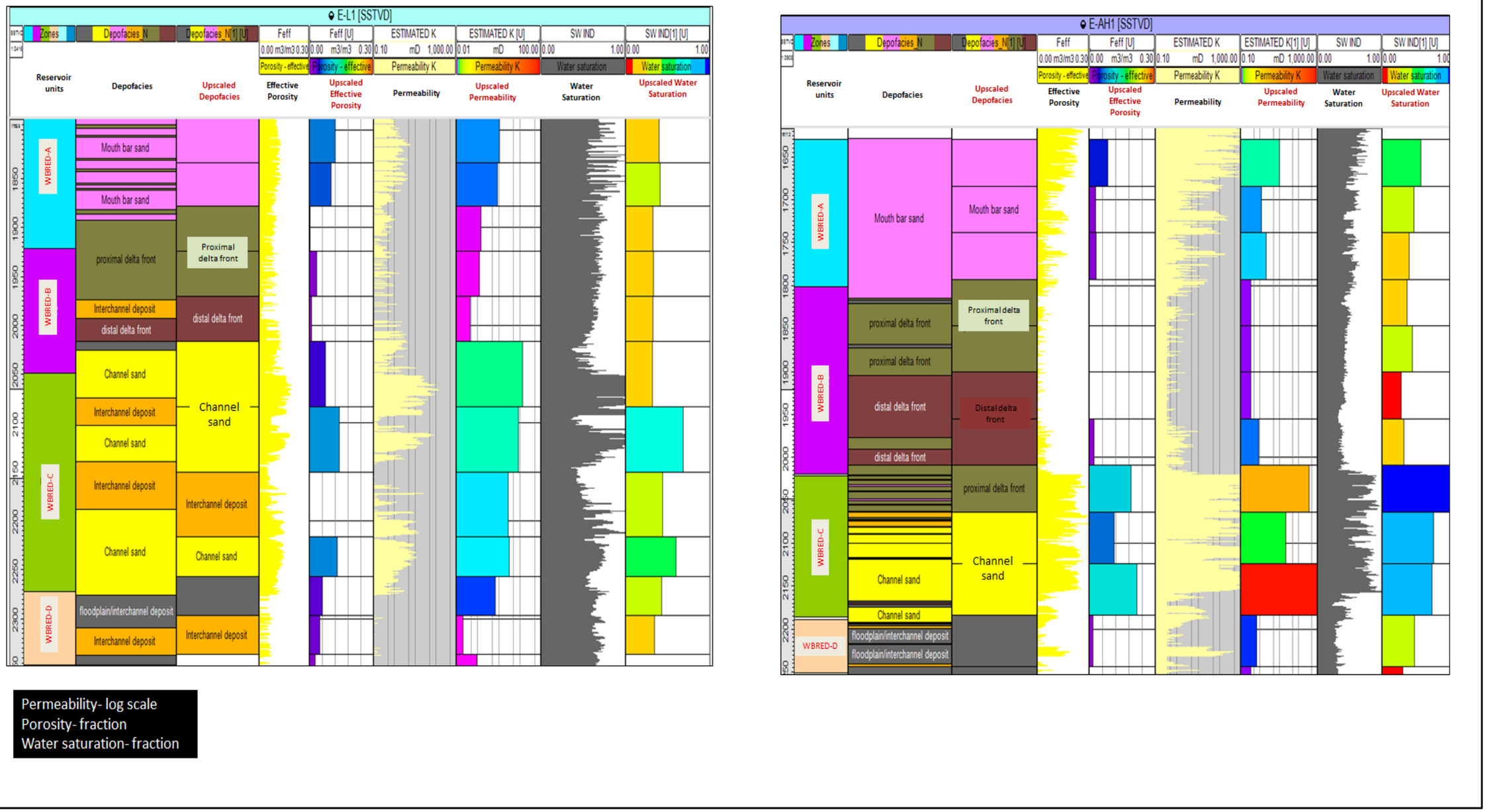

Figure 6.1: Examples of selected well logs for well E-L1 and E-AH2, showing the overall character of distribution preserved and good visual match of the vertical variability of the raw and upscaled logs.

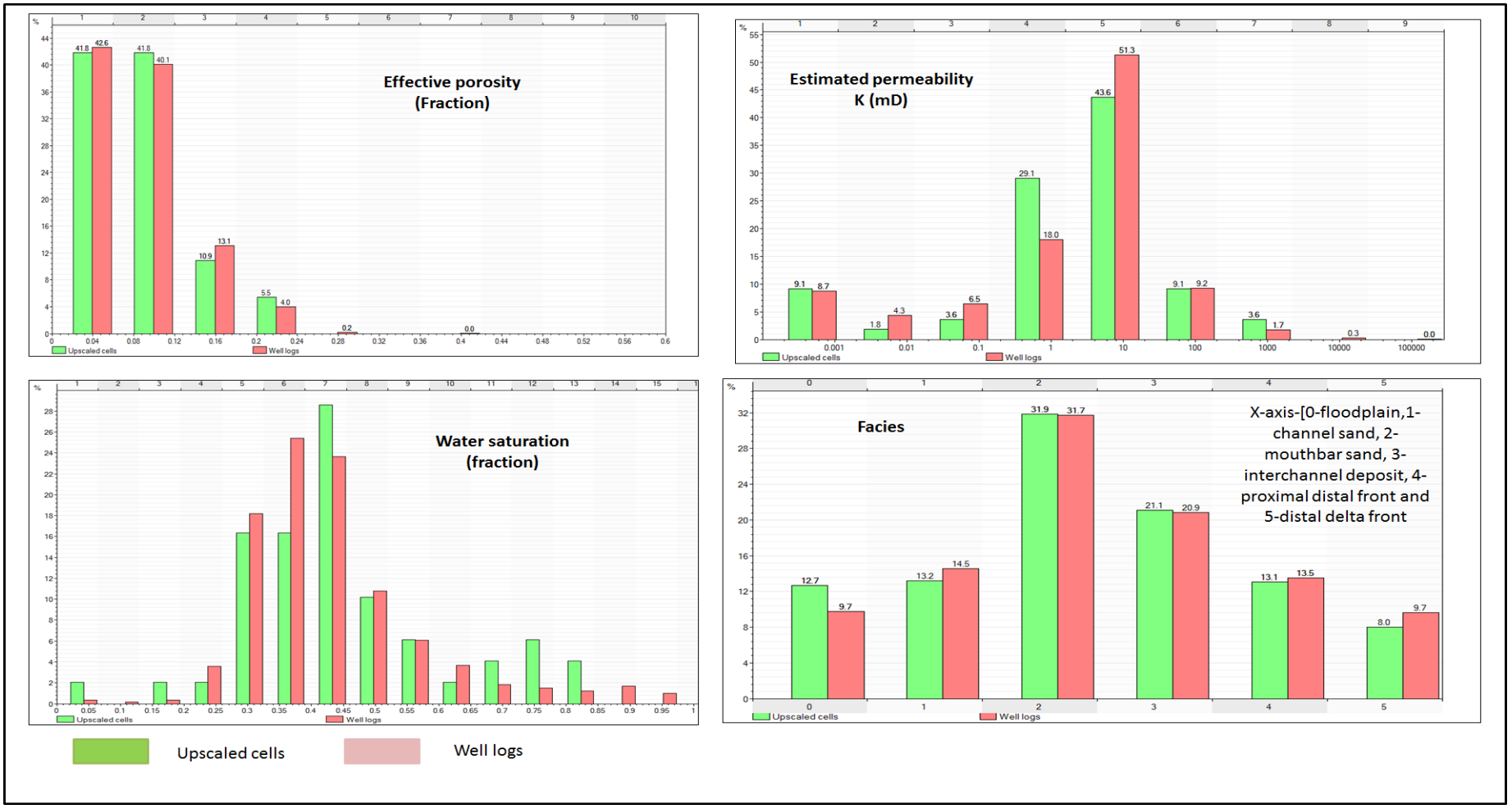

Figure 6.2: Histogram analyses of raw green and upscaled pink well logs (i.e. porosity, permeability, water saturation and depofacies) of selected wells in the study area, showing a good overall match of raw and upscaled log values.

Table 6.1: Well log upscaling results, showing different optimal averaging upscaling methods utilized within the different WBRED reservoir unit in this study

Facies		Effective Porosity		Permeability		Water saturation S_w	
Reservoir units	Upscaling Method BEST	Reservoir units	Upscaling Method BEST	Reservoir units	Upscaling Method BEST	Reservoir units	Upscaling Method BEST
WBRED-A	Averaging (most of)	WBRED-A	Averaging (arithmetic mean)	WBRED-A	Averaging (arithmetic mean)	WBRED-A	Averaging (arithmetic mean)
WBRED-B	Averaging (most of)	WBRED-B	Averaging (arithmetic mean)	WBRED-A	Averaging (harmonic)	WBRED-B	Averaging (mid point pick)
WBRED-C	Averaging (most of)	WBRED-C	Averaging (arithmetic mean)	WBRED-A	Averaging (geometric)	WBRED-C	Averaging (arithmetic median)
WBRED-D	Averaging (most of)	WBRED-D	Averaging (arithmetic mean)	WBRED-A	Averaging (geometric)	WBRED-D	Averaging (arithmetic median)

Table 6.2: Fine and simulation grid model dimensions generated for this study.

Model	Grid dimensions		Number of cells
WBRED fine grid model (all units)	Cell length (x): 25m Cell width (y): 25m Cell thickness- average (z): 59m	742x926x10 –(nİ x nĵ x n grid layers)	13815920
WBRED-C fine grid model	Cell length (x): 25m Cell width (y): 25m Cell thickness- average (z): 59m	746x926x3 –(nİ x nĵ x n grid layers)	2072388
Upscaled WBRED-C simulation model	Cell length (x): 100m Cell width (y): 100m Cell thickness average (z): 65m	181x227x3	123261

Table 6.3: Simulation grid property results.

Model upscaling				
Fine grid property	Sampling method	Weighting factors	Upscaling Methods	Remarks
Effective Porosity	All intersected cells within assigned range of fine grid layers	Net volume	Averaging (arithmetic mean)	Proved effective
Permeability		Net volume	Flow-based upscaling	Provided I, J, and K permeabilities.
Water Saturation		Pore volume	Averaging (arithmetic mean)	Pairs of fine and coarse cross sectional models showed good visual match
Depofacies		Gross volume	Averaging (arithmetic mean)	Proved effective

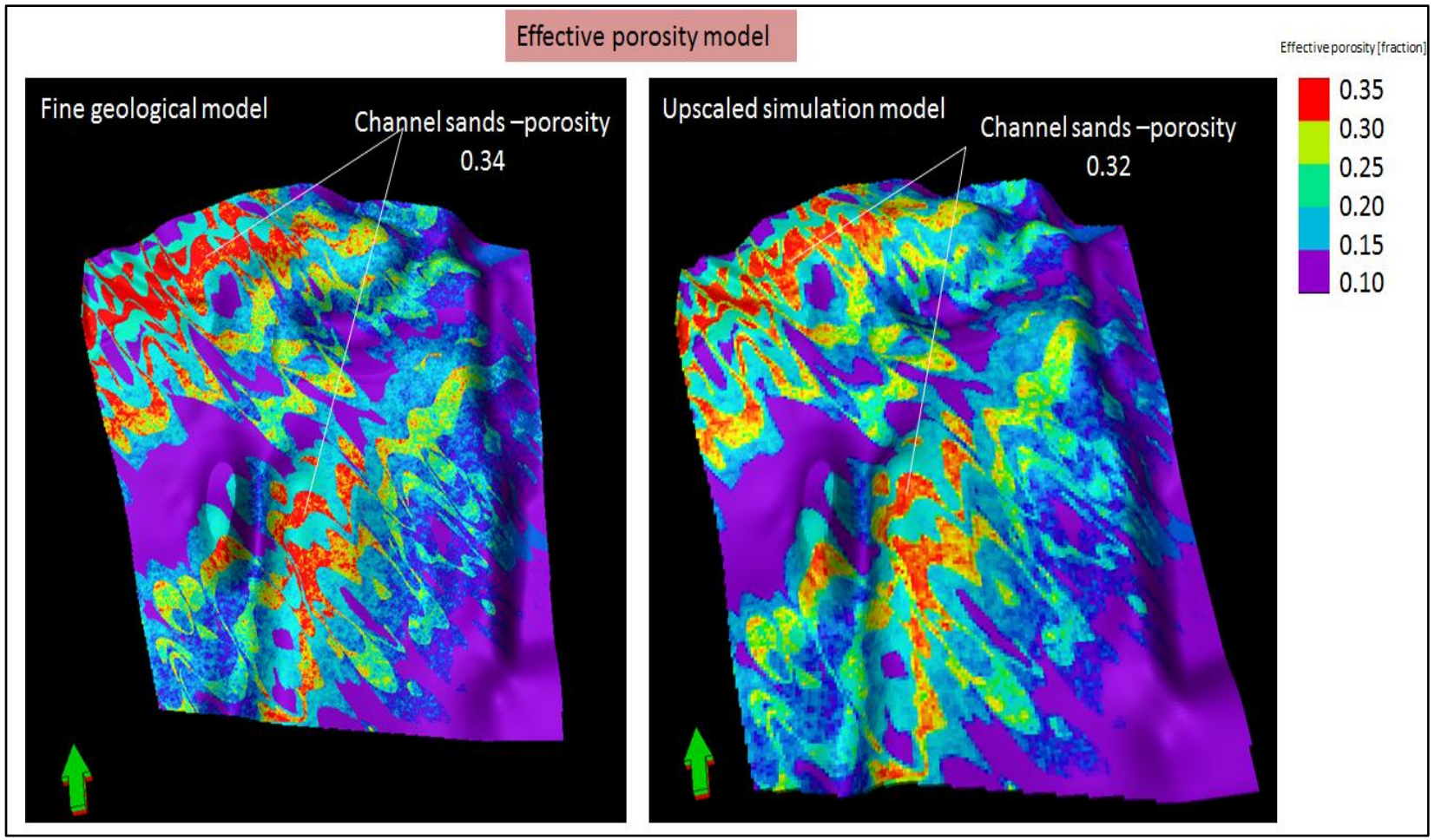

Figure 6.3: Examples of planar view of fine geological model (left) and upscaled simulation model (right) of WBRED-C, showing good visual match of upscaled reservoir facies properties such as effective porosity.

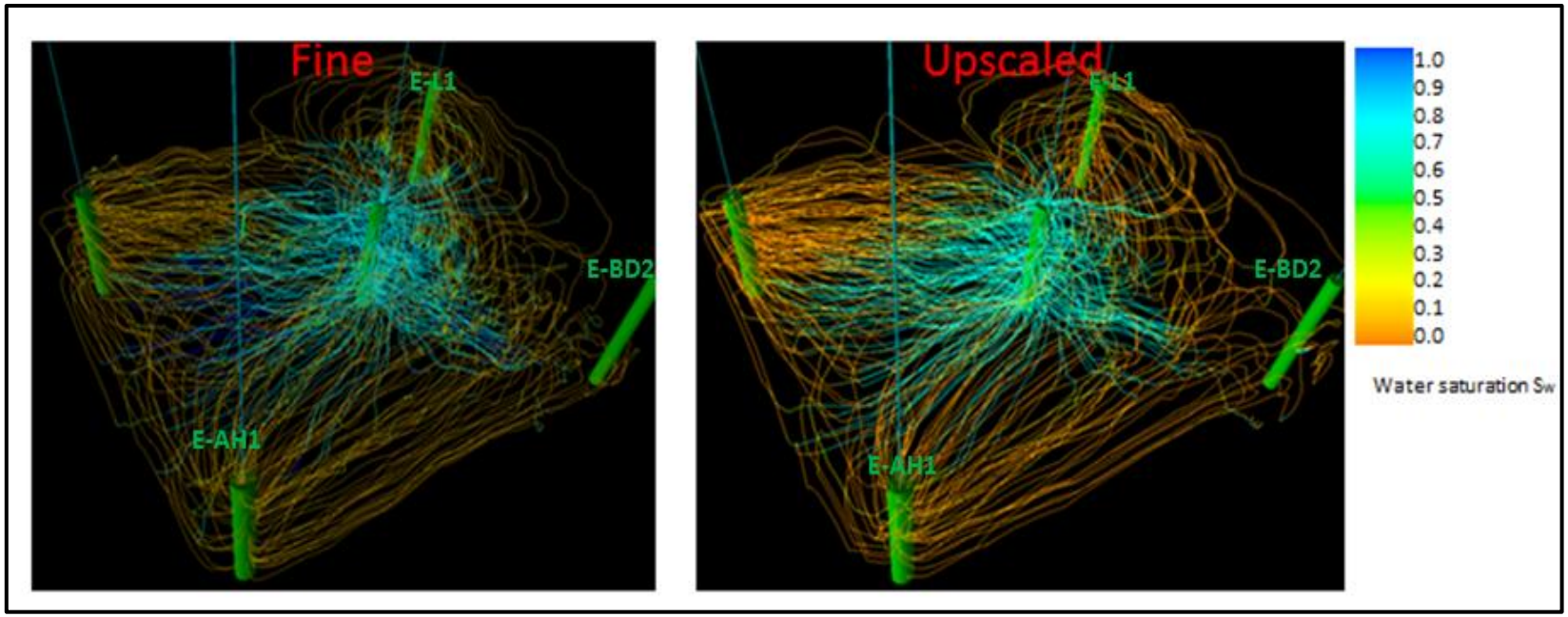

Figure 6.4: Examples of water-flood simulations runs results for (WBRED-C unit) using averaging (arithmetic mean) based upscaling. There is a close match between the upscaled and the fine model. The two unnamed wells are dummy wells used to better constrain the simulation.

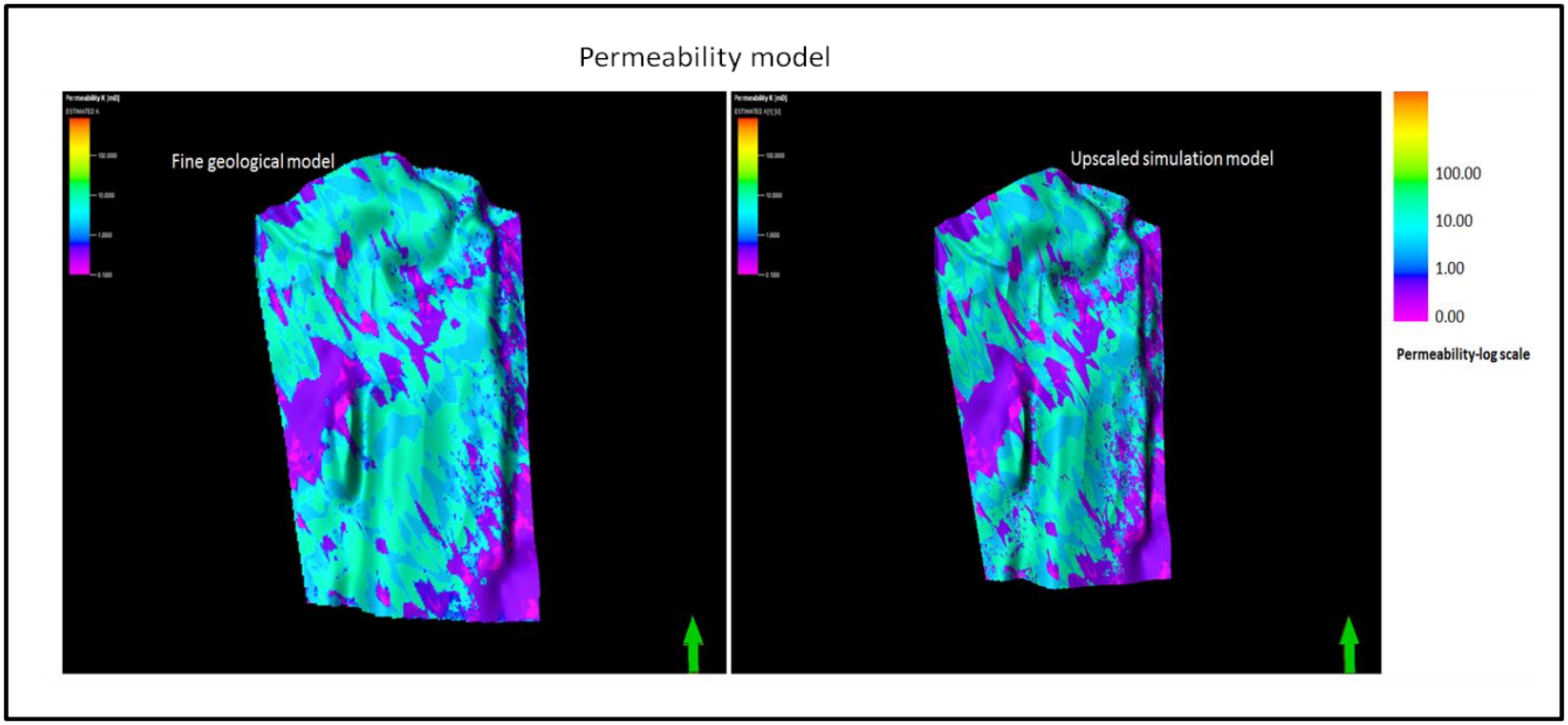

Figure 6.5: Examples of aerial view of fine geological model (left) and upscaled simulation model (right) of WBRED-C, showing good visual match of upscaled permeability.

6.4 Flow simulation modelling

After carrying out the upscaling process, the next step is to achieve the end objectives of establishing two-phase fluid-flow behaviour together with the investigation of a number of sensitivities (i.e. upscaling method, two-phase flow parameters and reservoir facies). Reservoir initial conditions, fluid PVT properties, rock physics functions, development strategies are pulled together to define a simulation case. Upon running various defined simulation case scenarios, the biggest impact on two-phase flow production results are studied against stated sensitivities. Table 6.4 shows a brief summary of key simulation input parameters.

6.4.1. Fluid PVT properties

Defining fluid PVT properties remains critical in performing flow simulation numerical calculations. To do this, the black oil (PVT) in the Eclipse simulator is selected as appropriate for the fluid PVT representation of the WBRED-C model and as part of efforts to reduce the complexity of the simulation study. Existing data from previous studies in nearby fields were used to assign fluid PVT.

6.4.2 Two-phase flow rock properties

Relative permeability is a dynamic rock property that is very important for estimating the flow of reservoir fluids. To characterize the WBRED-C reservoir rock physics and the interaction between rock and fluids, routine (RCAL) and special core analysis data (SCAL) of all examined core in the study area were utilized. Besides, it provided data for generating relative permeability tables for oil-water and oil-gas systems and establishing a simple averaged relative permeability relationship that corresponds to average J-functions correlations for each defined depofacies in WBRED-C. Leverette suggested the idea of J-functions, in effect to characterizing heterogeneous rock characteristics sufficiently by combining porosity and permeability in a parameter

correlation (Fanchi et al., 1999). J-functions have proved invaluable in correlating capillary pressure data within a lithology rock type (Crain's petrophysical handbook, 2008). The mixed wet rock curves for each depofacies are shown in Fig 6.6.

A systematic and robust workflow is initiated in assigning initial water saturation, residual oil saturation and irreducible water saturation and defining end points by combining rock types (i.e. depofacies of the WBRED-C unit) together with the reservoir quality index [RQI=0.0314*(K/Ø$^{1/2}$] methodology.

6.4.3 Development strategy and simulation case

Development strategies are established in order to describe to the reservoir simulator on how a field would be developed (Schlumberger, reservoir engineering handbook, 2011). For this study, the prediction depletion strategy is selected in PETREL to set up the WBRED-C model. The prediction depletion strategy relies on the use of appropriate primary drive mechanisms towards depleting hydrocarbon resource in the reservoir in question. In this instance, all wells (E-L1, E-AH1 and E-BD2) are added to the strategy and placed under production with minimum bottom-hole pressure.

Simulation input parameters	
Parameters	Remarks
Relative permeability End-points(K_{ro}, K_{rw} and K_{rg})	End point scaling were generated based on rock quality (i.e. criteria of -good to bad) of the different depofacies in the WBRED-C model and on the average plot values of relative permeability water saturation of depofacies
Oil-water relative permeability	Based on (RCAL) and (SCAL) data measurements of available cores.
Horizontal permeability Vertical Permeability (K_h/K_v)	Based on existing field data a range of vertical permeability schemes are developed which includes upscaled permeabilities, used as a function of horizontal permeability
PVT for reservoir fluids	PVT for reservoir fluids relied on existing PVT data generated from nearby oil fields.

Table 6.4: Summary of key simulation input parameters

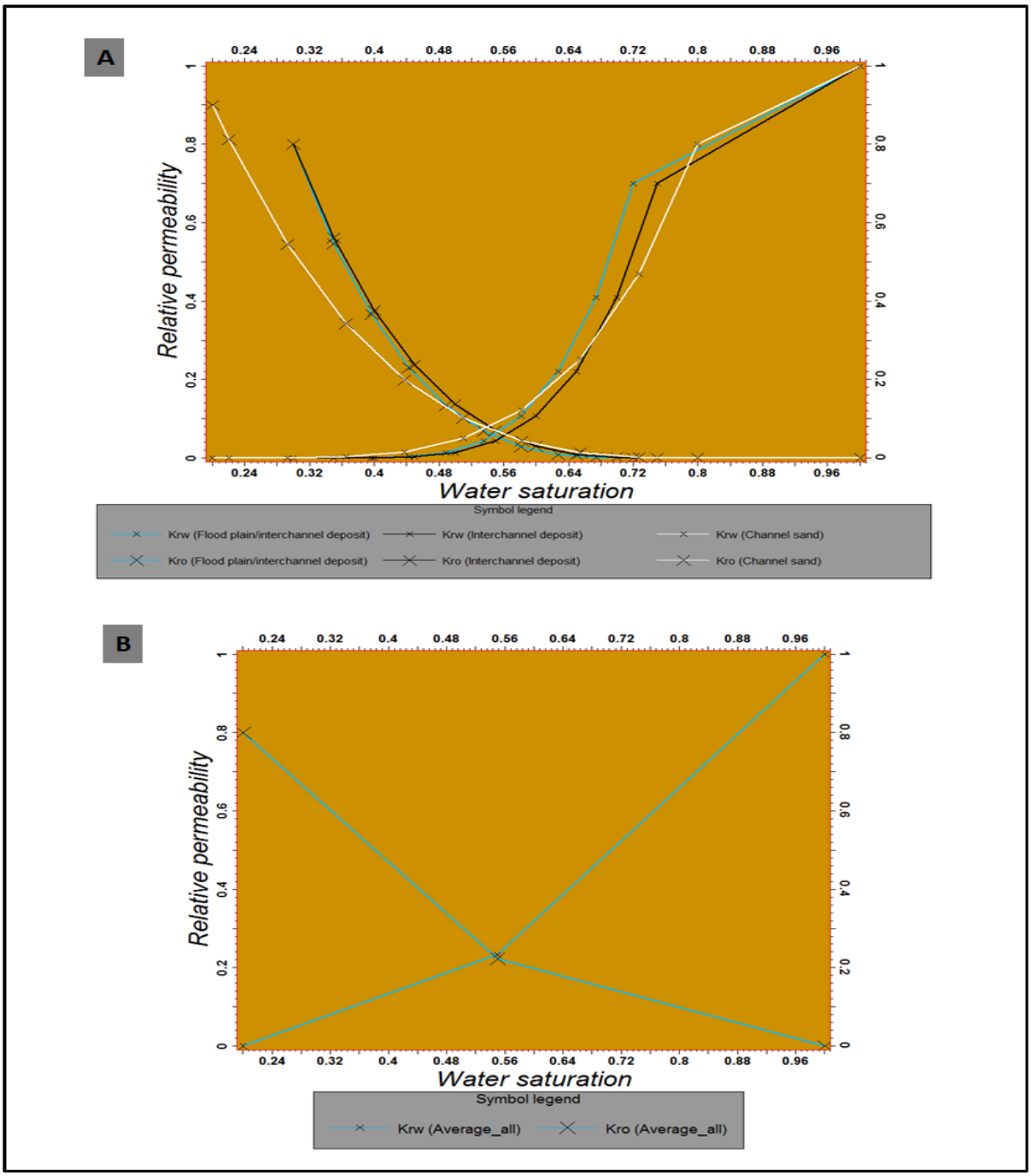

Figure 6.6: [A]-Two-phase flow rock curves for defined depofacies, and [B] - Plot of average values of upscaled relative permeability and water saturation based on two-phase rock curves for defined depofacies.

6.5 Flow simulation results

6.5.1 Prediction case scenarios

Production profiles are generated for the WBRED-C model for a period of twenty years (2000-2020) under two prediction case scenarios. Case 1 (constrained) is defined using the two-phase flow rock curves for defined depofacies, while Case 2 (unconstrained) is defined using average values. The rock-curves and cumulative production profiles are shown in (Figs 6.6 and 6.7) respectively.

From the production profiles result, an increase in cumulative production of oil and gas is observed in case 1 against case 2. It is determined that there is significant impact of facies heterogeneity on two-phase flow fluid behaviour in the study area. The overall prediction forecast suggest that for a good reservoir performance and management, understanding of horizontal and vertical heterogeneity in the case study area is crucial to successful mobile oil and gas productivity.

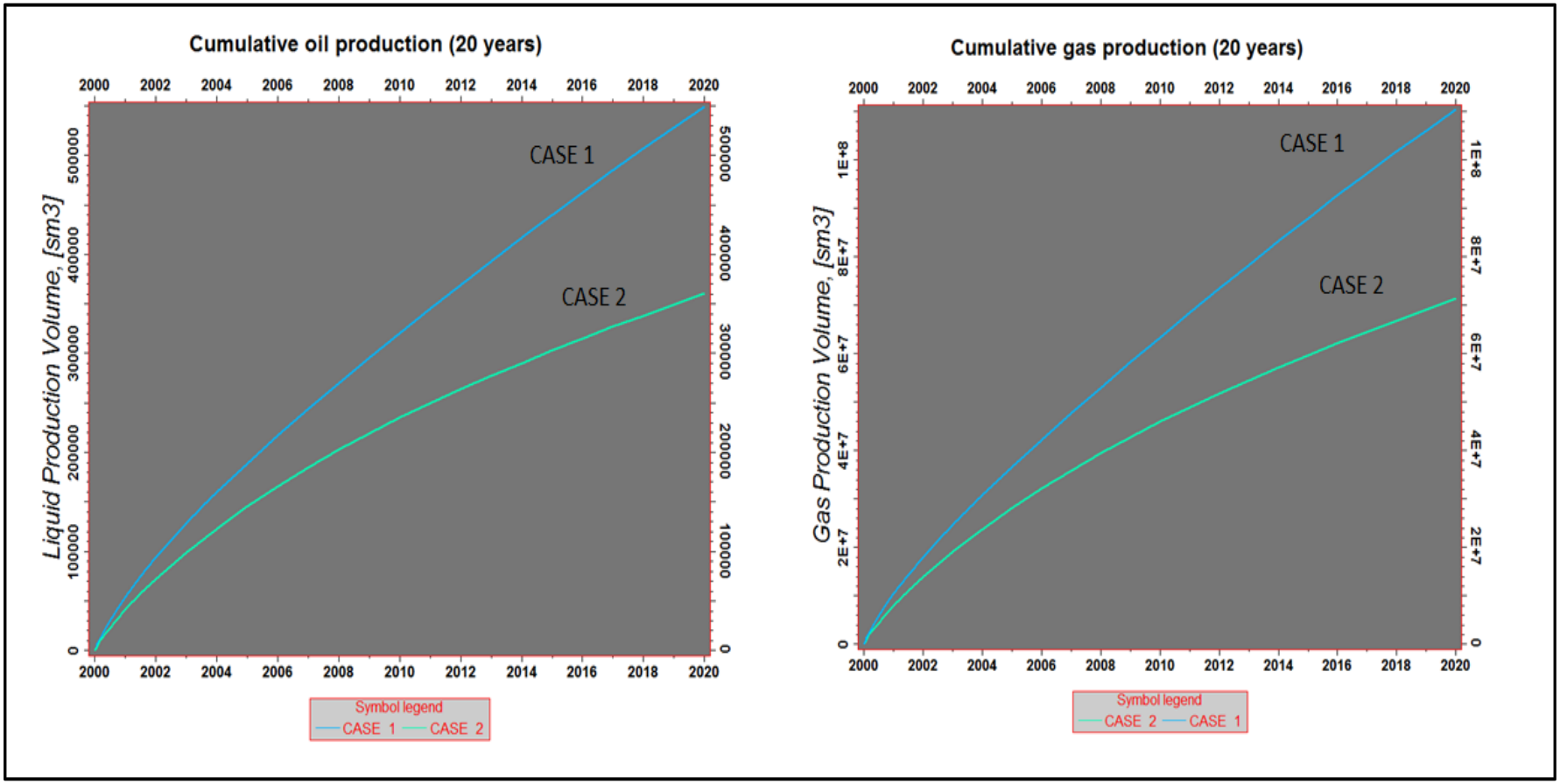

Figure 6.7: Comparison of the cumulative production profiles of the two defined case scenarios. Cumulative oil production results predict very promising recoverable estimates of (30-35 billion barrels) on comparison with (20-25 billion barrels) from the nearby Sable oil field. This suggests significant hydrocarbon potential in the western section of the Bredasdorp Basin. Full details of recoverable oil data estimates of Sable oil field based on 20-40 year duration period are presented in the Petroleum Agency Brochure, 2008 and PetroSA asset evaluation report, 2008.

CHAPTER SEVEN

CONCLUSION AND RECOMMENDATIONS

7.1 Conclusions

In this thesis, identified sandstone reservoir units within the 9At1 and 14At1 sequence boundary in the Western Bredasdorp Basin have been studied extensively based on available subsurface data. Even though the data are generally insufficient and a number of the 2-D seismic sections are of low quality, prudent adjustments and precautions have been useful to arrive at the several stochastic realizations generated in both the static and dynamic modelling stages towards delivering accurately the understanding of subsurface conditions. Based on the evaluations carried out in each section of this study, the following conclusions are made:

1. The studied stratigraphic reservoir intervals fall into the post-rift stage and within the transitional (early drift) phase (9At1- 14At1) that began in the late Albian and continues to the present structural development of the Bredasdorp Basin and neighbouring sub-basins in the Outeniqua Basin. Within these intervals no active fault systems are identified on studied seismic sections.
2. The reservoirs units identified are deposited in a fluvial-deltaic setting within a slope to shallow marine environment. Core and well data confirmed the presence of stacked sand–prone channels and overbank inter-channel facies together with the presence of clay-rich debris flow deposits. Six depofacies (proximal and distal mouth bar, delta fro, distributary channel deposits, and floodplain/inter channel deposits) characterize the 9A to 14A sequences; WBRED-A-(proximal, distal mouthbar and delta front), WBRED-B- (distributary channel deposits and delta front), WBRED-C- (distributary

channel deposits and over bank/inter-channel deposits) and WBRED-D - (distributary channel deposits and floodplain/inter-channel deposits).

3. A general knowledge of existing depositional models has been re-appraised using 2-D seismic data, regional studies and well data; hence the mouthbar and channel geometry within the E-L1, E-AH1, and E-BD2 tract are confirmed. Though, confirmations of the geometry of this sandbodies based on existing depositional models have originated more from the central part of the Bredasdorp Basin.
4. Two main reservoir types (distributary channel-fill and inter- channel reservoirs) exist within the studied intervals based on observed sediment stacking pattern of depositional units on well logs/cores.
5. Reservoir connectivity within the channel-belts/inter-channel seems to be complex and this is particularly obvious in WBRED-B, WBRED-C and WBRED-D where amalgamation is observed both vertically and laterally. The intersecting channel complexes within WBRED-B, WBRED-C and WBRED-D show good character of enhancing sand-body connectivity, hence favourable reservoir conditions.
6. WBRED-A, WBRED-B and WBRED-C and WBRED-D all show fairly-strong flow characteristics against characterized vertical and lateral heterogeneities.
7. Moderate to excellent poro-perm relationship is confirmed within the two main reservoir types-distributary channel-fill and inter-channel reservoirs.
8. Ten stratigraphic flow units (1-10) define predictable hydraulic conductivity, storage and porosity of reservoir sandbodies. Flow units 6 and 10 are considered potential shale barriers.
9. While the underlying goal of upscaling as an averaging procedure is to approximate static and dynamic characteristics of a fine-scale geological model by that of a coarse scale simulation model, preserving reservoir architecture and heterogeneity is vital

and has to be realized during the upscaling process. The upscaling approach adopted proved to be ideal and effective.

10. Geostatistics and streamline-simulations techniques provided a quick and scientifically based approach for quality checking and validating the upscaling process.
11. Well log upscaling of the following depofacies were important -distal mouth-bar, delta front and inter-channel deposits.
12. Small-scale upscaling during well log upscaling of WBRED-A may not be important due to good connectivity of massive sand units.
13. A good understanding of the multi-scale facies variations, model energy balance, and fluid migrations between reservoirs (channel-fill reservoirs and inter-channel deposits) is vital for accurate two-phase fluid-flow performance characterization in the basin. Multi-scale facies variation has a major impact.

7.2 Recommendations

Flow simulations results show that two-phase flow parameters and the associated uncertainties should be assessed rigorously and taken into account when developing potential oil and gas field in the basin. As these, when put into economic considerations (cash flow) can have significant impact on development decisions as to whether or not to develop potential fields.

7.2.1 Remaining uncertainties and way forward

The data available for this project is considerably insufficient and have created uncertainties in the model building and calibration process. The following are suggested:

1. Additional wells are required to appraise the north-west and south-west flank (Fig 4.10). Also, more sub-surface data (e.g. 3-D seismic, image logs and drill stem/repeated formation test in untested intervals of the selected wells are required and substantiated by the illustrations of hydrocarbon saturation–water saturation (S_{hc}-S_w) overlays shown in WBRED-C petrophysical figures (Figs 5.2. 5.3 and 5.4)
2. Due to lack of representative PVT data uncertainties in model initialization are created. Obtaining these PVT data would enhance accurate fluid-flow characterisation
3. With more dynamic data, this work could be reviewed and then suitable for high level water flood studies and enhanced oil recovery (EOR) assessment and screening.
4. With regards to understanding fully static and dynamic uncertainties, a comprehensive uncertainty analysis should be performed

REFRENCES

Aarnes, J.E., Krogstad, S. & Lie, K. 2006, "A hierarchical multi-scale method for two-phase flow based upon mixed finite elements and non-uniform coarse grids", *Multi-scale Modelling & Simulation*, vol. 5, no. 2, pp. 337-363.

AAPG Explorer Hand book, Petroleum Geology, 2013

Adedokun, O.A. 1981, "Petrology, provenance, and depositional environments of the reservoir sandstones of Ossu-izombe Oilfield, Imo state, Nigeria", *Journal of Petroleum Geology*, vol. 4, no. 1, pp. 35-56.

Allen, J. 1973, "Features of cross-stratified units due to random and other changes in bed forms", *Sedimentology*, vol. 20, no. 2, pp. 189-202.

Barker, J.W. & Dupouy, P. 1999, "An analysis of dynamic pseudo-relative permeability methods for oil-water flows", *Petroleum Geoscience*, vol. 5, no. 4, pp. 385-394.

Barker, J. & Thibeau, S. 1997, "A critical review of the use of pseudo-relative permeabilities for upscaling", *SPE Reservoir Engineering*, vol. 12, no. 2, pp. 138-143.

Barton, K. and Frewin, J., 1999, Re-appraisal of the E-CB oil and gas field based on the 1998 reprocessing of the 3-D seismic data. SOEKOR internal report, SOE-EXP-RPT-0472, 40p.

Begg, S., Carter, R. & Dranfield, P. 1989, "Assigning effective values to simulator grid-block parameters for heterogeneous reservoirs", *SPE reservoir engineering*, vol. 4, no. 4, pp. 455-463.

Ben-Avraham, Z., Hartnady, C. & Kitchin, K. 1997, "Structure and tectonics of the Agulhas-Falkland fracture zone", *Tectonophysics*, vol. 282, no. 1, pp. 83-98.

Bin Rabaa, A. & Heine, C. 2006, "A Facies-Based Approach to Distribution of Petrophysical Properties in an Aeolian Sandstone Reservoir, Unayzah Formation, Saudi Arabia", *SPE Annual Technical Conference and Exhibition*.

Branets, L.V., Ghai, S.S., Lyons, S.L. & Wu, X. 2009, "Challenges and technologies in reservoir modelling", *Communications in Computational Physics*, vol. 6, no. 1, pp. 1-23.

Branets, L., Ghai, S., Lyons, S. & Wu, X. 2009, "Efficient and accurate reservoir modelling using adaptive gridding with global scale up", *SPE Reservoir Simulation Symposium*.

Broad, D., Jungslager, E., McLachlan, I. & Roux, J. 2006, "Offshore Mesozoic basins", *The Geology of South Africa. Geological Society of South Africa/Council for Geoscience, Pretoria*, pp. 553-571.

Broad, D. & Mills, S. 1993, "South Africa offers exploratory potential in variety of basins", *Oil and Gas Journal ;(United States)*, vol. 91, no. 49.

Brown, K.M. & Ransom, B. 1996, "Porosity corrections for smectite-rich sediments: Impact on studies of compaction, fluid generation, and tectonic history", *Geology*, vol. 24, no. 9, pp. 843-846.

Brown, L.F., Benson, J.M., Brink, G.J. et al 1995, "Sequence stratigraphy in offshore South African divergent basins, an atlas on exploration for Cretaceous lowstand traps by SOEKOR (Pty) Ltd. AAPG Studies in Geology", 41.

Brown, W.R., Rust, D., Summerfield, M.A., Gleadow, A.J.W. and M.C.J., D.W., 1990. An early Cretaceous phase of accelerated erosion on the south western margin of Africa: Evidence from apatite fission track analysis and the onshore sedimentary record. Nuclear Tracks and Radiation Measurements, 17: 339-351.

Burden, P., 1996, “Depositional models for the 14A sequence in the Bredasdorp Basin. SOEKOR internal report, SOE-EXP-RPT-0343, 17p.

Burden, P.L.A & Davies, C.P.N. 1997a, “Oribi field is South Africa's first offshore crude oil production", *Oil and Gas Journal,* vol. 95, no. 37, pp. 63-65.

Burden, P.L.A. and Davies, C.P.N. 1997b, “Exploration to first production on block 9 off South Africa”, Oil and Gas Journal, 1, 92-98.

Burden, P. 1992, "Soekor, partners explore possibilities in Bredasdorp basin off South Africa", *Oil and Gas Journal ;(United States),* vol. 90, no. 51.

Campbell, C.V. 1967, "Lamina, laminaset, bed and bedset", *Sedimentology,* vol. 8, no. 1, pp. 7-26.

Christie, M. 1996, "Upscaling for reservoir simulation", *Journal of Petroleum Technology,* vol. 48, no. 11, pp. 1004-1010.

Christie, M. & Blunt, M. 2001, "Tenth SPE comparative solution project: A comparison of upscaling techniques", *SPE Reservoir Evaluation & Engineering,* vol. 4, no. 4, pp. 308-317.

Clifton, H.E. 1981, "Progradational sequences in Miocene shoreline deposits, south-eastern Caliente Range, California", *Journal of Sedimentary Research,* vol. 51, no. 1, pp. 165-184.

Clifton, H.E., Hunter, R.E. & Phillips, R.L. 1971, "Depositional structures and processes in the non-barred high-energy near-shore", *Journal of Sedimentary Research,* vol. 41, no. 3, pp. 651-670.

Cloud, P. 1976, "Major features in crustal evolution: Alex du Toit Mem".

Corbeanu, R.M., Wizevich, M.C., Bhattacharya, J.P., Zeng, X. & McMechan, G.A. 2004, "Three-dimensional architecture of ancient lower delta-plain point bars using ground-penetrating radar, Cretaceous Ferron Sandstone, Utah", *The Fluvial-Deltaic Ferron Sandstone: Regional-to-Wellbore-Scale Outcrop Analog Studies and Applications to Reservoir Modelling*, .

Crain, A. 2008, "Relative Permeability" in *Crain Petrophysical Handbook.*

Dalrymple, R.W., Baker, E.K., Harris, P.T. & Hughes, M.G. 2003, "Sedimentology and stratigraphy of a tide-dominated foreland-basin delta (Fly River, Papua New Guinea)", *Special Publication-SEPM,* vol. 76, pp. 147-174.

Darman, N., Pickup, G. & Sorbie, K. 2002, "A comparison of two-phase dynamic upscaling methods based on fluid potentials", *Computational Geosciences,* vol. 6, no. 1, pp. 5-27.

Davies, C. P. 1997a, "Hydrocarbon evolution of the Bredasdorp Basin, offshore South Africa: from source to reservoir". PhD Thesis, University of Stellenbosch.

Davies, C.P.N. 1997b,"Hydrocarbon families in the Bredasdorp Basin, offshore South Africa". Proceedings of the 4th AAPG Conference, Arusha, Tanzania.

Dewan, J.T. 1983, "*Essentials of Modern Open-Hole Log-Interpretation",* PennWell Books.

Dingle, R.V. 1993, "Structural and sedimentary development of the continental margin off south-western Africa". Communications of the Geological Survey of Namibia, 8, 35 – 44.

Dingle, R.V., Siesser, W.G. and Newton, A.R. 1983,"Mesozoic and tertiary geology of South Africa". A.A. Balkema, Rotterdam, 375, pp. 22.

Du Toit, S. R. 1976. "Mesozoic geology of the Agulhas Bank, South Africa". Ph.D. Thesis. Faculty of Science, University of Cape Town South Africa.

Dubrule, O. & Damsleth, E. 2001, "Achievements and challenges in petroleum geostatistics", *Petroleum Geoscience,* vol. 7, no. S, pp. S1-S7.

Dubrule, O. 1989, "A review of stochastic models for petroleum reservoirs" in *Geostatistics* Springer, pp. 493-506.

Durlofsky, L.J. 1998, "Coarse scale models of two phase flow in heterogeneous reservoirs: volume averaged equations and their relationship to existing upscaling techniques", *Computational Geosciences,* vol. 2, no. 2, pp. 73-92.

Ebanks, W.J. Jr., Scheihing, M.H., Atkinson, C.D., 1992. Flow units for reservoir characterization. In: D. Morton-Thompson, A.M. Woods (Eds.), Development Geology Reference Manual, Amer. Assoc. Petrol. Geol. Methods in Exploration Series No. 10, pp. 282–284.

Ewing, R.E. 1997, "Aspects of upscaling in simulation of flow in porous media", *Advances in Water Resources,* vol. 20, no. 5, pp. 349-358.

Fanchi, J.R., Pagano, T.A. & Davis, T.L. 1999, "State of the art of 4D seismic monitoring: the technique, the record, and the future", *Oil and Gas Journal,* vol. 97, no. 22, pp. 38-43.

Farmer, C. 2002, "Upscaling: a review", *International Journal for Numerical Methods in Fluids,* vol. 40, no. 1-2, pp. 63-78.

Gallagher, K. & Brown, R. 1997, "The onshore record of passive margin evolution: Thematic set: Tectonic, magmatic and depositional processes at passive continental margins", *Journal of the Geological Society,* vol. 154, pp. 451-457.

Galloway, W.E. & Hobday, D.K. 1996, "Slope and base-of-slope systems" in *Terrigenous Clastic Depositional Systems* Springer, pp. 186-230.

Gauthier, B., Garcia, M. & Daniel, J. 2002, "Integrated fractured reservoir characterization: a case study in a North Africa field", *SPE Reservoir Evaluation & Engineering,* vol. 5, no. 4, pp. 284-294.

Grobbler, N. 2005, "The Barremian to Aptian gas fairway, Bredasdorp Basin, South Africa", *18th World Petroleum Congress*.

Gunter, G., Finneran, J., Hartmann, D. & Miller, J. 1997, "Early determination of reservoir flow units using an integrated petrophysical method", *SPE Annual Technical Conference and Exhibition*.

Gunter, W., Wiwehar, B. & Perkins, E. 1997, "Aquifer disposal of CO2-rich greenhouse gases: extension of the time scale of experiment for CO2-sequestering reactions by geochemical modelling", *Mineralogy and Petrology,* vol. 59, no. 1-2, pp. 121-140.

Haldorsen, H. & Damsleth, E. 1990, "Stochastic Modelling (includes associated papers 21255 and 21299)", *Journal of Petroleum Technology,* vol. 42, no. 4, pp. 404-412.

Haldorsen, H. & Lake, L. 1984, "A new approach to shale management in field-scale models", *Old SPE Journal,* vol. 24, no. 4, pp. 447-457.

Haq, B.U., Hardenbol, J. & Vail, P.R. 1988, “Mesozoic and Cenozoic chronostratigraphy and eustatic cycles of sea-level change”. In: Wilgus, C.K., Hastings, B.S., Posamentier, H., van Wagoner, J., Ross, C.A. & Kendall, C. G. St C. (eds) Sea-level changes: An integrated Approach. Special Publication of the Society of Economic Paleontologists and Mineralogists, 42, 71 - 108.

He, C., Edwards, M.G. & Durlofsky, L.J. 2002, "Numerical calculation of equivalent cell permeability tensors for general quadrilateral control volumes", *Computational Geosciences,* vol. 6, no. 1, pp. 29-47.

Hohn, M.E., 1988, “Geostatistics and Petroleum Geology”. VanNostrand, New York.

Hoosbeek, M.R. & Bryant, R.B. 1992, "Towards the quantitative modelling of pedogenesis—a review", *Geoderma*, vol. 55, no. 3, pp. 183-210.

Journel, A.G. 1994, "Modelling uncertainty: some conceptual thoughts" in *Geostatistics for the next century* Springer, pp. 30-43.

IPIMS, “International Human Resources Development Corporation Website” From Waples 2011, reprinted with permission of Burgess Publishing Co.

Journel, A.G., 1989. Fundamentals of Geostatistics in Five lessons, Vol. 8 of Short Courses in Geology, AGU, Washington DC.

Jungslager, E.H. 1999, "Petroleum habitats of the Atlantic margin of South Africa", *Geological Society, London, Special Publications*, vol. 153, no. 1, pp. 153-168.

Kamali, M.R., Omidvar, A. & Kazemzadeh, E. 2013, "3-D Geostatistical Modelling and Uncertainty Analysis in a Carbonate Reservoir, SW Iran", *Journal of Geological Research*, vol. 2013.

Kamel, M.H. & Mabrouk, W.M. 2002, "An equation for estimating water saturation in clean formations utilizing resistivity and sonic logs: theory and application", *Journal of Petroleum Science and Engineering*, vol. 36, no. 3, pp. 159-168.

King, P. R., S. V. Buldyrev, N. V. Dokholyan, S. Havlin, Y. Lee, G.Paul, H. E. Stanley, and N. Vandesteeg, 2001, Predicting oil recovery using percolation theory: Petroleum Geoscience, v. 7, p. 105–107.

King, M. 2007, "Upgridding and upscaling: current trends and future directions", *SPE Distinguished Lecture.*

King, M., MacDonald, D., Todd, S. & Leung, H. 1998, "Application of novel upscaling approaches to the Magnus and Andrew reservoirs", *European Petroleum Conference*.

King, P. 1989, "The use of renormalization for calculating effective permeability", *Transport in Porous Media*, vol. 4, no. 1, pp. 37-58.

King, P., Buldyrev, S., Dokholyan, N., Havlin, S., Lopez, E., Paul, G. & Stanley, H. 2002, "Percolation theory", *Dialog: London Petrophysical Society Newsletter*, Vol. 10, No. 3.

Labourdette, R., Crumeyrolle, P. & Remacha, E. 2008, "Characterization of dynamic flow patterns in turbidite reservoirs using 3-D outcrop analogues: Example of the Eocene Morillo turbidite system (south-central Pyrenees, Spain)", *Marine and Petroleum Geology*, vol. 25, no. 3, pp. 255-270.

Leung, J.Y and Srinivasan, S. 2008, Analysis of uncertainty introduced by scale-up of log derived porosity in carbonate settings. Proc., Eight International Geostatistics Congress, Santiago, Chile, 1-5 December, Vol.2, 1059-1064.

Li, D. 1995, Scaling and upscaling of fluid flow through permeable media.

Lowry, P. & Jacobsen, T. 1993, "Sedimentological and reservoir characteristics of a fluvial-dominated delta-front sequence: Ferron Sandstone Member (Turonian), east-central Utah, USA", *Geological Society, London, Special Publications*, vol. 69, no. 1, pp. 81-103.

Massonnat, G., Viszkok, J. & Vrignon, M. 2002, "Hierarchical organization of flow network in fractured carbonate reservoirs: Identification and characterization of key parameters", *SPE Annual Technical Conference and Exhibition*.

Massonnat, G. 1997, "Sampling space of uncertainty through stochastic modelling of geological facies", *SPE Annual Technical Conference and Exhibition*.

Mattax, C. & Dalton, R. 1990, "Reservoir Simulation (includes associated papers 21606 and 21620)", *Journal of Petroleum Technology*, vol. 42, no. 6, pp. 692-695.

McMillan, I.K. 1990. Foraminiferal biostratigraphy of the Barremian to Miocene rocks of the Kudu 9A-1, 9A-2 and 9A-3 boreholes. Communications of the Geological Survey of Namibia, 6, 23 - 29.

McMillan, I., Brink, G., Broad, D. & Maier, J. 1997, "Late Mesozoic sedimentary basins off the south coast of South Africa", *Sedimentary Basins of the World*, vol. 3, pp. 319-376.

Mijnssen, F.C.J. 1991, "Characterization of deltaic rocks for numerical reservoir simulation",

Mikeš , D., Barzandji, O., Bruining, J. & Geel, C. 2006, "Upscaling of small-scale heterogeneities to flow units for reservoir modelling", *Marine and Petroleum Geology*, vol. 23, no. 9, pp. 931-942.

Mikeš, D. & Geel, C. 2006, "Standard facies models to incorporate all heterogeneity levels in a reservoir model", *Marine and Petroleum Geology*, vol. 23, no. 9, pp. 943-959.

Morse, D.G. 1994, "Siliciclastic reservoir rocks", *Memoirs-American Association of Petroleum Geologists*, pp. 121-121.

Moulton, J.D., Dendy, J.E. & Hyman, J.M. 1998, "The black box multi-grid numerical homogenization algorithm", *Journal of Computational Physics*, vol. 142, no. 1, pp. 80-108.

Olariu, C. & Bhattacharya, J.P. 2006, "Terminal distributary channels and delta front architecture of river-dominated delta systems", *Journal of Sedimentary Research*, vol. 76, no. 2, pp. 212-233.

Oreskes, N., Shrader-Frechette, K. & Belitz, K. 1994, "Verification, validation, and confirmation of numerical models in the earth sciences", *Science*, vol. 263, no. 5147, pp. 641-646.

Peaceman, Donald W. 2000. "Fundamentals of numerical reservoir simulation", pp. 351-367

Petroleum Agency South Africa, 2007-2011, *Petroleum Exploration Information and Opportunities*.

Pickup, G., Stephen, K., Ma, J., Zhang, P. & Clark, J. 2005, "Multi-stage upscaling: Selection of suitable methods", *Transport in Porous Media*, vol. 58, no. 1-2, pp. 191-216.

Pöppelreiter, M., Balzarini, M.A., De Sousa, P., Engel, S., Galarraga, M., Hansen, B., Marquez, X., Morell, J., Nelson, R. & Rodriguez, F. 2005, "Structural control on sweet-spot distribution in a carbonate reservoir: Concepts and 3-D models (Cogollo Group, Lower Cretaceous, Venezuela)", *AAPG Bulletin*, vol. 89, no. 12, pp. 1651-1676.

Qi, D. & Hesketh, T. 2005, "An analysis of upscaling techniques for reservoir simulation", *Petroleum Science and Technology*, vol. 23, no. 7-8, pp. 827-842.

Qi, D. & Hesketh, T. 2004, "Quantitative evaluation of information loss in reservoir upscaling", *Petroleum Science and Technology*, vol. 22, no. 11-12, pp. 1625-1640.

Qi, D. & Hesketh, T. 2004, "REV grid technique for reservoir upscaling", *Petroleum Science and Technology*, vol. 22, no. 11-12, pp. 1595-1624.

Readings, H.G., 1981, "Sedimentary environments and facies", *Blackwell science publications*, 569pp.

Renard, P. & De Marsily, G. 1997, "Calculating equivalent permeability: a review", *Advances in Water Resources*, vol. 20, no. 5, pp. 253-278.

Ringrose, P., Sorbie, K., Corbett, P. & Jensen, J. 1993, "Immiscible flow behaviour in laminated and cross-bedded sandstones", *Journal of Petroleum Science and Engineering*, vol. 9, no. 2, pp. 103-124.

Robinson, A. 2008, "The future of geological modelling in hydrocarbon development: introduction", *Geological Society, London, Special Publications*, vol. 309, no. 1, pp. 1-3.

Roux, J. 2007, Republic of South Africa 2007 license round-Area C: Proximal Bredasdorp Basin. Petroleum Agency South Africa, pp. 1-26.

Sharma, A., Leung, J., Srinivasan, S. & Kim, Y. 2008, "An Integrated Approach to Reservoir Uncertainty Assessment: Case Study of a Gulf of Mexico Reservoir", *SPE Annual Technical Conference and Exhibition*.

Schaller, M. F., and Fan, Y. (2009), River basins as groundwater exporters and importers: Implications for water cycle and climate modelling, Journal of Geophysical Research: Atmospheres, 114.

Schlumberger Oilfield Glossary, www.glossary.oilfield.slb.com.

Schlumberger Oilfield Review, 2008.

Schlumberger, 1991, "Principle and application of log interpretation," Schlumberger Education services, Houston.

Schlumberger, "Reservoir engineering manual, "Schlumberger Education services, Houston, 2009-2011.

V. Singh, I. Yemez e J. Sotomayor 2013, Key Factors Affecting 3-D Reservoir Interpretation and Modelling Outcomes: Industry Perspectives. British Journal of Applied Science & Technology

Sonibare, W., Mikeš, D. & Cole, D. 2011, "Facies architecture of kookfontein shelf edge delta, Tanqua-Karoo Basin (South Africa): Implications for facies analysis and modelling", *South African Journal of Geology*, vol. 114, no. 3-4, pp. 299-324.

Sonibare, W.A., Sippel, J., Scheck-Wenderoth, M. and Mikeš, D. (2014: In press), Crust-scale 3-D model of the Western Bredasdorp Basin (Southern South Africa): data-based insights from combined isostatic and 3-D gravity modelling. Basin Research, BRE-026-2013.

Tamhane, D., Wang, L. & Wong, P. 1999, "The role of geology in stochastic reservoir modelling: the future trends", *SPE Asia Pacific Oil and Gas Conference and Exhibition*.

Thomson, K. 1999, "Role of continental break-up, mantle plume development and fault reactivation in the evolution of the Gamtoos Basin, South Africa", *Marine and Petroleum Geology*, vol. 16, no. 5, pp. 409-429.

Thomson, K. 1998, "When did the Falklands rotate?" *Marine and Petroleum Geology*, vol. 15, no. 8, pp. 723-736.

Turner, 2000, "Geological Models for Sequences 14a and 13a, Block 9, Bredasdorp Basin, Offshore Republic of South Africa. SOEKOR internal report, SOE-EXP-RPT-0440, 40p.

Turner, J., Grobbler, N. & Sontundu, S. 2000, "Geological modelling of the Aptian and Albian sequences within Block 9, Bredasdorp Basin, offshore South Africa", *Journal of African Earth Sciences*, vol. 31, no. 1, pp. 80.

Turner, 1991, "Geological Models for sequence 13a, Block 9, Bredasdorp Basin, Offshore Republic of South Africa. SOEKOR internal report, SOE-EXP-RPT-0112, 30p.

Tye, R.S. & Hickey, J.J. 2001, "Permeability characterization of distributary mouth bar sandstones in Prudhoe Bay field, Alaska: How horizontal cores reduce risk in developing deltaic reservoirs", *AAPG Bulletin*, vol. 85, no. 3, pp. 459-475.

Vail, P., Hardenbol, J. & Todd, R. 1984, "Jurassic unconformities, chronostratigraphy, and sea-level changes from seismic stratigraphy and biostratigraphy".

Warren, J. & Price, H. 1961, "SPE-001579-G-Flow in Heterogeneous Porous Media", *Old SPE Journal*, vol. 1, no. 3, pp. 153-169.

Webber, K. & Van Geuns, L. 1990, "Framework for constructing clastic reservoir simulation models", *Journal of Petroleum Technology*, vol. 42, no. 10, pp. 1248-1253, 1296-1297.

Weber, K. 1986, "How heterogeneity affects oil recovery", *Reservoir characterization*, vol. 487.

Wen, R., Allard, W.M., Arve, N. & Ringrose, P. 1998, "Three-Dimensional Simulation of Small Scale Heterogeneity in Tidal Deposits–A Process-Based Stochastic Simulation Method",

Wen XH, Gómez-Hernández JJ. 1996,"Upscaling hydraulic conductivities": an overview Hydrol; 183(1–2): ix–xxxii.

Wiggins, M. & Startzman, R. 1990, "An approach to reservoir management", *SPE Annual Technical Conference and Exhibition*.

Zijl, W. & Trykozko, A. 2002, "Numerical homogenization of two-phase flow in porous media", *Computational Geosciences*, vol. 6, no. 1, pp. 49-71.

APPENDIXES

APPENDIX A: DESCRIPTION OF SUBSURFACE DATA AND ASSOCIATED ELEMENTS

List of Reservoir Data	Complete suites of digitized data in the selected wells (E-L1, E-AH1 and E-BD2)
1. Updated base maps 2. Digitized wire-line log data (tif, las and asci format) 3. 2D Seismic profiles , 17 seismic lines- SEGY format 4. Well survey data (well co-ordinates, well header) 5. Well completion report 6. Well test report and data 7. Stratigraphic data (Well tops) 8. Check shot data 9. Core samples, core plugs, routine and special core analysis report (including core photographs)	1. SP (spontaneous potential log) 2. GR (gamma ray log) 3. DT(sonic log) 4. RHOB(density log) 5. Resistivity log (shallow, medium and deep) 6. Caliper (borehole diameter) 7. Sonic porosity 8. Neutron log –missing in well E-BD2

APPENDIX A: DESCRIPTION OF SUBSURFACE DATA AND ASSOCIATED ELEMENTS

Well name	Surface X	Surface Y	Latitude	Longitude	TVD	MD
E-L1	517755.48	6115584	35”06’8.64’S	21”0834.93E	3984	3974
E-AH1	513022.58	6106191	35”11’13.8’S	21”0834.93E	3703	3729
E-BD2	524341.76	6102958	35”12’58.00”S	21”16’2.85”E	2874	2900

Seismic Profile	Length (km)	Seismic Profile	Length (km)
E-89-002	27	E-90-713	27
E-90-013	22	E-90-714	27
E-90-072	25	E-90-715	27
E-90-703	26	E-90-728	29
E-90-710	26	E-90-730	29
E-90-711	26	E-90-731	29
E-90-712	26	E-90-732	29
E-90-716	26	E-90-734	29
		E-90-744	26

S/n	Well name	Total Depth (m)	Elevation, KB (m)	Water Depth (m)	Seafloor (m)	Core Start depth-End Depth (m)	No of available core sample	Core sample length (m)
1	E-L1	2900	25	100	125	2579-2632	2	25.7
2	E-AH1	3729	26	91	117	2471-3161	2	14
3	E-BD2	4886	26	89	115	2798-3300	1	7

APPENDIX B: DATA PREPARATION AND QUALITY CHECKING

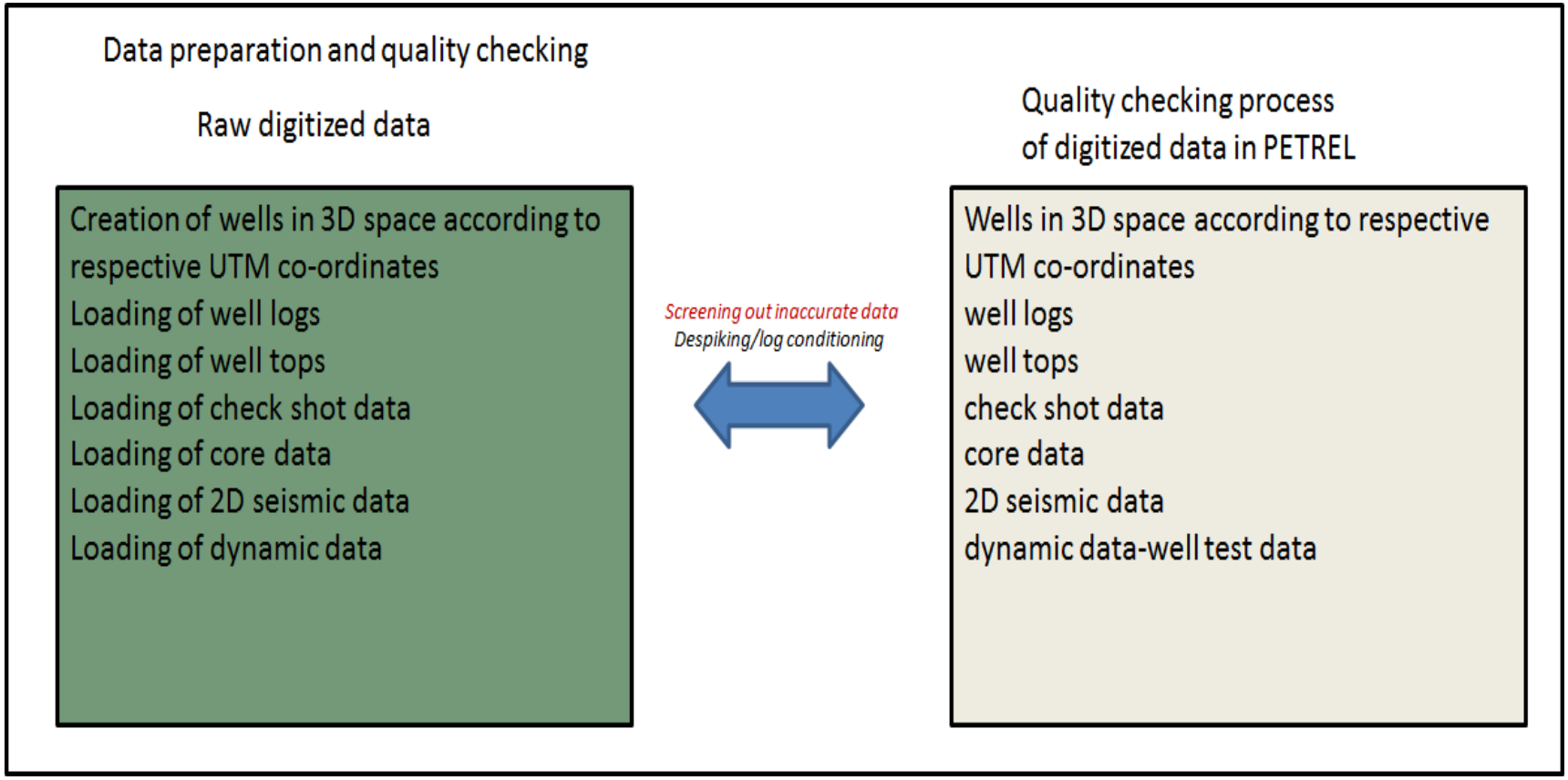

APPENDIX C: SEDIMENTARY CORE LOGS FOR WELL E-L1, E-AH1 AND E-BD2

Well E-L1:

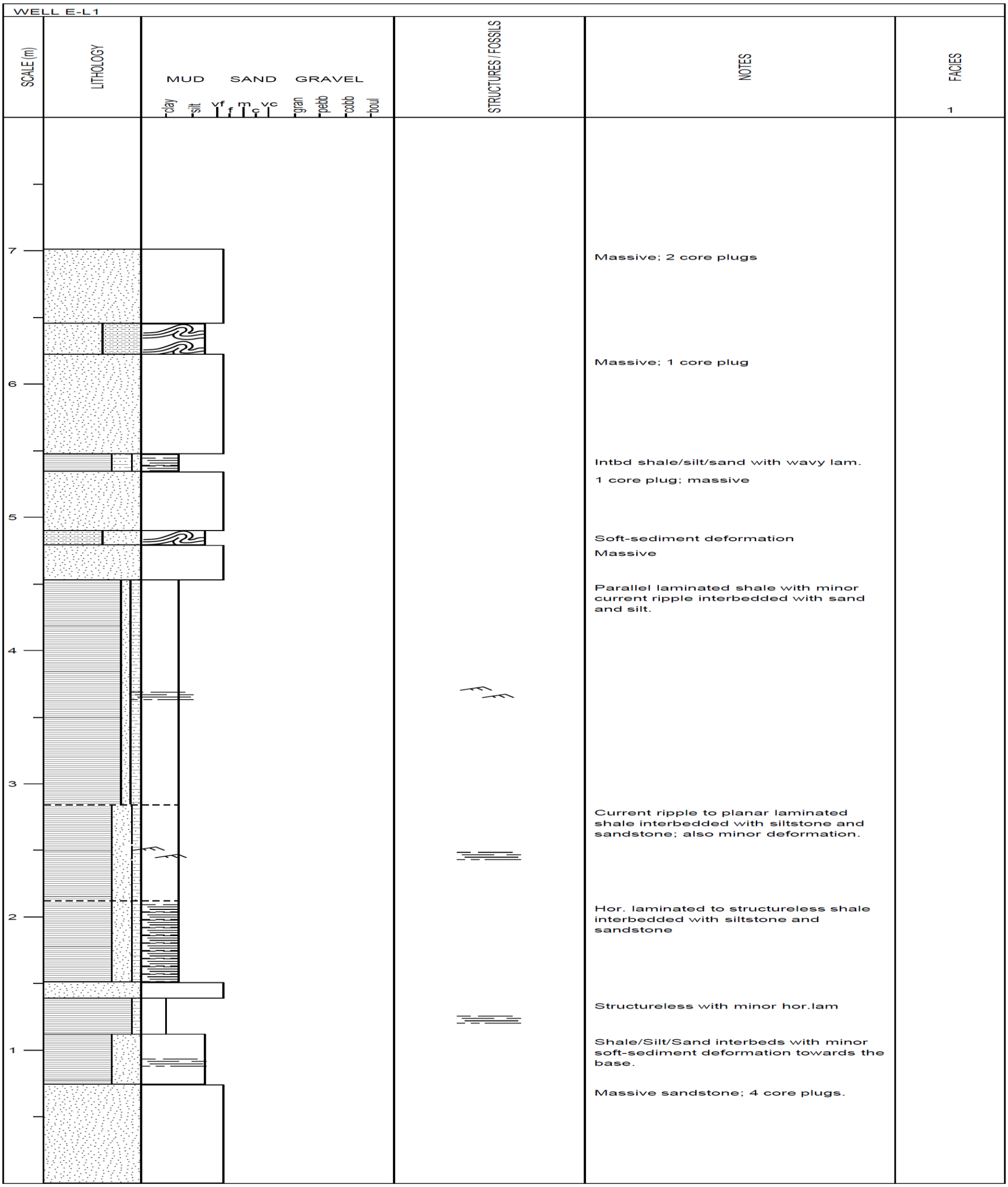

Well E-AH1:

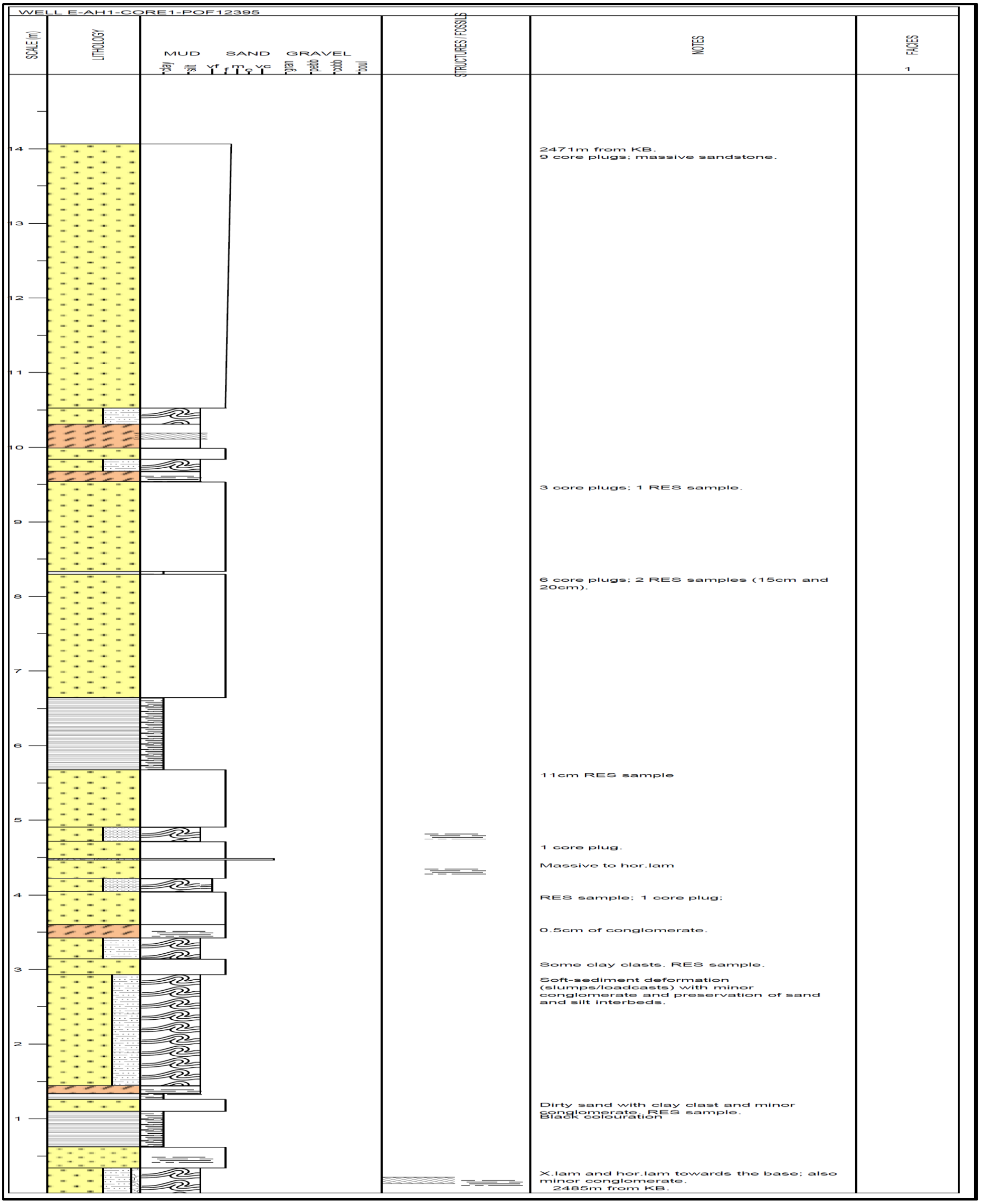

Well E-BD2:

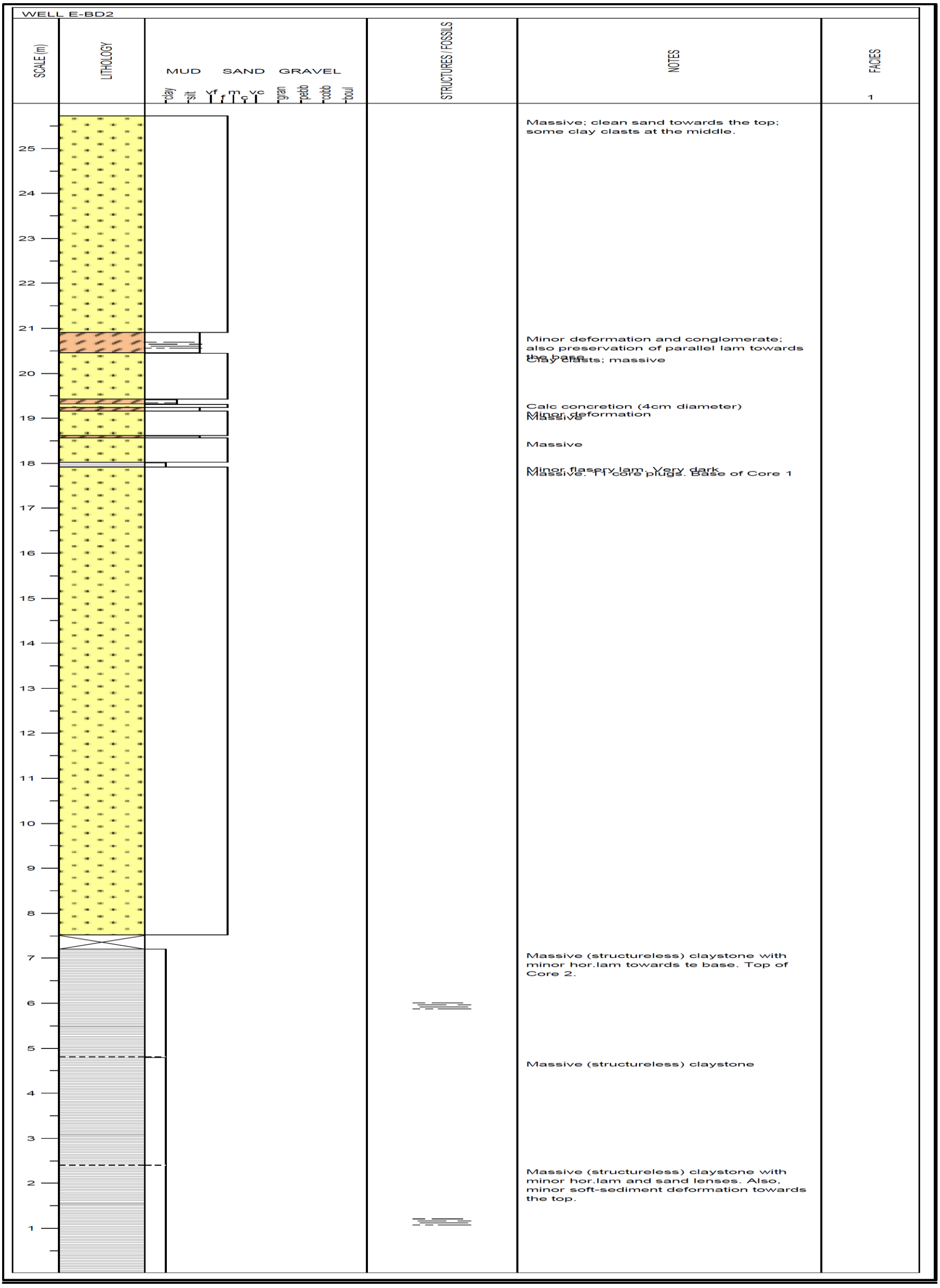

APPENDIX D: CHARACTERISTICS OF SELECTED WELL LOGS IN THE STUDY AREA AND THE BASIC INTERPRETATION GOALS

Log	Property measured	Units	Interpretation goals
SP-spontaneous potential	Natural electric potential	Millivolts	Gross lithology (reservoir vs. non reservoir), estimation of shale content, identification of deposition environment, correlations of formations from well to well and qualitative indication of permeability.
Resistivity	Resistance to electric flow	Ohm-meters	Fluid evaluation and true formation resistivity R_t.
Gamma-ray	Natural radioactivity – related to K, Th, U (Potassium, Thorium and Uranium)	API units	Gross lithology (shaliness), correlation of formations and clay typing.
Sonic	Velocity of compressional sound wave	Microsecond/metre	Identification of porous zones (from interval transit time, DT) lithological identification (with density and neutron) synthetic seismograms (with density) and seismic time-to- depth conversion.
Neutron	Concentration of hydrogen (water and hydrocarbons) in pores	Per cent porosity	Porosity (displayed directly on the log), lithology identification (with sonic or density) and gas indication with density.
Density	Bulk density (electron density) includes pore fluid in measurement	Kilograms per cubic metre (kg/cm^3)	Porosity (from bulk density, RHOB), lithology identification, gas indication (with the neutron log), and synthetic seismograms- deriving acoustic impedance with the sonic log).
Combination Neutron-density Log	Apparent porosity of both neutron and density.	Per cent porosity	This log is routinely recorded in mostly in all reservoir sections in determining porosity that is free of lithology effects and detect hydrocarbon effects (i.e. gas mainly).

APPENDIX E: CORE DATA AND PORO-PERM PLOT

Well E-L1:

Depth	Porosity	K_h	K_v	S_w	S_g	Grain density
3293.1	0.071	0.34	0.26	0.44	0.56	2.65
3293.4	0.086	0.57	0.37			2.67
3293.65	0.075	0.13	0.09			2.67
3293.9	0.058	0.14	0.08	0.41	0.59	2.66
3294.33	0.072	0.27	0.17			2.67
3294.58	0.067	0.13	0.07			2.67
3294.78	0.05	0.06	0.03			2.68
3294.95	0.04	0.06	0.03	0.65	0.35	2.66
3295.45	0.064	0.02	0.01			2.7
3295.71	0.032	0.02	0.01			2.68
3298.37	0.015	0.01	0.01			2.69
3298.76	0.016	0.01	0.01			2.69
3299.49	0.076	0.14	0.08	0.46	0.54	2.65
3300.1	0.087	0.55	0.36			2.66
3300.21	0.074	0.62	0.41	0.4	0.6	2.65

K_h-Horizontal permeability
K_v-Vertical permeability
S_w-Water saturation
S_g- Gas saturation

Well E-AH1:

DEPTH	Porosity	K_h	K_v	S_w	S_o	S_g	Grain density
2471	0.134	33	39	0.44	0.16	0.4	2.64
2471.38	0.174	45	53				2.72
2471.61	0.167	40	47				2.71
2471.84	0.141	32	38				2.67
2471.88	0.139	38	45	0.54	0.17	0.29	2.65
2472.23	0.136	28	34				2.66
2472.48	0.139	26	31				2.68
2472.73	0.13	23	28				2.66
2472.9	0.149	33	39	0.59	0.15	0.26	2.68
2473.27	0.138	30	36				2.65
2473.52	0.14	32	38				2.69
2473.76	0.153	22	27	0.75	0	0.25	2.67
2473.9	0.141	23	28				2.65
2474.22	0.123	15	19				2.67
2474.47	0.124	20	24				2.67
2474.71	0.117	15	18				2.67
2474.89	0.111	10	13	0.65	0	0.35	2.67
2475.26	0.117	6.6	8.6				2.71
2475.51	0.04	0.02	0.03				2.7
2475.76	0.063	0.06	0.11				2.68
2475.95	0.131	53	61	0.79	0	0.21	2.69
2476.31	0.065	0.02	0.04				2.77
2476.56	0.034	0.02	0.03				2.73
2476.75	0.128	33	39	0.79	0	0.21	2.66
2476.98	0.131	26	31				2.66
2477.21	0.13	26	31				2.66

2477.44	0.124	25	30				2.67
2477.67	0.182	50	58				2.77
2477.72	0.182	48	56	0.81	0	0.19	2.78
2478.12	0.142	42	49				2.66
2478.37	0.153	45	53				2.65
2480.77	0.048	0.02	0.04	0.45	0	0.55	2.63
2481.55	0.143	63	73				2.66
2481.8	0.191	80	91				2.81
2481.96	0.165	65	75	0.41	0.14	0.45	2.77
2482.2	0.189	57	66				2.83
2482.47	0.077	2.5	3.5				2.69
2482.72	0.139	79	90				2.65
2482.84	0.185	83	94	0.57	0.16	0.27	2.81
2483.25	0.085	74	9.5				2.68
2483.48	0.169	15	19				2.94
2483.71	0.101	12	15				2.67
2483.94	0.147	53	61	0.41	0.15	0.44	2.63

Well E-BD2

Depth	Porosity	K_h	K_v	Grain density
2579.3	0.197	929	935	2.64
2580.35	0.186	497	503	2.67
2580.6	0.184	276	283	2.66
2580.85	0.174	228	235	2.65
2581.6	0.192	670	673	2.64
2581.85	0.167	116	121	2.64
2582.35	0.195	645	645	2.64
2582.64	0.191	486	489	2.64
2583.8	0.159	159	166	2.64
2584.3	0.171	150	157	2.64
2585.8	0.188	421	422	2.64
2586.32	0.194	747	755	2.67
2586.82	0.197	198	204	2.64
2587.35	0.174	64	68.1	2.64
2587.85	0.157	174	178	2.64
2588.1	0.18	296	300	2.64
2588.35	0.188	393	393	2.64
2588.6	0.183	446	448	2.64
2588.85	0.187	530	532	2.66
2589.1	0.169	142	147	2.64
2589.35	0.171	198	201	2.64
2589.6	0.17	207	211	2.64
2589.85	0.167	240	243	2.64
2590.1	0.171	248	253	2.64

2590.35	0.173	239	245	2.65
2590.6	0.171	215	222	2.64
2590.89	0.173	230	238	2.64
2591.17	0.168	184	190	2.64
2591.42	0.174	259	262	2.64
2591.69	0.168	151	158	2.65
2591.94	0.166	189	193	2.64
2592.19	0.174	201	205	2.64
2592.44	0.158	103	108	2.64
2592.69	0.158	155	160	2.64
2592.94	0.14	103	107	2.64
2593.19	0.185	197	200	2.72
2593.5	0.164	145	149	2.65
2593.75	0.177	145	150	2.65
2594	0.17	90.8	97.1	2.65
2594.28	0.168	175	179	2.64
2594.53	0.166	117	121	2.64
2594.78	0.173	115	120	2.65
2595.03	0.167	108	112	2.64
2595.28	0.177	212	216	2.65
2595.53	0.14	76.1	79.7	2.65
2595.78	0.163	146	152	2.64
2596.05	0.168	154	160	2.65
2596.3	0.168	155	159	2.66

(CORE PORO-PERM) PLOT FOR EACH SELECTED WELL

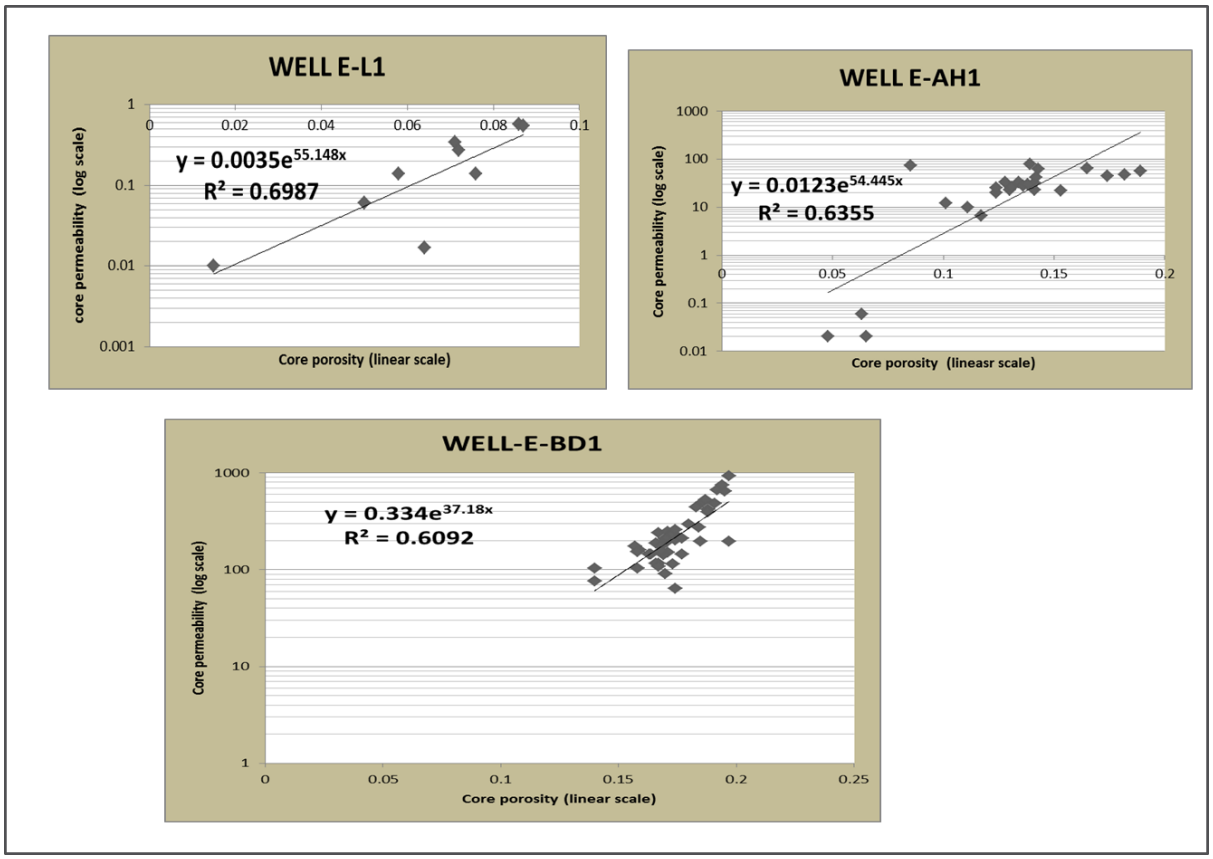

APPENDIX F: SUMMARISED DESCRIPTION OF INTERPRETED LITHOFACIES OF CORES FROM THE SELECTED WELLS E-L1, E-AH1, AND E-BD2

Lithofacies WELL E-AH1	Lithology	Sedimentary Structures	Facies Thickness	Facies Association	Notes	Micropaleontology/ Bioturbation	Estimated Sand: Silt ratio
A	Sand	Massive clean sand, minor horizontal lamination with occurrences of soft sediment deformation with minor conglomerate and sand and silt interbeds. Presence of occasional clay clast and high angle bedding towards the base.	~7.5m	Sandstone	Massive sandstone well sorted and glauconitic	Presence of bivalve shells	95:5%
B	Interbedded sand stone and siltstone	Minor horizontal lamination and presence of minor conglomerates	~1.7m	Mudstone		Abundant radiolaria	60:40%
C	Clay stone/Shale	Near Horizontal bedding	~1.20m	Sandstone			50:50%
D	Soft sediment deformation	Homogenous fine sand/silt with slump	~ 2.4m	Sandstone			30:70%
Lithofacies WELL E-BD2							
A	Sand	Massive clean sand, irregular clay clast and sandstone interbeds present, occurrence of stylolitic development and low angle cross stratification, erosional contact present	~17.7m	Sandstone	Massive sandstone, well-sorted, glauconitic, bedding indistinct, minor irregular sub mm-2cm sandstone laminae	Presence of bivalve shells at the top	95:5%
B	Interbedded sandstone and siltstone	Rounded calcareous concretions present, irregular siltstone laminae	~0.5m	Mudstone	Siderite lenses present		60:40%
C	Claystone/shale	Massive structure less clay stone with minor horizontal lamination towards base, minor sandstones and siltstone lenses present	~7.4m	Sandstone	Massive uniform clay stone, bedding indistinct, occasional clay flake inclusions		60:40%
D	Soft sediment deformation						
Lithofacies WELL E-L1							
A	Sand	Massive sandstone, presence of stylolite's at top of core. Irregular plus soft sediment compaction distortion, sub horizontal clay clast present	~2.7m	Sandstone			90:10%
B	Claystone/shale	Presence of wavy lamination	~4.05m	Mudstone			30:70%
C	Interbedded sandstone and siltstone	Minor horizontal lamination to structureless shale, occasionally parallel laminated shale with minor current ripple interbedded with sand and silt	~0.15m	Sandstone			70:30%
D	Soft sediment deformation	Homogenous fine sand/silt with slump	~0.2m	Sandstone			40:60%